NERA

**Network of European Research Infrastructures for Earthquake Risk Assessment and Mitigation**

# Report

## Inventory of Operational Near-Fault Observatory Networks and Data

| | |
|---|---|
| Activity: | *Networking Near-Fault Observatories* |
| Activity number: | *NA5, Task 5.1* |
| Deliverable: | *Inventory of Operational Near-Fault Observatory Networks and Data* |
| Deliverable number: | *D5.1* |
| Responsible activity leader: | *Kristín S. Vogfjörd* |
| Responsible participant: | *Icelandic Meteorological Office (IMO)* |
| Authors: | *K. S. Vogfjörd (IMO), P. Bernard (CNRS), L. Chiaraluce (INGV), D. Fäh(ETHZ), G. Festa (AMRA), Can Zulfikar (BOUN).* |

**Seventh Framework Programme**
**EC project number: 262330**

# Summary

This report summarizes networks, systems, instrument types, software, data and operational procedures in use at six European near-fault observatories. The report constitutes deliverable D5.1 of NERA WP5, Networking of Near-fault Observatories and its purpose is to serve as an inventory of infrastructure, data and operations in the six observatories being networked in WP5. The six observatories are: The **South Iceland Seismic Zone** in Iceland, the **North Anatolian Fault in the Marmara Sea** in Turkey, the **Alto Tiberina Fault** and the **Irpinia Fault**, both in Italy, the **Corinth Rift** in Greece and the **Valais Region** in Switzerland. The goal with this pan-European near-fault network is to facilitate scientific and technological collaboration among the observatories, to establish common operational and data quality standards and to generate common archives of multiparameter near-fault observatory data. The report forms a basis for planning and decision making within the work package, for the systems and data to be networked. It will be reviewed at the scheduled workshops of WP5.

# Contents

# 1 Introduction

The seismic hazard generated by fault zones slipping in large earthquakes and the need for mitigation of risk to population and structures drive the pursuit to understand the physics of faulting and the near-surface response to shaking. To facilitate research into the faulting process and its effects, near-fault observatories (NFO) comprised of dense, multidisciplinary geophysical networks have been constructed in many European fault zones. Six such European NFO's are networked in NERA's WP5. The emphasis varies between observatories, but as a whole, they have collected a wealth of data of great imporance for the advancement of knowledge of the faulting process and near-fault site effects.


***Figure 1.1*** *Location of near-fault observatories to be networked in the NERA project*

The fault zones represented by the six observatories (Figure 1.1) to be networked are in different tectonic regimes: i) The **South Iceland Seismic Zone** (SISZ) in Iceland, the **Marmara Sea** in Turkey and the **Corinth Rift** in Greece are at plate boundaries, with strike-slip faulting characterizing the SISZ and the Marmara Sea, while normal faulting dominates in the Corinth Rift. ii) The **Alto Tiberina** (ATF) and **Irpinia** faults, dominated by low- and medium-angle normal faulting respectively, are in the Appennine mountain range in Italy. iii) The **Valais Region**, characterized by both strike-slip and normal faulting is located in the Swiss Alps. The fault structures range from well developed long faults, such as in the Marmara Sea, to more complex networks of smaller, book-shelf faults such as in the SISZ.

All the fault zones can generate large earthquakes (M≥6) posing substantial earthquake hazards. Two of the zones, Marmara Sea and Corinth, are under ocean causing additional tsunami hazard, while steep slopes and sediment-filled valleys in the Valais give rise to hazards from landslides and liquefaction. Induced seismicity has repeatedly occurred in connection with geothermal drilling and water injection in the SISZ and in the Valais region. The active volcanoes flanking the SISZ also bring the added dimension of volcano-tectonic interaction.

The focus of the observatories varies, ranging from small- to large-scale seismicity and includes: i) earthquake early-warning and rapid response ii) the internal structure of the fault systems, iii) the role different parameters, such as fluids play in fault initiation, iv) site effects and v) derived processes such as earthquake generated tsunamis and vi) landslides. The sites include surface and sub-surface observations from seismic, deformation, strain, geochemical and electromagnetic equipment, thus representing a wide spectrum of near-fault observations. An overview of the observation systems at each NFO is given in Table 1.1.

***Table 1.1*** *Types of systems and numbers of stations to be networked from the near-fault observatories.*

| NFO | Seism. SP/BB | Accel. | OBS | Tide guage | GPS | Strain | Bore hole water level | Chem. | Magnet/ EM | Deep drill |
|---|---|---|---|---|---|---|---|---|---|---|
| **SISZ** | 18/3 | 2[1)] +2 | | | 12 +3[3)] | 4 | x [3)] | x [3)] | | x [3)] |
| **NAFZ** | 0/39 | 27 | 5 | | 58 | | . | . | x[5)] | . |
| **ATF** | 15[6)]/13 | 6[1)] | | | 10 | | | | | |
| **CRL** | 13/8 | 3[1)] +14 +1[4)] | | 1 | 9 | 2 | 1 | x[3)] | x[3)] | x[3)] |
| **IF** | 12/6 | 31[1)] | | | | | | | | |
| **VA** | 4/10 | 4[1)] +34 | | | (11+20[2)]) [3)] | 1[3)] | | 1 | 1[2)] | |

[1)] Co-located with seismic station
[2)] Planned installation
[3)] Not owned by NERA partner
[4)] Array
[5)] With OBS's
[6)] Three are vertical arrays

The observatories are either operated by a single national organisation, such as in the case of Irpinia and ATF, by different national institutions, such as in the SISZ and the Valais, or by different national and European organisations, such as in the Marmara Sea, and Gulf of Corinth.

# 2 Description of observatories:

## 2.1 South Iceland Seismic Zone

**[63.75N - 64.25N; 21.5W – 19.5W]**

### Tectonic setting and observatory overview

The South Iceland Seismic Zone (SISZ) is a 20 km wide and 80 km long transform zone on the Mid-Atlantic rift, the plate boundary between Eurasia and North America. The rift, which comes on land on the Reykjanes Peninsula (RP on Figure 2.1.1) in SW Iceland spreads at a full rate of 18-19 mm/yr (Sella et al., 2002). Due to the rifts interaction with the mantle plume under east central Iceland, it shifts roughly 80 km eastward along the SISZ to the Eastern volcanic zone (EVZ), which takes over most of the rifting (LaFemina et al., 2005). The displacement along the E-W trending SISZ is left-lateral strike slip, but on the surface all the major faults strike approximately N-S with right-lateral motion exhibiting a pattern of book-shelf faulting (Einarsson and Eiríksson, 1982; Hackman et al., 1990; Clifton & Einarsson, 2005; Einarsson, 2008).

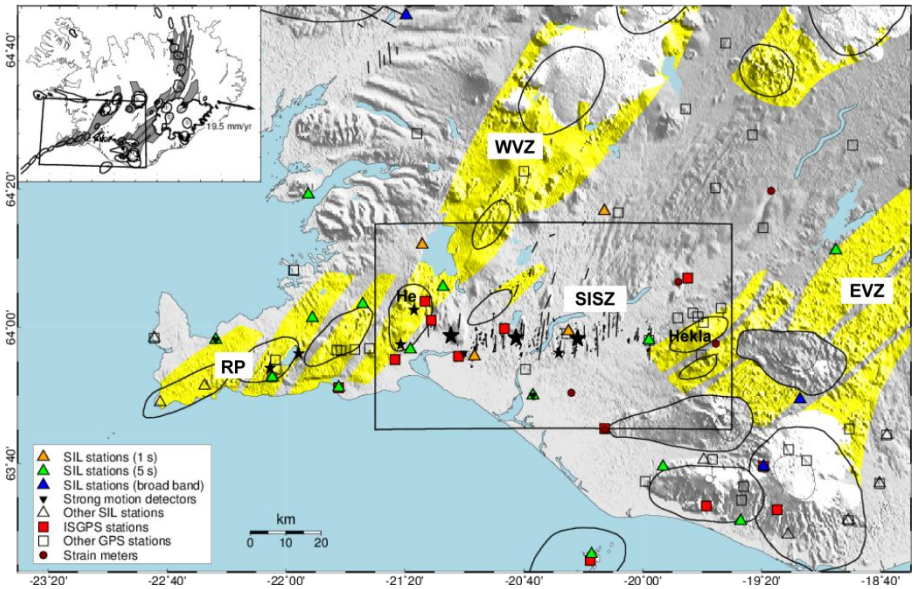


***Figure 2.1.1*** *Map of SW Iceland showing the active segments of the Mid-Atlantic rift in Iceland (yellow) and the location of the SISZ. Mapped faults in the SISZ are outlined (black lines) and recent M>5 events are shown as stars. Locations of Hekla and Hengill (He) volcanoes are indicated. The boxed area marks the outlines of the SISZ near-fault observatory. The inset shows the rift zones and the spreading direction. Seismic, GPS and borehole strain network stations are shown. Stations networked in NERA are coloured.*

History reveals that every century a sequence of M6-7 events on N-S oriented, strike-slip faults moves through the ZISZ. Each sequence can last from weeks to years and usually starts in the east (Figure 2.1.2) (Einarsson et al., 1981; Stefánsson and Halldórsson, 1988). A major earthquake sequence is presently ongoing, including two $M_W$6.5 events near the center of the SISZ in 2000 (Árnadóttir et al., 2001; 2003; 2005; Björnsson et al., 2001; Jónsson et al., 2003; Pedersen et al., 2001; 2003; Decriem et al., 2011) and a $M_W$6.3 earthquake farther west in 2008 (Hreinsdóttir et al., 2009; Vogfjörd et al., 2009; Decriem et al., 2010) (Figure 2.1.1). The fault planes of the two June-2000 earthquakes and their triggered events, as well as the two fault planes of the 2008 earthquake have been mapped

through high-precision realtive earthquake locations of aftershocks (Vogfjörd et al., 2005a; 2005b, 2009; Hjaltadóttir and Vogfjörd, 2005; Hjaltadóttir, 2010) Less than half of the accumulated shear stress was released by these three events and earthquake hazard remains high in the SISZ (Decriem et al., 2011). Dynamic triggering of significant earthquakes ($M_W$>5.5) at up to 70 km distance is an observed characteristic of the SISZ (Clifton et al., 2003; Pagli et al., 2003; Árnadóttir et al., 2004; Vogfjörd et al., 2005b; Antonioli et al., 2006). On average around 2,000 earthquakes are recorded yearly in the SISZ, but the number can excede 20,000 during years of major events (Jakobsdóttir et al., 2002). Events as small as M-0.7 are detected, but the magnitude of completeness is around M0.6.

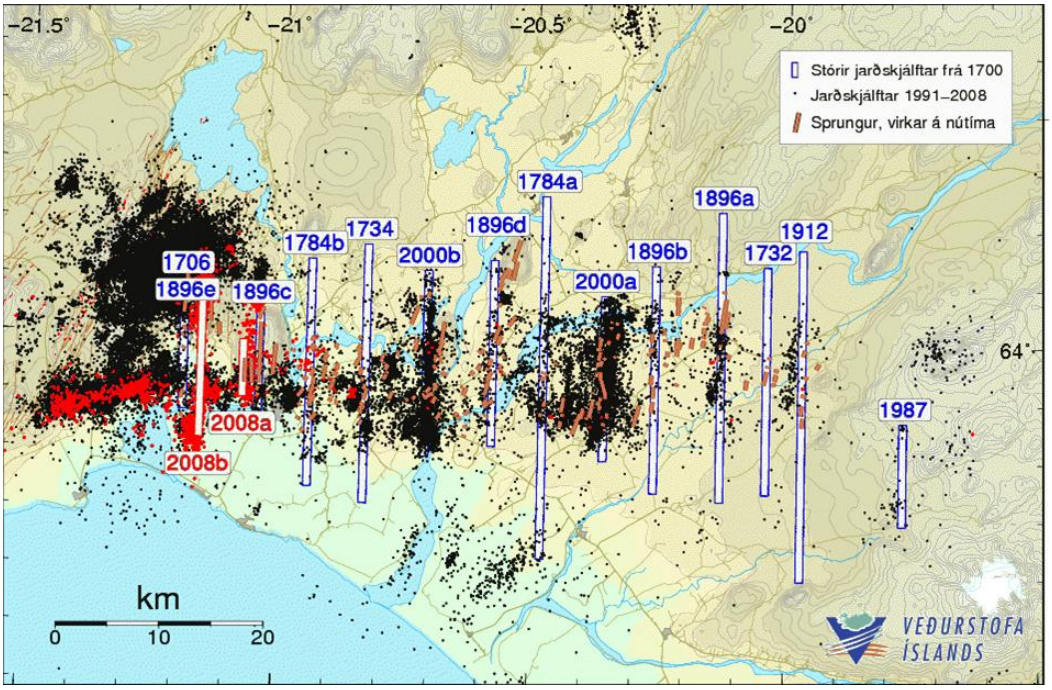


***Figure 2.1.2.*** *Map showing seismicity in the SISZ (black dots) between 1991-2007, and 2008 (red dots). Estimated location orientation and length of large earthquakes since 1700 are shown (Roth, 2004). Mapped surface faults are shown with brown lines. Fault surfaces of major earthquakes since 1991 have been mapped with high-precision, realtive earthquake locations (Vogfjörd et al., 2005a, Vogfjord et al., 2009).*

Low temperature geothermal activity is commonly associated with faults in the SISZ and tens of wells for municipal heating have been drilled throughout the zone. Two volcanoes flank the SISZ, Hekla in the East and Hengill at the NW margin (Figure 2.1.1), and volcano-tectonic interaction occurs between activity in the volcanoes and faults in the zone. Uplift in the Hengill region in 1994-1998 induced numerous swarms on nearby faults in the SISZ, amounting to nearly 100,000 recorded microearthquakes and ending with two events of $M_W$5.5 and 5.2 (Sigmundsson et al., 1997; Feigl et al., 2000; Clifton et al., 2002; Vogfjörd et al., 2005a). Two geothermal power plants with associated production wells are sited in the high-temperature geothermal fields of the Hengill region. Drilling and injection into (~2 km deep) wells has occationally induced microseismicity in rececent years. In 2009 the intensity of induced seismicity increased significantly and an on-going injection activity continues to induce earthquakes. In 2011 around 2,000 induced earthquakes were recorded, the two largest being of $M_W$4.

The focus of the SISZ observatory is on microseismicity and deformation in the SISZ, mapping of fault structures through relative location of the microseismicity, analysis of short- and long-term precursors and early warning of the larger events (Pétursson and Vogfjörd, 2010; Vogfjörd et al., 2010). Inside the area defining the observatory are seismic and strong

motion networks and analysis systems, a continuous GPS network and a borehole strain meter network (Figure 2.1.1). IMO operates the national seismic network, SIL the strain-meter network and the GPS network, ISGPS (Geirsson et al., 2006). The seismic network is fully ownded by IMO, while the strain-meter network is co-owned with the Carnegie Institue of Washington, Department of Terrestrial magnetism and the GPS network is owned by nine different institiutions. IMO will contribute data from its own stations in the systems that are relevant to the SISZ near-fault observatory. These include: Data from 21 SIL stations in and around the SISZ, of which two sites have co-located accelerometers, data from all 6 borehole strain meter stations and data from 12 ISGPS stations. Three GPS stations withiin the SISZ are owned by the Institute of Earth Sciences (IES) at the University of Iceland. Access to their data can be granted by IES. Over the course of the next two years, 2013-2014, some or all of these stations could become incorporated into IMO's ISGPS national network.

Other systems, such as a strong motion network and automatic observations of water level in boreholes exist in the SISZ, but are owned by institutions not participating in NERA. However, to strengthen the effectiveness of the operational seismic-early-warning processes in the SISZ observatory and to increase the number of parameters networked in NERA, IMO has initiated collaboration with the Earthquake Engineering Research Center (EERC) at the University of Iceland to exchange data streams from accelerometers. This will add two additional strong motion stations to the observatory; one in the western part of the SISZ and one in the eastern part, bringing the number of strong motion stations to four. In addition IMO will initiate discussions with owners of borehole water-level data to seek inclusion of data from a few such sites in the SISZ near-fault observatory. Other observation systems previously operated by IES in the SISZ, such as radon monitoring in boreholes, have been temporarily discontinued. However one well at Selfoss, may still be viable and inclusion of the radon data stream in the observatory will be examined.

The real-time seismic system (SIL) automatically locates and determines magnitude for all earthquakes in Iceland. Upgradable Alert- and ShakeMaps for events of $M_W$>2, starting 2 minutes after the event are also automatically generated, and automatic GPS processing delivers 24hr displacement solutions for all GPS stations. These results and time series from all strain stations are all immediately displayed on the IMO web site www.vedur.is.

## Network descriptions

### 2.1.1 Seismic and strong motion networks

#### *2.1.1.1 Network and hardware*

The first eight stations of the Icelandic national seismic network, SIL were installed in 1991 in and around the South Iceland Seismic Zone. The original goal of the network was to record microseismicity and therefore all the initial stations were short-period (Stefánsson et al., 1993; Bödvarsson et al., 1996, 1998; Rögnvaldsson and Slunga 1993, 1994; Slunga et al., 1995), but since then the network has grown and expanded to cover most of Iceland and to include broadband instruments, as well as accelerometers. Most stations are located in quiet rural areas, often on farms. Each station consists of a seismic sensor and recording equipment located in a semi-submerged vault, usually within a few hundred metres from a house with access to power, where the site computer is usually located. Three stations contributing data to the SISZ near-fault observatory are located in remote areas without access to electricity. These sites generate their own power and do not have a site computer. Locations of stations are shown in Figure 2.1.1 and listed in Table 2.1.1.

***Table 2.1.1*** *List of seismic stations contributing data to the SISZ near-fault observatory.*

| Station name | Latitude °N | Longitude °E | Elevation m | Sensor depth m |
|---|---|---|---|---|
| asb | 64.74818 | -21.32535 | 94 | 1.5[1)] |
| asm/ASM | 63.83361 | -20.61474 | 22 | 1.5 |
| bja | 63.94590 | -21.30258 | 57 | 1.5 |
| esk | 63.52503 | -19.45080 | 95 | 1.5 |
| god | 63.65976 | -19.32236 | 1,200 | 1.5 |
| gyg | 64.28107 | -20.21483 | 119 | 1.5 |
| hau | 63.96851 | -19.96471 | 96 | 1.5 |
| hei | 64.19978 | -21.23604 | 162 | 1.5 |
| kas | 64.02290 | -21.85200 | 108 | 1.5 |
| kri | 63.87810 | -22.07646 | 146 | 1.5 |
| kro | 64.09806 | -21.11976 | 147 | 1.5 |
| kud | 64.32059 | -21.87472 | 28 | 1.5 |
| mid | 63.65833 | -19.88573 | 132 | 1.5 |
| san | 64.05601 | -21.57013 | 208 | 1.5 |
| sau | 63.98983 | -20.41519 | 74 | 1.5 |
| sly | 63.82402 | -19.11732 | 633 | 1.5 |
| sol | 63.92896 | -20.94357 | 30 | 1.5 |
| vat | 64.18664 | -18.91768 | 573 | 1.5 |
| ves | 63.44291 | -20.28664 | 55 | 1.5 |
| vog/VOG | 63.96967 | -22.39285 | 7 | 1.5 |
| vos | 63.85279 | -21.70357 | 8 | 1.5 |
| sel | 63.93678 | -21.00247 | ~30 | 0 |
| eerc-2[2)] | - | - | - | - |

[1)] Average depth of sensors in the vaults
[2)] Data streaming not yet active.

Of the 21 SIL stations in southwestern Iceland considered part of the SISZ observatory, 18 have short-period velocity sensors (Table 2.2). Of these 5 have a corner frequency of 1Hz (Lennartz 1s) and 13 have a corner frequency of 0.2 Hz (Lennartz 5s). Three station have broadband sensors, one with flat velocity responses at periods under 120 s (STS2), and two at periods under 60 s (CMG-3ESPC and -3ESPCD). The sensitivity of the short period sensors is 400 V/m/s, while the sensitivities of the broad band sensors are 1500 V/m/s (STS2) and 2000 V/m/s (CMG-3ESP) Two sites have accelerometers (CMG-5T) co-located with short-period sensors. Their sensitivities are 1.02 V/m/s$^2$, with a maximum range of ±1g. The Cusp-3C strong motion sensors have an integrated digitizer and recorder. Their maximum range is ±5g. The digitizers operated with the five 1 Hz sensors and five of the 0.2 Hz sensors are short period (Nanomertics RD3), with a corner frequency around 0.5 Hz and a gain of 1.47 µV/bit. The other 14 stations have digitizers with a flat response (CMG-DM24) and gains between 1 and 3.5 µV/bit. All SIL stations sample at 100 sps, while the two EERC strong motion stations sample at 200 sps.

A phase detector running on the SIL site computers continuously transmits phase information data in real time to the data center, where they are fed into an automatic event location system which operates on the phase logs only. The recorded waveform data are stored in a ring buffer at the site and originally only event based data was transmitted to the data center for archiving, but since summer 2012 the network has been converted to continuous archiving of all stations. The data streams from the remote stations without a site computer and from the two EERC strong motion stations are sampled continuously at the SIL data center.

***Table 2.1.2*** *Technical specifications of stations in the SISZ observatory*

| Station name | SP type, corner freq.$^{-1}$ | BB type, corner freq.$^{-1}$ | SM type | Sensor sensitivity V/m/s | Sensor sensitivity V/m/s$^2$ | Digitizer type | Digitizer gain µV/bit | Transmission | Power | Data[1)] | Sampling rate s$^{-1}$ |
|---|---|---|---|---|---|---|---|---|---|---|---|
| asb | | STS2 120 s | | 1500 | | CMG-DM24 | 1.0-3.5 | Internet | Mains | C | 100 |
| asm | Lennartz 5s | | CMG5T | | 1.02V/m/s$^2$ (p-p: ±1g) | CMG-DM24 | 1.0-3.5 | ISDN | Mains | C | 100 |
| bja | Lennartz 5s | | | 400 | | RD3 | 1.47 | ISDN | Mains | C | 100 |
| esk | Lennartz 5s | | | 400 | | CMG-DM24 | 1.0-3.5 | 3G | Mains | C | 100 |
| god | | CMG-3ESPC 60 s | | 2000 | | CMG-DM24 | 1.0-3.5 | ADSL | Wind & solar | C | 100 |
| gyg | Lennartz 1s | | | 400 | | RD3 | 1.47 | ISDN | Mains | C | 100 |
| hau | Lennartz 5s | | | 400 | | CMG-DM24 | 1.0-3.5 | Radio link | Mains | C | 100 |
| hei | Lennartz 1s | | | 400 | | RD3 | 1.47 | WiMax | Mains | C | 100 |
| kas | Lennartz 5s | | | 400 | | RD3 | 1.47 | ADSL | Mains | C | 100 |
| kri | Lennartz 1s | | | 400 | | CMG-DM24 | 1.0-3.5 | 3G | Mains | C | 100 |
| kro | Lennartz 5s | | | 400 | | RD3 | 1.47 | ISDN | Mains | C | 100 |
| kud | Lennartz 5s | | | 400 | | RD3 | 1.47 | 3G | Mains | C | 100 |
| mid | Lennartz 5s | | | 400 | | RD3 | 1.47 | 3G | Mains | C | 100 |
| san | Lennartz 5s | | | 400 | | RD3 | 1.47 | ADSL | Mains | C | 100 |
| sau | Lennartz 1s | | | 400 | | CMG-DM24 | 1.0-3.5 | 3G | Mains | C | 100 |
| sly | | CMG-3ESPD 60s | | 2000 | | CMG-DM24 | 1.0-3.5 | 3G/GPRS | Wind & solar | C | 100 |
| sol | Lennartz 1s | | | 400 | | RD3 | 1.47 | ADSL | Mains | C | 100 |
| vat | Lennartz 5s | | | 400 | | CMG-DM24 | 1.0-3.5 | 3G | Wind & solar | C | 100 |
| ves | Lennartz 5s | | | 400 | | CMG-DM24 | 1.0-3.5 | 3G | Mains | C | 100 |
| vog | Lennartz 5s | | CMG5T | | 1.02V/m/s$^2$ (p-p: ±1g) | RD3 | 1.47 | ADSL | Mains | C | 100 |
| vos | Lennartz 5s | | | 400 | | CMG-DM24 | 1.0-3.5 | 3G | Mains | C | 100 |
| sel | | | CUSP-3C | | (p-p: ±5g) | Linux | 1.0 µg/bit | LAN | Mains | C | 200 |
| eerc-2 | | | CUSP-3C | | (p-p: ±5g) | Linux | 1.0 µg/bit | | Mains | C | 200 |

SP: Short period; BB: Broad band SM: Strong motion
STS2: Streckeisen; CMG-3ESPC(D): Guralp Systems Ltd.; CUSP-3C: Cantebury Seismic Instruments, Ltd;
RD3: Nanometrics RD3; CMG-DM24: Guralp CMG-DM24
C: Continuous data recording;
[1)] Data archiving changed in summer 2012, from event based to continuous recording.

### *2.1.1.2 Software systems*

*Acquisition, detection and transmission software at the SIL stations*

At the seismic station computers, several automatic processes are run. These are written in C and Python by IMO staff and R. Bödvarsson at Uppsala University and include:

***SIL utility software****:* Data acquisition software with ASP drivers, ringbuffer in shared memory and real-time pre-processing of data. Includes: detector, with information on incoming wavelets, such as precise onset, signal- and noise amplitudes for all three components, apparent velocity and azimuth, spectral content et c. All packed into 128b data slices (*phase logs*) and transmitted in real-time to the data centre. (*C*; R. Bödvarsson).
***ffinnur****:* Event detector (*C*, R. Böðvarsson).
***alertrem****:* Real-time alert detector, transmitting warnings of large amplitudes or high background noise as well as estimates of band-passed 1-min averages of amplitudes on all components in the frequency bands: 0.5-1 Hz; 1-2 Hz; 2-4 Hz (*C*; R. Bödvarsson, S. Jakobsdóttir, E. Kjartansson).
***shakedet***: A detector on peak ground velocity (PGV) and peak ground acceleration (PGA), with an automatically adjusted background reference level. Including real-time transmission to the data center. Also applied to the data streams from the two EERC SM stations (*C*; E. Kjartansson).
***bctool***: Waveform data base and compression, including a runtime library and the utility bctool (*C*; E. Kjartansson).
***site*** and ***center****:* Software controlling communication with the SIL ananlysis center (*Python*; H. Gunnarsson; Ó. Arnarsson).
***Utility shell scripts***: (S. Ólafsson, S. Jakobsdóttir, G. Guðmundsson, H. Sveinbjörnsson, Ó. Arnarson).

*Automatic analysis software at the SIL data center*

Detections, or *phase logs* are continuously received at the data center, where automatic software analyzes them and locates events. Up until recently, when an event was detected, the center immediately sent a request for waveforms to the station and waveforms usually arrived within 10 minutes. Now archiving of waveforms has moved to continuous. real-time transmission of a few-second-long bc-files.

***alert****:* Processes the alert logs received from the stations. If predefined thresholds are exceded in any of the predefined alert regions, an auditory warning is played on workstations of the staff analysts. For the highest alert levels an e-mail and an SMS are also sent to relevant users and phones (*C*; R. Bödvarsson, S. S. Jakobsdóttir).
***anaaut, selector, lockina***: Automatic analysis of station phase logs to detect microearthquakes, locate them in 1D velocity models and determine their magnitude (*Fortran* and *C*; R. Slunga, R. Bödvarsson).
***phmag***: Calculates automatic local magnitudes from phase logs. (*C*; S. Rögnvaldsson)
***fetcher***: Issues fetch request for waveforms from stations. (*C*; R. Böðvarsson) – Now obsolete
***ml***: Calculates local magnitude $M_L$, by fitting 1.5 Hz high-passed, peak-to-peak amplitudes to a local magnitude relation (*Fortran*; G. B. Gudmundsson).
***shake2a*** and ***locs***: ***shake2a*** performs real-time processing of *PGV*, *PGA* and onset to prepare input into ***locs***, which locates events and determines magnitude ($M_w$) for events of $M_w$>2, based on attenuation relations for *PGV* and *PGA*. Immediate and upgradeable web publishing of PGV and first arrival times of P at the sites on an ***Alert map*** starting 2 minutes after the event origin time (*C*; E. Kjartansson).

***ShakeMap***: Immediate processing of input values from ***locs***, including location, $M_w$, and *PGV* and *PGA* values from the stations, and including also maps of near-surface S-wave velocity, $V_S^{30}$ which are based on surface geology (USGS).
***Safer1,2***: Automatic near-real time process under testing in the SISZ. The process runs every 5 minutes, starting after waveforms from two stations have arrived at the data center. It correlates the new waveforms with waveforms from previous near-by, high-quality library events already located with relative methods (***Slunga1,2,3***). The relative arrival times are then inverted for high-precision locations within 20 minutes after an earthquake. The procedure is repeated when more waveforms arrive. (Analysis software: *Fortran*; R. Slunga. Automatic process: *Perl*; G. Gudmundsson).
***Scripts*** for real-time web publishing of automatic earthquake locations and magnitudes (*Perl*; G. Gudmundsson).

*Manual analysis software*

All automatically located events are reviewed by the seismic analyst who adjusts and adds phase arrival picks and polarities of P and S waves. The event is then relocated and local magnitudes and fault plane solutions calculated. Analysis of selected data sets may also include high-precision, relative earthquake locations. The software is written in C and Fortran and include:

***lokimp***: An interactive phase picking and location software in 1D velocity models. Can also be rerun in batch mode (*Fortran* and *C*; R. Slunga, R. Bödvarsson).
***skiaut***, ***spgaut***: Process to determine focal mechanisms of earthquakes. Performs a grid search in 4° increments over strike dip and rake, to fit polarity determinations of P and S waves and inverts parameters of P- and S-wave amplitude spectra for seismic moment. Estimates local magnitude based on the moment $M_{wL}(M_0)$ and stress drop (*Fortran* and *C*; R. Slunga, R. Bödvarsson).
***slunga1,2,3*** and ***quakelook***: ***slunga1,2,3*** perform correlation of P- and S-waves from earthquakes and invert the relative times for high-precision relative location. ***quakelook*** enables interactive analysis of graphically displayed results to determine common faults of microearthquakes and combined mechenism (*Fortran* and *C*; R. Slunga)
***sjatrem***: Graphic display of 1-min-averages of amplitudes on 3 components and in 3 frequency bands (0.5-1 Hz; 1-2 Hz; 2-4 Hz). Automatically updates when new packets arrive every 5 minutes (*C*; E. Kjartansson)
***EWIS***: Interactive web-based examination and analysis mapping tool, displaying event distributions as a function of time, latitude, longitude and depth. Accesses automatic and reviewed event locations from relational database (db2) (*java script*, C++; B. Jónsson, E. Eiríksson, V. Eyjólfsson, K. Bjarnason, M. Roberts)
***ZMap***: (S. Wiemer et al. at ETHZ)

*Quality control processes*

Automatic or routine quality control processes are not applied to the seismic data streams or to parameter data, but definition of quality control protocols has just started. Technicians and monitoring staff flag data errors and other problems, which are then fixed by the technical staff. Background noise curves are not routinely calculated, but have been determined for about 1/3 of the stations.

*Data formats, accessible data bases and available data*

The SIL data is stored in ASCII files in a Unix file tree structure. Parameter data is also uploaded into a relational data base (db2). Quality checking of parameter data is not

routinely performed, but work is starting on reviewing and correcting data in the data base and making it searchable on the web. Waveform files are presently not on the web.

The seismic waveform data is archived in an in-house compressed binary data format labelled ***bc-format***.

### *2.1.1.3 Station installation procedures*

When a new seismic station is sited a careful search for an appropriate location on bedrock is carried out. Temporary instruments are operated for a few days to weeks in a few locations and waveforms from local earthquakes examined and noise curves from calm as well as windy days analysed. The criteria are for low background noise conditions and clear, short P- and S-waveforms, void of near-surface ringing effects. Seismic stations are placed on bedrock, generally where soil cover is thick enough to allow submergence of the vault. The vault is usually a 1 - 1,5 m in diameter cylindrical plastic ceptic tank, with the bottom removed. A concrete slab, 0.5 - 1 m in diameter, is cemented on the bedrock and gravel filled in between the vault and the concrete to decrease noise effects generated by wind vibration of the vault. A drain to lower ground is also included in the vault to prevent flooding in spring when the winter-snow melts. The sensor and digitzer are placed on the concrete pier, but the electronics are often mounted on the side of the vault. The vault colses on top with a ~25 cm high plastic lid. The GPS antenna providing the accurate clock synchronization is located a few meters from the vault. Examples of setup from stations **esk** and **vos** are shown in Figure 2.1.3.

***Figure 2.1.3.*** *(Upper left) Picture shows the black lid on the seismic vault at station* ***esk****. A cable links the vault to the site computer located inside the farmhouse in the background (Upper right) Inside the vault: Lennartz 5s sensor (blue), RD3 digitizer (brown) on the concrete platform. (Lower left) Black lid on the seismic vault and GPS antenna at seismic station* ***vos;*** *GPS station* ***VOGS****. (Lower right) Inside the vault: Lennartz 5s sensor (blue), RD3 digitizer (brown) and GPS receiver (yellow) on the concrete platform.*

At most stations a site computer is located in a near-by house (farm) with access to power. A 300-1200 m cable is plowed into the ground, connecting the vault to the station computer. The cable carries power to the vault and the signal from the digitizer to the computer.

Due to the northerly latitude of Iceland, the winter days (especially December and January) are too short for solar panels to generate enough power, making a windmill a necessary part of the station installation. The wind mill is usually located 10-20 m from the vault to decrease its effect on the seismic signal. A typical setup is shown on Figure 2.1.4.

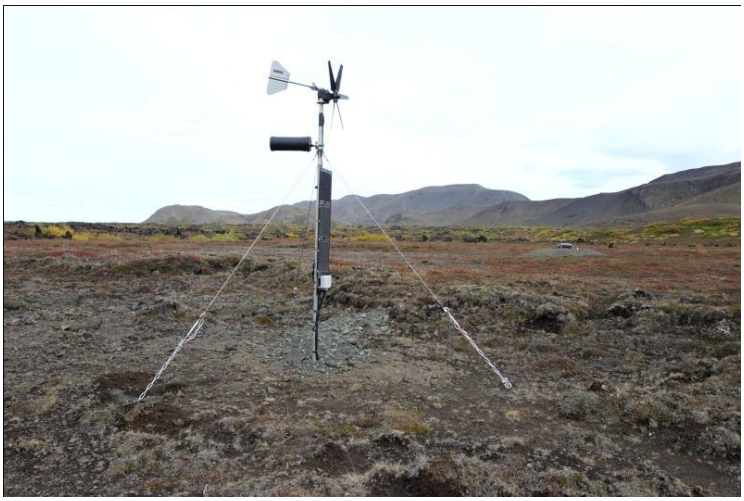

***Figure 2.1.4.*** *Typical setup of power generation at a seismic station. The windmill is on a few-m-high mast, which is anchored to the bedrock. The solar panels and transmission antenna are mounted on the mast. The battery is inside the seismic vault, which is seen in the background to the right. The solar panels are vertically mounted and facing south, to decrease snow accumulation and icing during winter.*

In remote mountaineous sites, where there is little or no soil a much smaller vault sits on top of the rock outcrop, and is anchored to the rock. In these locations the power for data acquisition and transmission to the nearest farm or town is generated on site by a wind mill, backed up by solar panels (vertically mounted) and batteries. An example of a mountaineus site, ***god*** at the edge og a glacier is shown in Figure 2.1.5.

***Figure 2.1.5.*** *Picture shows the small seismic vault (with a green lid) at station* ***god*** *at 1200 m elevation at the edge of a glacier. The digitizer and electronics are inside the red drum and GPS antenna and wind mill are seen in the background.*

## 2.1.2 GPS network

### *2.1.2.1 Network and hardware*

The first 4 stations of the Icelandic continuous GPS network were installed in the western part of the SISZ in 1999 (Geirsson et al. , 2006). Since then the network has expanced to cover much of Iceland and as of 2012, the GPS network is owned by many institutions: IMO, IES, the National Land Survey of Iceland, the power company Landsvirkjun, University of Savoie, King Abdullah University of Science and Technology, University of Arizona, Pennsylvania State University and IGS. IMO maintains and downloads data from around 70 stations, but only 14 stations are actually owned by IMO. The 12 IMO stations located in and around the SISZ will be networked in the NERA project. Access to data from other GPS stations, including 3 IES stations within the SISZ is through the relevant owner. Additional data may be acessible through other avenues: Data from the University of Arizona stations is available through UNAVCO and data from IGS stations are also openly available. Location of the 12 ISGPS stations contributing to the observatory as well as other stations are shown in Figure 2.1.1 and listed in Table 2.1.3.

***Table 2.1.3.*** *List of GPS stations contributing data to the SISZ near-fault observatory*

| Station name | Latitude °N | Longitude °E | Elevation m |
|---|---|---|---|
| GOLA | 63.659700839 | -19.322083918 | 1259.6467 |
| HLID | 63.921105074 | -21.389694954 | 111.0574 |
| HVER | 64.017153197 | -21.184809774 | 150.041 |
| ISAK | 64.119328479 | -19.747177587 | 319.3864 |
| KIDJ | 63.996582887 | -20.774844239 | 122.8777 |
| OLKE | 64.063126546 | -21.219892806 | 550.5941 |
| SELF | 63.928979737 | -21.032223174 | 79.9481 |
| SOHO | 63.552474681 | -19.246644082 | 857.5202 |
| STOR | 63.752670145 | -20.212084858 | 124.7944 |
| THEY | 63.561467995 | -19.643419855 | 195.2938 |
| VMEY | 63.426989303 | -20.293559884 | 135.2542 |
| VOGS | 63.852688632 | -21.703645972 | 72.9799 |

At each site, the GPS antenna is mounted on a ~1 m high stainless steel quadripod, which is bolted and cemented into stable bedrock (Table 2.1.4). To enable high accuracy replacement of the antennas, a geodetic monument is also installed. Power for the stations is provided through the national power grid when possible, but two of the stations are placed in remote areas, where a combination of wind generator and solar panels are used to provide power.
Most of the data from the networked stations are sampled at 15 sps, but the network is gradually moving to higher sample rates and presently 4 of the networked stations sample at 1 sps.

***Table 2.1.4.*** *Technical specifications of ISGPS stations in the SISZ observatory*

| Station | Receiver type and model | Antenna type | Height of antenna m | Transmission | Power | DATA | Sampling interval s |
|---|---|---|---|---|---|---|---|
| GOLA | Trimble NetRS | TRM41249.00 | 1.0340 | Radio link | Wind & solar | C | 1 |
| HLID | Trimble 4000 | TRM29659.00 | 0.9141 | ISDN | Mains | C | 15 |
| HVER | Trimble 4700 | TRM29659.00 | 0.9843 | ISDN | Mains | C | 15 |
| ISAK | Trimble 5700 | TRM29659.00 | 1.0047 | ISDN | Mains | C | 15 |
| KIDJ | Trimble NetRS | TRM29659.00 | 1.0050 | Radio link | Mains | C | 1 |
| OLKE | Trimble 4700 | TRM29659.00 | 0.9742 | GSM | Wind & solar | C | 15 |
| SELF | Trimble R7 | TRM29659.00 | 1.0108 | Radio link | Mains | C | 15 |
| SOHO | Trimble NetR9 | TRM57971.00 | 1.0121 | 3G | Mains | C | 1 |
| STOR | Trimble NetRS | ASH701945C_M | 0.9720 | ADSL | Mains | C | 1 |
| THEY | Trimble 4700 | TRM29659.00 | 1.0271 | ISDN | Mains | C | 15 |
| VMEY | Trimble 4000 | TRM29659.00 | 0.999 | Internet | Mains | C | 15 |
| VOGS | Trimble 4700 | TRM29659.00 | 0.9721 | ISDN | Mains | C | 15 |

C: Continuous data

#### *2.1.2.2 Software systems*

*Acquisition software*

The data is acquired and stored by the GPS receivers on site. Depending on communication link and sampling rate, the data is downloaded an prepared for the processing software at a 24 hour (15 s data) or one hour (1 Hz data) interval. The software used to convert the data from receiver specific format to rinex format varies depending on receiver types

(See: http://facility.unavco.org/software/download_transfer/download_transfer.html) but in all cases the final conversion to rinex format is done using the ***teqc*** software (see: http://facility.unavco.org/software/teqc/teqc.html).

*Automatic analysis software*

Data sampled at 15 sps are processed on a daily basis calculating 24-hour average coordinates. The processing is done using the GAMIT/GLOBK 10.4 software. For accurate coordinates estimation a number of IGS stations are used in the processing in order to constrain the final coordinates in an ITRF2005 reference frame. The solutions are then plotted in a time series relative to the IGS station REYK (located in Reykjavík).

*Manual analysis software*

Same as the automatic analysis software.

*Quality control processes*

Quality control is done as a part of the analyses procedures. Stations with hig RMS values and little data are automaticaly deleted from the processing. In addition, the reference stations are tested for consistency with their ITRF2005 coordinates and stations with high residuals are removed as reference stations.

*Data formats and accessible data bases*

The data is archived in rinex format and the final processed data are copied to an ftp site (http://hraun.vedur.is/ja/gps/rinex/) wich is access controlled.

#### *2.1.2.3 Station installation procedures*

The GPS stations are installed on stable bedrock. The antenna is mounted on a ~1 m high stainless steel quadripod, bolted and cemented into the rock. The antenna is covered by a raydome to protect it from the harsh environment. Directly under the antenna a geodetic monument is installed to enable high accuracy replacement of the antennas. The receivers, are generally mounted on the quadripod, but where GPS stations are co-located with seismic stations, they are located in the seismic vault.

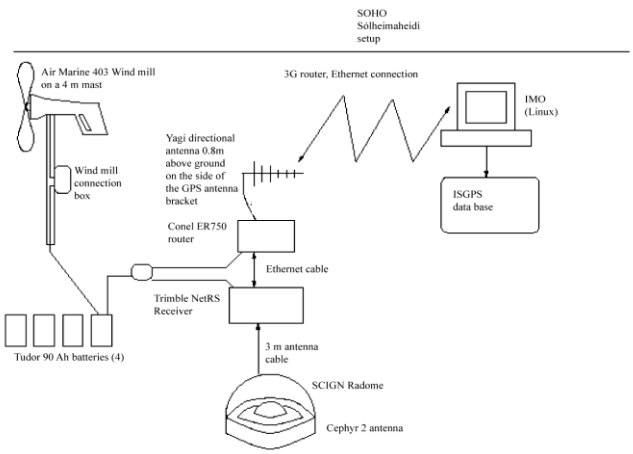


***Figure 2.1.6.*** *(left) Picture shows quadripod with GPS antenna and raydome at mountain station* ***SOHO*** *at the edge of a glacier. The receiver (inside the box) and transmission antenna are mounted on the quadripod. A wind mill is mounted on top of a 4 m high mast. The battery pack is buried at the base of the mast. (right) Schematic diagram showing setup at station* ***SOHO****.*

In remote stations, where access to power mains is not possible, the power is generated and stored on-site. These stations are equipped with solar panels and batteries. Due to the northerly latitude, however solar panels are insufficient power generators in winter. The stations, therefore also have a wind generator, mounted on a few-m-high pole. To maintain stability in strong winds, the pole is anchored with wire harnesses. An example of GPS-station setup in a remote location is shown in Figure 2.1.6 and at a site colocated with a seismic station in Figure 2.1.3.

## 2.1.3 Borehole strain meters

### *2.1.3.1 Network and hardware*

The Icelandic strain network was installed in 1979 as a collaborative venture between IMO and the Carnegie Institution of Washington, Department of Terrestrial Magnetism (CIW). IMO is responsible for the operation of the network, with operational support provided by CIW. The strainmeter network was initially intended to record crustal deformation caused by strong earthquakes in SISZ (Ágústsson, 1999), but it has proved essential for monitoring volcanic eruptions of Hekla (Linde et al., 1993; Águstsson et al., 2000). The station BUR is positioned ~14.3 km north-west from the volcano's summit. Compressive strain signals recorded at BUR tens of minutes before the February 2000 eruption of Hekla enabled a public warning to be issued before the eruption began.

When originally installed, the Iceland network comprised seven stations - three of which are operational today. The strain meters were grouted into boreholes in and around the SISZ. A new strainmeter was installed in September 2010, in a purpose-drilled borehole ~5 km south-east of the summit of Hekla; it is estimated that this station (HEK) is at least five times more sensitive to magma movements than BUR. Alongside the installation of HEK, a network-wide upgrade of strain acquisition and telemetry hardware took place between 2010 and 2011. Further expansion of the strain network is planned in coming years. The location of each functioning station is given in Table 2.1.5.

***Table 2.1.5.*** *List of strain stations contributing data to the SISZ near-fault observatory.*

| Station name | Latitude °N | Longitude °E | Elevation m | Sensor depth m |
|---|---|---|---|---|
| BUR | 64.10972 | -19.79735 | 260 | 181 |
| HEK | 63.96257 | -19.58565 | 739 | 179 |
| HEL | 63 84160 | -20.39923 | 37 | 393 |
| STO | 63.75115 | -20.21035 | 55 | 401 |

The strain meters are all Sacks-Evertson dilatometers sensitive to volumetric strain with a resolution of 0.1 nanostrain (Sacks et al., 1971).
Until 1986, continuous readings from the network were saved as analogue tracings on paper drums at each station. Subsequently multiplexed measurements from the stations were telemetered via radio to IMO, where the data were deplexed and stored on magnetic tapes. Since 1991, data have been archived at IMO on hard-drives and compact discs. The conversion to digital telemetry enabled continuous, 20-bit data-streaming from the strain network. Following upgrade work in 2011, each station records 24-bit data at 50 samples per second (sps), with auxiliary data sampled at 1 sps and 20-bit resolution (Table 2.1.6).

***Table 2.1.6.*** *Technical specifications of strain stations in the SISZ observatory*

| Station name | Strain sensor type | Recorder type | Transmission | Power | Data | Sampling rate $s^{-1}$ |
|---|---|---|---|---|---|---|
| BUR | Sacks-Evertson | SHOE-box | Radio link | Mains | C | 50 |
| HEK | Sacks-Evertson | SHOE-box | Radio link* | Wind & solar | C | 50 |
| HEL | Sacks-Evertson | SHOE-box | 3G | Mains | C | 50 |
| STO | Sacks-Evertson | SHOE-box | ADSL | Mains | C | 50 |

C: Continuous data
*: Radio link uses a repeater antenna mid-way between the station and the nearest connection to the internet.

### *2.1.3.2 Software systems*

*Acquisition software*

All functioning strain stations use a custom-built acquisition system (by Michael Acierno at CIW) for handling strainmeter functions and data processing. The software is Linux-based, operating on an ARM single-board computer. The computer runs a programme called ***dap24***, which collects data from a micro-controller. Data are held in memory buffers before being written to Flash memory at 1 second and 1 hour intervals.

*Automatic analysis software*

Strain data, sampled at 1-second intervals are downloaded automatically and displayed at IMO in near real-time for monitoring purposes. The lag-time between data collection and display at IMO is less than three minutes. All other data, including 50 sps files, are downloaded at hourly periods.

*Manual analysis software*

CIW have developed a dedicated software interface, known as ***dtscope***, for viewing strain data. This software is in daily use at IMO and it is compatible with Linux and Mac operating systems. Because of the standardised nature of the SAC file format, strain data can be read using a variety of analysis software, including SAC, PQL II, and the RSEIS package for R.

*Quality control processes*

Quality control processes have not been defined yet for the strain data recording and data base.

*Data formats and accessible data bases*

Strain data collected between 1986 and 2010 are stored at IMO at 1-second and 1-minute intervals. Since 2011, data are stored in SAC format, in 50 sps files compressed using bzip2. Strain data are presently unavailable via the web, although work is in progress to enable this.

### *2.1.3.3 Station installation procedures*

Wherever possible, disused boreholes are used to host strainmeters. Such boreholes are either drilled for geothermal prospecting (e.g. HEL and STO) or for geological assessment purposes (e.g. BUR). Consequently, most strainmeters in the Icelandic network have been designed to fit specific borehole apertures.

In the case of HEK, the station's 179-m borehole was purposedly drilled due to the remoteness of the site. The procedure was as follows: (i) An ODEX hammer drill was used to sink a welded, 6.5-inch steel casing to a depth of 166.5 m. After the base of the steel casing was cemented into place, the borehole was drilled a further 12 m using a 3-7/8-inch rotary Tricone bit. Throughout the drilling work, rock fragments were sampled at 2-m depth intervals; these samples were examined to help determine the suitability of the borehole. The base of the borehole was cemented and re-drilled several times to ensure a uniformly smooth installation surface. Down-hole calliper measurements and video-camera inspections were performed at various stages of the Tricone drilling and cementing work; this information was used to assess the integrity and smoothness of the cemented walls. A test piece having the same dimensions as the actual strainmeter was lowered to installation depth without jarring in the borehole; this was confirmed by line-tension measurements during the descent and ascent of the test piece.

All in cases, expansive grout is used for mechanical coupling between the strainmeter and the surrounding rock. Before the instrument is lowered into place, a grout mixture is prepared on the surface and then delivered to the base of the borehole using a several-metre-long bailer. This device is designed to eject the grout on contact with the base of the borehole, hence preventing dissolution or splattering of the mixture. The strainmeter is allowed to sink through the grout until the tip of the instrument is near the base of the borehole. To ensure complete immersion, additional grout is pumped via a narrow plastic pipe onto the top of the strainmeter, backfilling the borehole several metres above the instrument. The stainless steel cable used to install the strainmeter is then fixed in place using a ‘Chinese finger’ bolted to the top of the casing. The installation cable is also used to support the electrical cable, which stems from the top of the strainmeter. A thick, copper cable is attached to the top of the casing; this cable serves as a single grounding point for the strainmeter and the surface electronics. A schematic diagram of the set-up is shown in Figure 2.1.7.

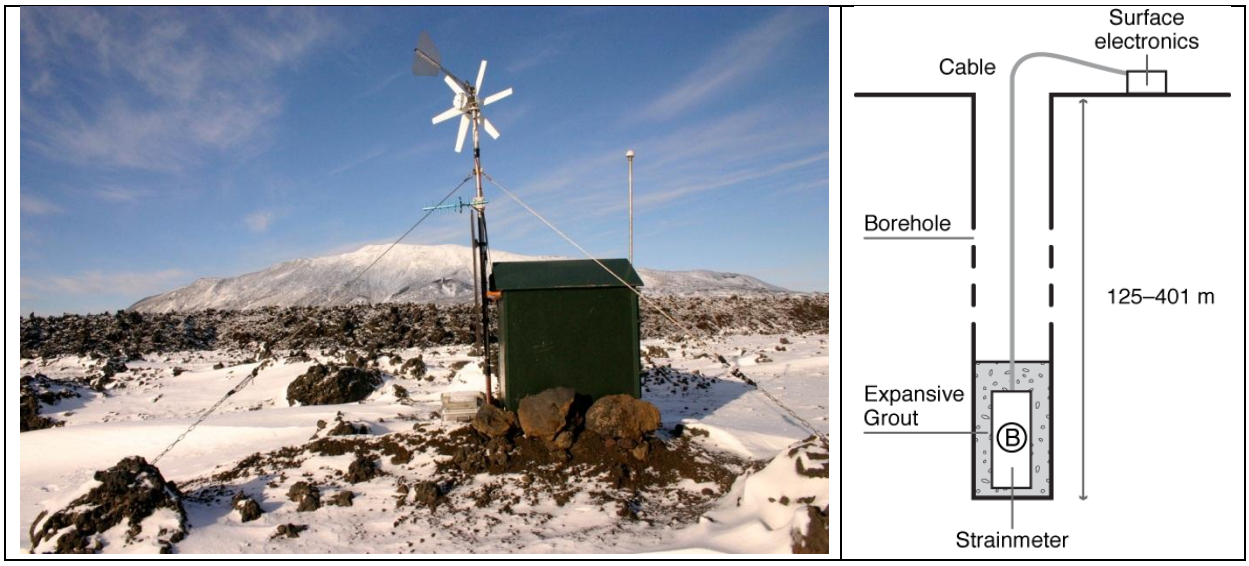


***Figure 2.1.7.*** *(left) Picture showing hut above the strain meter at station* ***HEK****, housing the SHOE box recorder and electrocnics. The wind mill, solar panels and transmission antenna are mounted on the mast and the GPS antenna is mounted on the hut. Hekla volcano is in the background. (right) Schematic diagram showing typical strainmeter installation in a borehole.*

The electrical and grounding cables from the borehole are routed to a surface enclosure located near to the borehole. The enclosure contains the SHOE-box single-board computer, components for supplying and regulating electrical power, and telemetry equipment. An example of the surface setup is shown in Figure 2.1.7.

For several weeks following the installation, a compressive signal dominates the volumetric time-series due to thermal expansion of the grout. Long-period signals, signifying stress changes in the surrounding rock, become discernible typically a few months after installation. Such signals are caused primarily by Earth and oceanic tides and variations in atmospheric pressure.

### 2.1.4 Water level guages in boreholes

Water level is automatically monitored in many boreholes in the SISZ and following the June 2000 earthquakes in the SISZ, observed water level changes were in agreement with earthquake focal mechanisms (Björnsson et al., 2001). IMO does not have ownership of these data. For information and access to data contact the Icelandic Geosurvey (www.isor.is)

### 2.1.5 Deep drilling

Tens of boreholes, a few hundred m deep, exist in the SISZ area. Most have been drilled for utilization of geothermal water for house heating. Several boreholes, 1-2 km deep have also been drilled in the Hengill region, in the western part of the SISZ supplying energy to the two geothermal power plants operated in the area (Nesjavellir and Hellisheidi). Initial plans for deep drilling (> 3 km) in the Hengill region (He in Figure 2.1.1) have been put on hold for several years, due to the financial crash in Iceland in 2008. Substantial induced seismicity has been recorded during fluid injections in the Hengill region during 2009-2012.

### 2.1.6 Future Goals and Developments of the SISZ Observatory

Future goals for the SISZ observatory include strengthening of all permanent networks and systems in operation.

For the seismic network this entails: more automation of high-precision earthquake locations and strengthening of seismic early warning processes; increased resiliency to large earthquakes by improving acces to strong motion data, partly through increased networking with the EERC; mapping of all significant active faults in the SISZ whith high-precision locations of microearthquakes; installations of seismic broad-band and borehole instruments at selected sites.

For the crustal deformation networks the focus will be on establishing a sustainable, permanent GPS network in and around the SISZ, dense enough to resolve variations in deformation in space and time, and continued build-up of the borehole strain network in particular to monitor deformation of the volcanoes flanking the SISZ.

In general emphasis will be on incresing access to multiparameter time series collected in the SISZ, e.g. access to water pressure in boreholes in the SISZ may be obtained through networking with other Icelandic institutions operating such pressure monitoring systems.

[B.G. Ófeigsson, M.J. Roberts, G. B. Gudmundsson also provided material, or reviewed the description of the SISZ observatory.]

## 2.2 Marmara Sea, The North Anatolian Fault Zone
### [39N – 42N; 26E – 32E]

### Tectonic Setting of the Marmara Region

The North Anatolian Fault Zone (NAFZ) is one of the largest plate-bounding transform faults that separate the Anatolia and Eurasian plates and extends for 1600 km between Eastern Anatolia and the Northern Aegean (USGS, 2000). The Anatolian block is moving westward with respect to the collision zone between the Eurasian and Arabian Plates, at a rate of ~25mm/yr east of the Sea of Marmara (Hegert et al., 2010). The movement continuously produces major strike-slip and also N-S extensional normal-faulting earthquakes south of the Marmara region (Bulut et al., 2009). In the North Anatolian Fault a series of large earthquakes started in 1939 near Erzincan in eastern Anatolia and propagated westward toward the Istanbul-Marmara region, located in northwestern Turkey where the 1999 Izmit earthquake occurred (Figure 2.2.1.a) (Bulut et al., 2009). Also west of the Izmit rupture a ‘‘seismic gap’’ exists along ~100 km long segment below the Sea of Marmara which connects the Ganos (1912) and Izmit (1999) ruptures (Bulut et al., 2009, Toksöz et al., 1979, Stein et al., 1997, Reilinger, et al., 2000) (see Figure 2.2.1. a). It is believed that this segment is capable of generating an earthquake with a magnitude equal to or larger than 7.4 (Hubert-Ferrari et al., 2000), or a number of smaller events with normal faulting regime (Armijo et al., 2002) or it could even rupture in a single large event (Le Pichon et al., 1999)

The 1999 Mw 7.4 Izmit and 1999 Mw 7.1 Düzce events are the two most recent major earthquakes to occur in NW Turkey, rupturing a 200 km long segment of the North Anatolian Fault Zone east of the Marmara region (Tibi et al., 2001;Barka et al., 2002; Aktar et al., 2004]. After the Izmit event, the Düzce event occurred 3 months later where the rupture in the first event extended from the Sea of Marmara to the Düzce area. The rupture length of Düzce event was 50 km long, extending to the East (Bulut et al., 2009)

It is argued that the western end of the 1999 rupture is located in the eastern Sea of Marmara below the Çınarcık Basin (Wright et al., 2001). Moreover, the rupture may have extended to south of the Princes Islands, which are located (Bouchon et al., 2002; Ozalaybey et al., 2002) within 20 km distance of the city of Istanbul with its more than 12.5 million inhabitants. On the other hand, Pinar et al. (2001) argue that the rupture did not enter the Çınarcık Basin but terminated close to Hersek, west of the Izmit Gulf (Bulut et al., 2009). At the western end of the Izmit rupture a branching of the NAFZ is observed, with streaks of similar, normal- or strike-slip faulting mechanisms along individual fault branches below the Çınarcık Basin (Orgulu and Aktar, 2001; Ozalaybey et al., 2002; Karabulut et al., 2002 Bulut et al., 2009). The estimated 30-year probability for an event of M ≥7 below the Sea of Marmara is 35– 70% (Wright et al., 2001; Parsons et al., 2000;Parsons, 2004 Bulut et al., 2009).

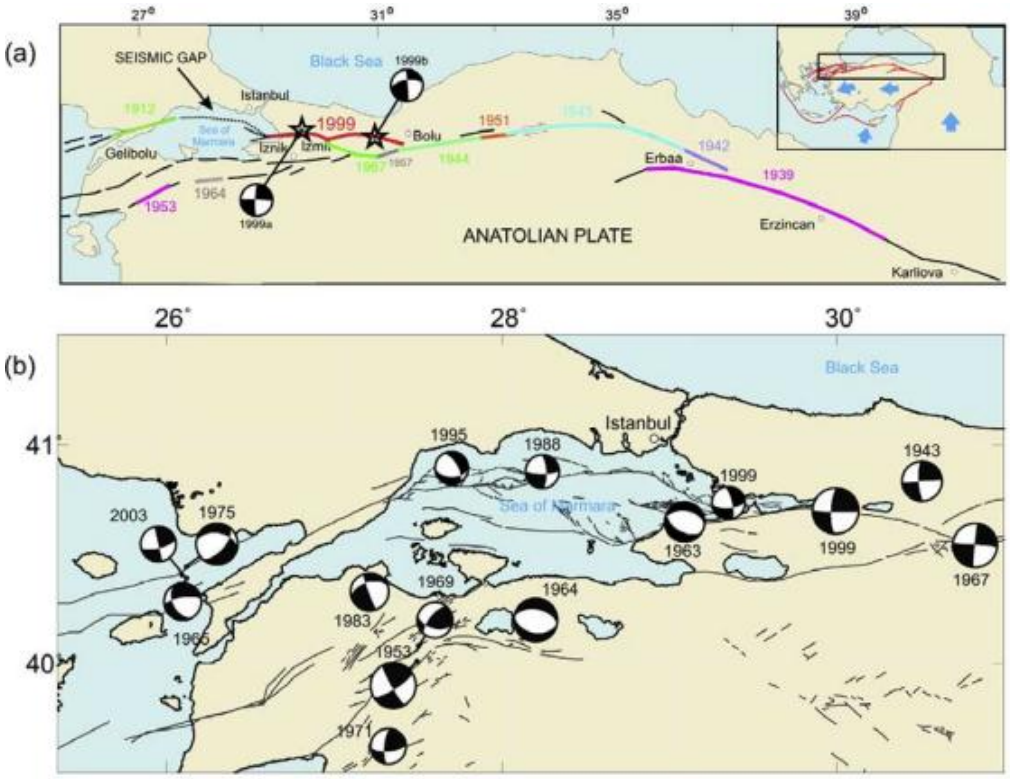


***Figure 2.2.1. (a)*** *Tectonic map of Anatolian-Aegean region (modified from U.S. Geological Survey(2000)): Westward movement of Anatolian plate causes destructive earthquakes along North Anatolian Fault Zone (black line). Rupture zones associated with destructive earthquakes are represented by different colors. In this study we focused on the westernmost part of 1999 (Izmit 17 August 1999 Mw 7.4 and Düzce 12 November 1999 Mw 7.2) rupture zone in which a destructive earthquake is expected to occur in the next decades.* ***(b)*** *Fault plane solution for M > 5.0 size earthquakes that have occurred within the vicinity of Sea of Marmara region since 1943 (compiled from Orgulu and Aktar, (2001), Pinar et al.(2003), and Şengör et al. (2005)). Fault lines are taken from Turkey General Directorate of Mineral Research and Exploration, and Armijo et al. (2005).*

## Network descriptions

### 2.2.1 Seismic and strong motion networks

#### *2.2.1.1 Network and hardware*

The Kandilli Observatory and the Earthquake Research Institute National Earthquake Monitoring Centre currently have 126 broad band and 60 strong motion stations operating nationwide (Figure 2.2.2). 39 of the broad band and 27 of the strong motion stations are in operation in order to observe the seismicity of the Sea of Marmara region (Figure 2.2.3). 6 of the 39 broad band stations were in operation as short period, but between September 2006 and May 2008 each of them was renewed with a broad band instrument. The list of broad band and strong motion stations are given in Table 2.2.1 and Table 2.2.3 respectively. Technical specifications are also listed in Table 2.2.2 and Table 2.2.4.

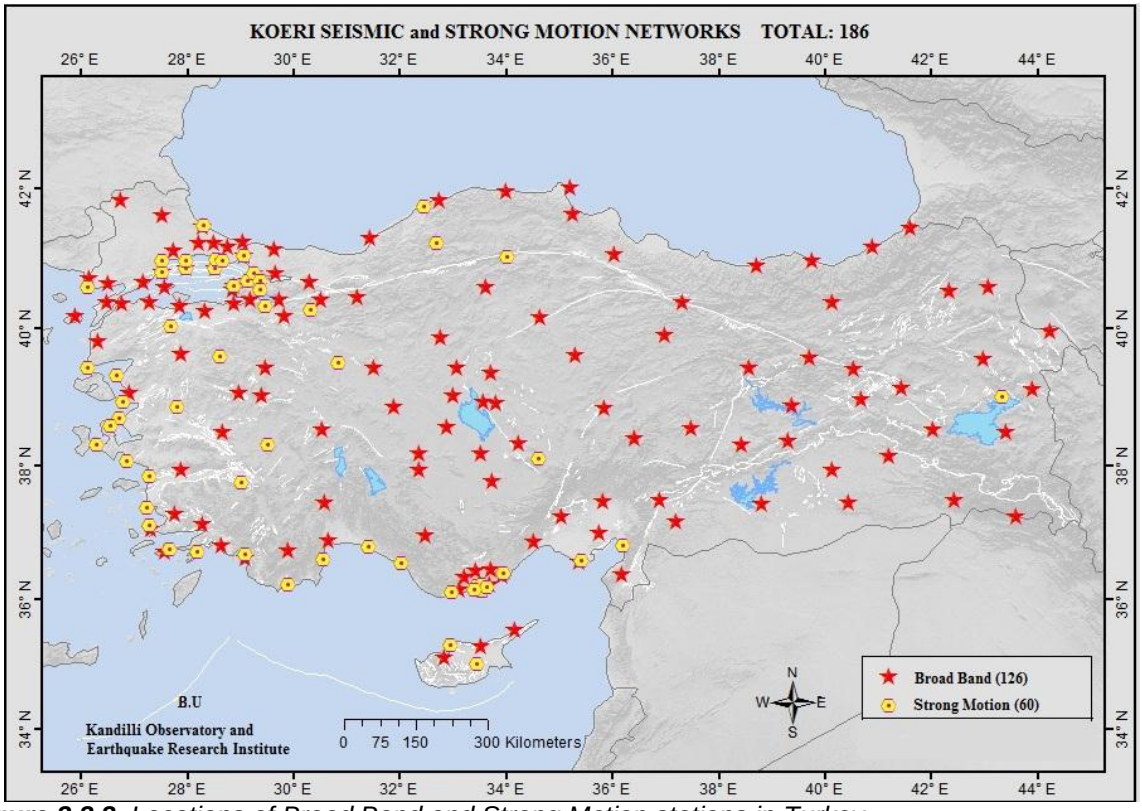


***Figure 2.2.2.*** *Locations of Broad Band and Strong Motion stations in Turkey*

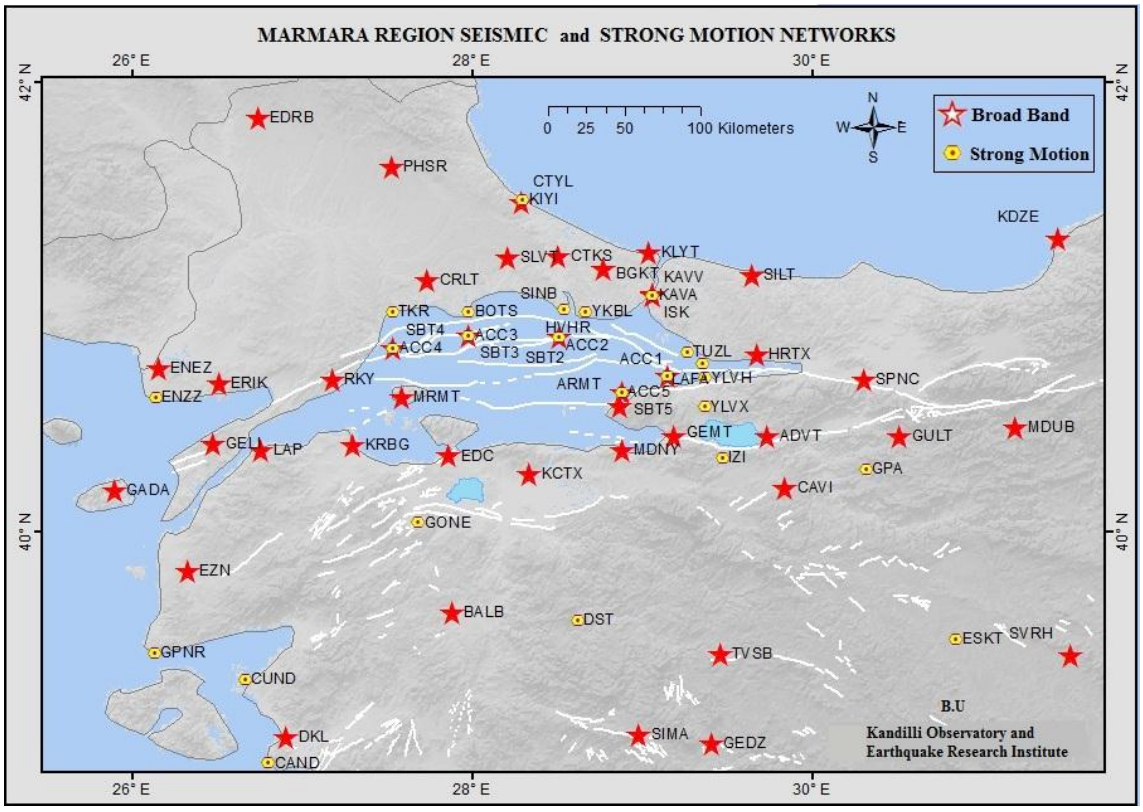


***Figure 2.2.3.*** *Locations of Broad Band and Strong Motion stations around the Sea of Marmara*

***Table 2.2.1.*** *List of near-fault observatory Broad Band stations located around The North Anatolian Fault Zone in the Marmara Sea*

| Station name | Latitude °N | Longitude °E | Elevation m | Sesnor depth m |
|---|---|---|---|---|
| ADVT | 40.4332 | 29,7383 | 193 | |
| ARMT | 40.5683 | 28,866 | 320 | |
| BALB | 39.64 | 27,88 | 120 | |
| BGKT | 41.181 | 28.773 | 80 | |
| CAVI | 40.2018 | 29.8377 | 670 | |
| CRLT | 41.129 | 27.736 | 230 | |
| CTKS | 41.2373 | 28.5072 | 47 | |
| CTYL | 41.476 | 28.2897 | 77 | |
| EDC | 40.3468 | 27.8633 | 269 | |
| EDRB | 41.847 | 26.7437 | 209 | |
| ENEZ | 40.7362 | 26.153 | 100 | |
| ERIK | 40.6708 | 26.5132 | 1500 | |
| EZN | 39.8267 | 26.3258 | 48 | |
| GADA | 40.1908 | 25.8987 | 130 | |
| GELI | 40.398 | 26.4742 | 129 | |
| GEMT | 40.435 | 29.189 | 220 | |
| GULT | 40.432 | 30.515 | 930 | |
| HRTX | 40.8217 | 29.668 | 645 | |
| ISK | 41.0657 | 29.0592 | 132 | |
| KCTX | 40.2625 | 28.3353 | 451 | |
| KDZE | 41.3132 | 31.443 | 410 | |
| KLYT | 41.253 | 29.042 | 30 | |
| KRBG | 40.3932 | 27.2977 | 75 | |
| LAP | 40.3727 | 26.7602 | 230 | |
| MDNY | 40.3708 | 28.8847 | 1000 | |
| MDUB | 40.4712 | 31.1978 | 110 | |
| MFTX | 40.7867 | 27.2812 | 924 | |
| MRMT | 40.6058 | 27.5837 | 702 | |
| PHSR | 41.6308 | 27.5238 | 263 | |
| SBT1 | 40.7056 | 29.1492 | -1260 | |
| SBT2 | 40.8786 | 28.5142 | - 810 | |
| SBT3 | 40.8848 | 27.9751 | -1204 | |
| SBT4 | 40.8282 | 27.5355 | - 1144 | |
| SBT5 | 40.6311 | 28.8804 | - 368 | |
| SILT | 41.153 | 29.643 | 100 | |
| SLVT | 41.23 | 28.21 | 180 | |
| SPNC | 40.686 | 30.3083 | 190 | |
| TKR | 40.9902 | 27.5357 | 140 | |
| YLVX | 40.5667 | 29.3728 | 829 | |

***Table 2.2.2.*** *Technical specifications of Broad Band Stations*

| Station Name | Sensor type Corner freq.$^{-1}$ | Sensor sensitivity V/m/s | Digitizer type | Digitizer gain µV/bit | Transmission | Power | Data | Sampling rate $s^{-1}$ |
|---|---|---|---|---|---|---|---|---|
| ADVT | CMG-3T | | DM24-3M | | Satellite | | C | |
| ARMT | CMG-3ESP | | DM24-3M | | Satellite | | C | |
| BALB | CMG-3T | | DM24-3M | | Satellite | | C | |
| BGKT | CMG-3ESP | | DM24-3M | | Satellite | | C | |
| CAVI | CMG-3ESP | | DM24-3M | | Satellite | | C | |
| CRLT | CMG-3ESP | | DM24-3M | | Satellite | | C | |
| CTKS | CMG-3ESP | | DM24-3M | | Satellite | | C | |
| CTYL | CMG-3T | | DM24-3M | | Satellite | | C | |
| EDC | CMG-3T | | DM24-3M | | Satellite | | C | |
| EDRB | CMG-3T | | DM24-3M | | Satellite | | C | |
| ENEZ | CMG-3T | | DM24-3M | | Satellite | | C | |
| ERIK | CMG-3ESP | | DM24-3M | | Satellite | | C | |
| EZN | CMG-3ESP | | DM24-3M | | Satellite | | C | |
| GADA | CMG-3T | | DM24-3M | | Satellite | | C | |
| GELI | CMG-3ESP | | DM24-3M | | Satellite | | C | |

| | | | | | | | | |
|---|---|---|---|---|---|---|---|---|
| GEMT | CMG-3T | | DM24-3M | | Satellite | | C | |
| GULT | CMG-3ESP | | DM24-3M | | Satellite | | C | |
| HRTX | CMG-3ESP | | DM24-3M | | Satellite | | C | |
| ISK | CMG-3T | | DM24-3M | | Network | | C | |
| KCTX | CMG-3ESP | | DM24-3M | | Satellite | | C | |
| KDZE | CMG-3T | | DM24-3M | | Satellite | | C | |
| KLYT | CMG-3T | | DM24-3M | | Satellite | | C | |
| KRBG | CMG-3ESP | | DM24-3M | | Satellite | | C | |
| LAP | CMG-3ESP | | DM24-3M | | Satellite | | C | |
| MDNY | CMG-3ESP | | DM24-3M | | Satellite | | C | |
| MDUB | CMG-3T | | DM24-3M | | Satellite | | C | |
| MFTX | CMG-40T | | HRD24-nmx | | Telemetry | | C | |
| MRMT | CMG-3T | | DM24-3M | | Satellite | | C | |
| PHSR | CMG-40T | | DM24-3M | | Satellite | | C | |
| SBT1 | CMG-3T | | DM24-3M | | Fiber +Satellite | | C | |
| SBT2 | CMG-3T | | DM24-3M | | Fiber +Satellite | | C | |
| SBT3 | CMG-3T | | DM24-3M | | Fiber +Satellite | | C | |
| SBT4 | CMG-3T | | DM24-3M | | Fiber +Satellite | | C | |
| SBT5 | CMG-3T | | DM24-3M | | Fiber +Satellite | | C | |
| SILT | CMG-3ESP | | DM24-3M | | Satellite | | C | |
| SLVT | CMG-3ESP | | DM24-3M | | Satellite | | C | |
| SPNC | CMG-3ESP | | DM24-3M | | Satellite | | C | |
| TKR | CMG-3ESP | | DM24-3M | | Satellite | | C | |
| YLVX | CMG-40T | | HRD24 nmx | | Telemetry | | C | |

***Table 2.2.3.*** *List of near-fault observatory Strong Motion stations located around The North Anatolian Fault Zone in the Marmara Sea*

| Station name | Latitude °N | Longitude °E | Elevation m | Sensor depth m |
|---|---|---|---|---|
| ACC1 | 40.7042 | 29.1517 | 1260 | |
| ACC2 | 40.8783 | 28.5133 | 810 | |
| ACC3 | 40.8850 | 27.9783 | 1204 | |
| ACC4 | 40.8283 | 27.5350 | 1144 | |
| ACC5 | 40.6311 | 28.8804 | 368 | |
| BOTS | 40.9902 | 27.9810 | 30 | |
| CAND | 38.9542 | 26.8031 | 157 | |
| CUND | 39.3360 | 26.6663 | 10 | |
| DST | 39.6041 | 28.6267 | 693 | |
| ENZZ | 40.6070 | 26.1406 | 11 | |
| ESK | 39.5212 | 30.8492 | 1295 | |
| GOKC | 40.1997 | 25.9183 | 118 | |
| GONE | 40.0466 | 27.6860 | 143 | |
| GPA | 40.2850 | 30.3167 | 570 | |
| GPNR | 39.4552 | 26.1329 | 55 | |
| HVHR | 40.9908 | 28.6678 | 22 | |
| IZI | 40.3368 | 29.4728 | 910 | |
| KAVA | 41.0628 | 29.0608 | 138 | |
| KIYI | 41.4844 | 28.3000 | 23 | |
| LAFA | 40.7598 | 29.3554 | 38 | |
| ORLT | 40.0452 | 28.8914 | 650 | |
| SINB | 40.9998 | 28.5392 | 59 | |
| TKR | 40.9902 | 27.5357 | 140 | |
| TUZL | 40.8128 | 29.2657 | 12 | |
| YKBL | 40.9908 | 28.6678 | 139 | |
| YLVH | 40.6953 | 29.3703 | 0 | |
| YLVX | 40.5658 | 29.3708 | 879 | |

***Table 2.2.4.*** *Technical specifications of Strong Motion Stations*

| Station name | Sensor type . | Sensor sensitivity V/m/s$^2$ | Digitizer type | Digitizer gain µV/bit | Transmission | Power | Data | Sampling rate s$^{-1}$ | Software |
|---|---|---|---|---|---|---|---|---|---|
| ACC1 | 5T | | DM24 | | Fiber- Satellite | | | | Scream |
| ACC2 | 5T | | DM24 | | Fiber- Satellite | | | | Scream |
| ACC3 | 5T | | DM24 | | Fiber- Satellite | | | | Scream |
| ACC4 | 5T | | DM24 | | Fiber- Satellite | | | | Scream |
| ACC5 | 5T | | DM24 | | Fiber- Satellite | | | | Scream |
| BOTS | 5T | | DM24 | | Satellite | | | | Scream |
| CAND | 5TD | | CD24 | | Turkcell 3G | | | | Scream |
| CUND | 5TD | | CD24 | | Turkcell 3G | | | | Scream |
| DST | 5TD | | CD24 | | GSM-GPRS | | | | Scream |
| ENZZ | 5TD | | CD24 | | Turkcell 3G | | | | Scream |
| ESK | 5TD | | CD24 | | GSM-GPRS | | | | Scream |
| GOKC | 5TD | | DM24 | | Turkcell 3G | | | | Scream |
| GONE | 5TD | | CD24 | | Satellite | | | | Scream |
| GPA | 5TD | | CD24 | | GSM-GPRS | | | | Scream |
| GPNR | 5TD | | CD24 | | Turkcell 3G | | | | Scream |
| HVHR | 5T | | DM24 | | Satellite | | | | Scream |
| IZI | 5TD | | CD24 | | Satellite | | | | Scream |
| KAVA | 5TD | | CD24 | | Network | | | | Scream |
| KIYI | 5TD | | CD24 | | Turkcell 3G | | | | Scream |
| LAFA | 5T | | DM24 | | Satellite | | | | Scream |
| ORLT | 5TD | | CD24 | | GSM-GPRS | | | | Scream |
| SINB | 5T | | DM24 | | Satellite | | | | Scream |
| TKR | 5TD | | CD24 | | Satellite | | | | Scream |
| TUZL | 5T | | DM24 | | Satellite | | | | Scream |
| YKBL | 5T | | DM24 | | Satellite | | | | Scream |
| YLVH | 5T | | DM24 | | Satellite | | | | Scream |
| YLVX | 3T | | DM24 | | GSM-GPRS | | | | Scream |

### *2.2.1.2 Station installation procedures*

The capacity of a seismic network is directly related to the signal and noise characteristics of the site. If the noise level at the site is too high, the seismic signal will be lost, also local soil conditions may affect the real signal negatively. In order to avoid these effects, the site selection process is carefully carried out mostly in rural areas and on bedrock.
An example of a standard site installation process is shown below. This broad band station was in operation over a short time, but after May 2008 the equipment were replaced by the newer ones.

***Figure 2.2.4.*** *Mudurnu (MDUB) Broad Band Station*

***Figure 2.2.5.*** *Infrastructure Work*

***Figure 2.2.6****. Installation of a* satellite communication antenna *(upper)* and GPS antenna *for time synchronization* (lower).

***Figure 2.2.7.*** *Installation of batteries and other equipment inside the building (upper) and thermal insulation after sonsor mounting (lower).*

***Figure 2.2.8.*** *Grounding process to protect the system from lightning*

### 2.2.2 Strong Motion Network in the Framework of Istanbul Early Warning and Rapid Response System

The 17 August 1999 Mw7.4 Kocaeli earthquake and the 12 November 1999 Mw 7.2 Düzce earthquakes caused 18.373 accounted deaths, 48.901 injuries, 16.400 heavily damaged and collapsed buildings, and 600.000 homeless people (Erdik, 2000). After these damaging earthquakes, and by taking into account the vital importance of Earthquake Early Warning Systems, Bogazici University Kandilli Observatory and Earthquake Research Institute prepared the project of **Istanbul Earthquake Rapid Response and Early Warning System**. (http://www.koeri.boun.edu.tr/depremmuh/eski/EWRR/EWEngWeb/TurAnaSayfa_eng1.htm)

#### *2.2.2.1 Network and hardware*

The list of strong motion stations and some of their technical specifications are given under chapter 2.2.1.1 above, in Table 2.2.3 and Table 2.2.4 and shown in Figure 2.2.3.

***Istanbul Earthquake Rapid Response System (IERRS)***

Modern technological developments allow measurements of strong ground shaking in near real time for urban areas exposed to earthquake risk. ShakeMaps which show the distribution of strong ground motion, building damage and casualties are prepared within a few minutes after an earthquake. In order to reduce casualties after an earthquake, the location and severity of damages can be rapidly assessed by the information from a Rapid Response Sytems. For this purpose, a dense strong motion network of **one hundred strong motion accelerometers** was established in populated areas of Istanbul, within an area of ~ 50x30 km. After being triggered by an earthquake, each station processes the streaming strong motion to yield the spectral accelerations at specific periods and sends the calculated parameters in the form of SMS messages to the main center in KOERI through ARIA GSM network service. After gathering information from stations, a shake map and damage distribution is automatically generated. In order to transmit the Rapid Response information to İstanbul Governorate, First Army Headquarters and Istanbul Municipality, digital radio modem and GPRS communication systems are used. Figure below shows the location of Rapid Response stations.

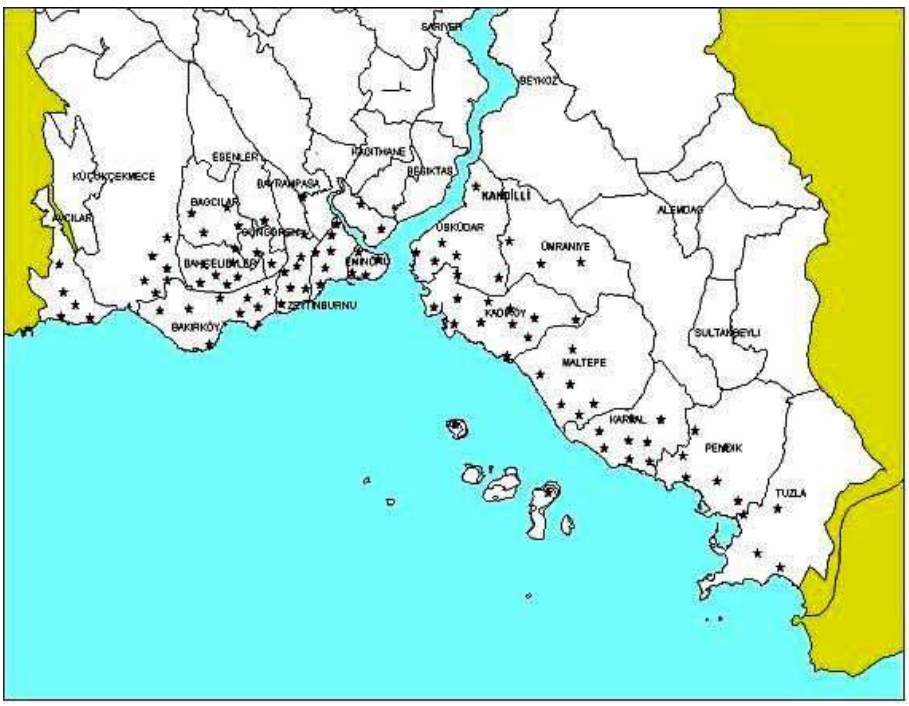


***Figure 2.2.9.*** *The locations of Rapid Response Stations*

### *Istanbul Earthquake Early Warning System (IEEWS)*

To enable Earthquake Early Warning, **ten strong motion stations**, with 24 bit resolution and on-line data transmission mode, are placed at locations as close as possible to the Great Marmara Fault zone. Continuous telemetry of data between these stations and the main data center is realized with digital spread spectrum radio modem system, involving repeater stations selected in the region.

Considering the complexity of fault rupture and the short fault distances involved, a simple and robust Early Warning algorithm is implemented, based on exceedance of a specified amplitude-level threshold in the time domain. The band-pass filtered accelerations and the cumulative absolute velocity (CAV-time integral of the absolute acceleration) are compared with specified threshold levels. When any acceleration or CAV (on any channel) at a given station exceeds specific selectable threshold values it is considered a vote. Whenever we have 2 or 3 (selectable) station votes within selectable time interval after the first vote, the first alarm is declared. The early warning information (consisting of three alarm levels) will be communicated to the appropriate servo shut-down systems of the recipient facilities, which will automatically decide proper action, based on the alarm level. Depending on the location of the earthquake (initiation of fault rupture) and the recipient facility the alarm time can be as high as about 8s.

The early warning signals will be transmitted to the end uses by employing several communication companies as “service providers”. The encrypted early warning signals (earthquake alarm) will be communicated to the respective end users by FM, UHF and satellite communication systems.


***Figure 2.2.10.*** *The locations of Early Warning Stations*

### *Technical Specifications of Instruments in the IEERS and IEEWS*

The system is designed by Kandilli Observatory and Earthquake Institute of Bogazici University and construction of the system is carried out by the GeoSig Inc. (http://www.geosig.com) and the Electrowatt-Ekono (www.ewe.ch) consortium. Rapid Response data communication is provided by ARIA GSM (http://www.aria.com.tr) service provider.

All of the Rapid Response (Dial-up), Early Warning (On-line) and Structural Monitoring (Off-line) stations use essentially the same instrumentation package.

- Sensor (Transducer)
- Digitizer/Recorder
- Communication Module
- Timing Module (GPS)
- Power Supply

*Sensor*
External, tri-axial (three orthogonal axis), force-balance (servo) type accelerometer
Range: +/- 2 g full scale (optionally adjustable)
Dynamic Range (Minimum): 108 dB (Dial-up and off-line), 144 dB (On-line)
Frequency Range: Flat between 0 and 50Hz (minimum)
Damping: Between 0.6-0.7 (Critical)
Linearity: 1% (minimum)
Cross axis sensitivity: 3dB-RMS (minimum)


***Figure 2.2.11.*** *Guralp CMG5T transducer*

*Digitizer/Recorder*
Sampling: Selectable up to 200 (minimum) sps/channel with anti-alias filtering.
Resolution (minimum): 18 bit (Dial-up and off-line), 24 bit (On-line).
Pre-event memory: 30s (minimum) selectable, at maximum sampling rate.
Post-event memory: 60s (minimum) selectable, at maximum sampling rate.
Recording Media: Memory Card with (minimum) 60 minute recording time at maximum sampling rate.
Triggering: Threshold and LTA/STA (optional).
Parametric Information: Instrumental Parameters, Peak Ground Acceleration, Event Duration, Spectral Acceleration (optional), Spectral Intensity (optional).

*Communication Module*
RS-232 based remote interrogation
For On-line stations: Spread Spectrum digital radio modem.
For Dial-up stations: GSM Modem (Data link and SMS) using Siemens M20 compatible specifications.

*Timing Module (GPS)*
Standard internal clock.
Integrated GPS timing to provide UTC time, clock correction and position (for all units).
12 Channel reception with 5 microsecond (minimum) resolution.
Separation with the station (if needed): 70m (minimum).

*Power Supply*
External charger voltage: 220 (+/- 20%).
Solar Panels for 4 (four) of the On-line stations.
12V internal battery that can provide (minimum) 72 Hour autonomy.
Provision for connection of 12 V external car battery.

The location of equipment installed in the main room of the Main Data Center is shown in the diagram below.

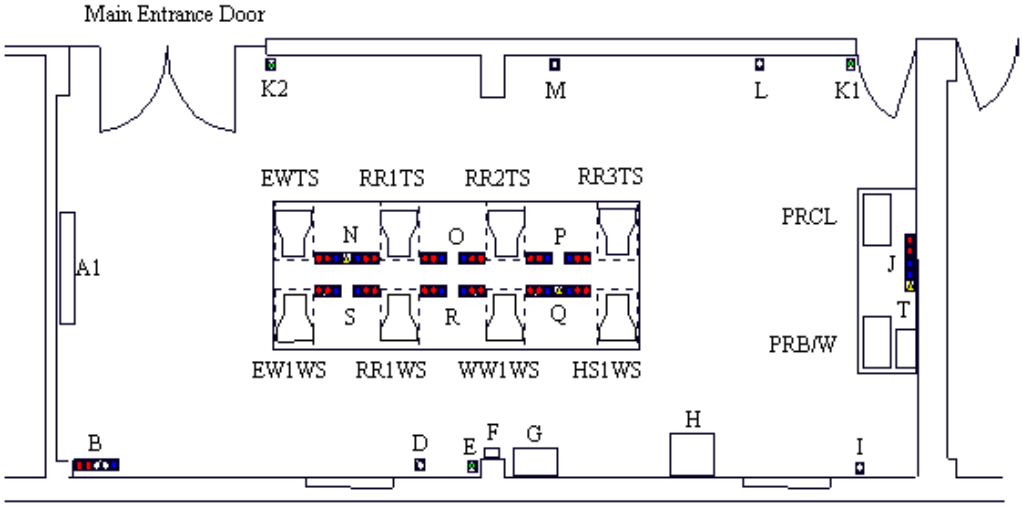


| Code | Item |
|---|---|
| A1 | Air conditioner |
| B | 2 AC-UPS outlets, 2 AC outlets, 1 Network outlets |
| D | 1 AC outlet |
| E | Emergency light switch |
| F | SMS notification module |
| G | GSM Rack |
| H | Network Rack |
| I | 1 AC outlet |
| J | 2 AC-UPS outlets, 2 Network outlets, 1 phone outlet |
| K1 | Centre light switch |
| K2 | Centre light switch |
| L | 1 AC outlet |
| M | 1 AC outlet |
| N | 4 AC-UPS outlets, 2 Network outlets, 1 Phone outlet |
| O | 4 AC-UPS outlets, 2 Network outlets |
| P | 4 AC-UPS outlets , 2 Network outlets |
| Q | 4 AC-UPS outlets, 2 Network outlets, 1 Phone outlet |
| R | 4 AC-UPS outlets, 2 Network outlets |
| S | 4 AC-UPS outlets, 2 Network outlets |
| T | Network print server |
| EWTS | Early Warning terminal server |
| RR1TS | Rapid Response terminal server 1 |
| RR2TS | Rapid Response terminal server 2 |
| RR3TS | Rapid Response terminal server 3 (spare) |
| EW1WS | Early Warning workstation (EWTS spare) |
| RR1WS | Early Warning workstation |
| WW1WS | Web server |
| HS1WS | Hot spare |
| PRB/W | Printer black and white |
| PRCL | Printer color |

***Figure 2.2.12.*** *The diagram of the locations of equipment in the main room of the Main Data center.*

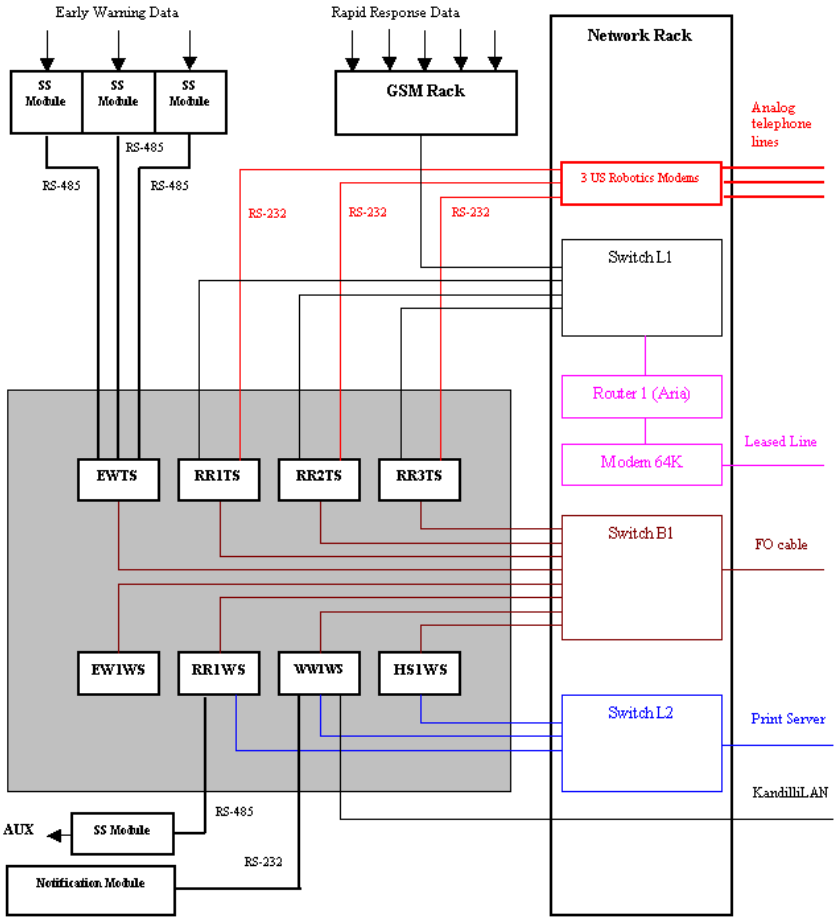


***Figure 2.2.13.*** *The diagram showing all computers in the Data Center, main modules and interconnection between them.*

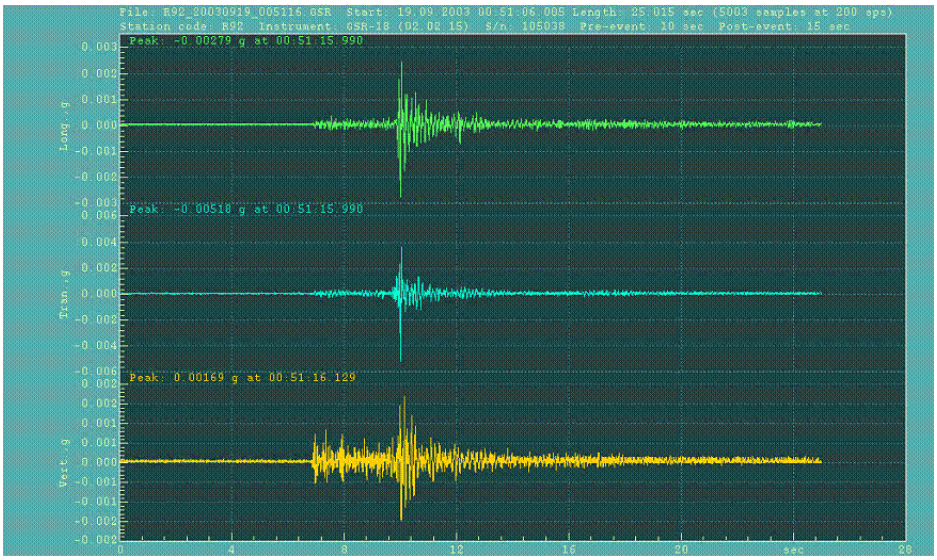


***Figure 2.2.14.*** *Record of UDAIO station on 19 September 2003, 00:51(GMT), Magnitude 3.1, Guzelyalı Istanbul Earthquake.*

#### *2.2.2.2 Software systems*

The general description of analysis and processing systems is given in chapter 2.2.2.1 above, under subheadings: *Istanbul Earthquake and Rapid Response System* and *Istanbul Earthquake Early Warning System*.

### 2.2.3 Ocean bottom sensors

#### *2.2.3.1 Network and hardware*

The Marmara Sea Ocean Bottom Observatory project has two main components: Land and Ocean Bottom Networks. The primary goal of this project is to fill the seismic network gap in the Sea of Marmara and combine the stations with the land networks. The following goals of the project are listed below (KOERI-NEMC., 2010).

- Encompass the Southern part of Marmara Sea with broad band stations.
- Make automatic solutions.
- Reach the capacity to issue a warning of a possible forthcoming earthquake and tsunami.
- Determine the physical properties of the seismic source.
- Provide observations of the post and ongoing rupture process synchronously.
- Determine the crustal properties and velocity model of the Marmara region more robustly and provide high quality and reliable data.
- Reach the capacity to determine the epicenter and the magnitude of earthquakes more robustly.
- Detect earthquakes with magnitude M<1.0.
- Observe heat, pressure and sea bottom flow in the Sea of Marmara.
- Determine the tectonics and active faults of the region more robustly.
- Issue rapid and reliable information to the public.
- Install state-of-the-art technology digital sensors a all 10 broad band stations around the sea of Marmara.
- Collect real time data and send information to KOERI with satellite system in real-time.

*LAND STATIONS*

The list and technical specifications of 10 broad band stations which are installed around the sea of Marmara are shown in the previous 2.2.1. section. Figure 2.2.17 shows the locations of these stations separately (KOERI-NEMC., 2010).

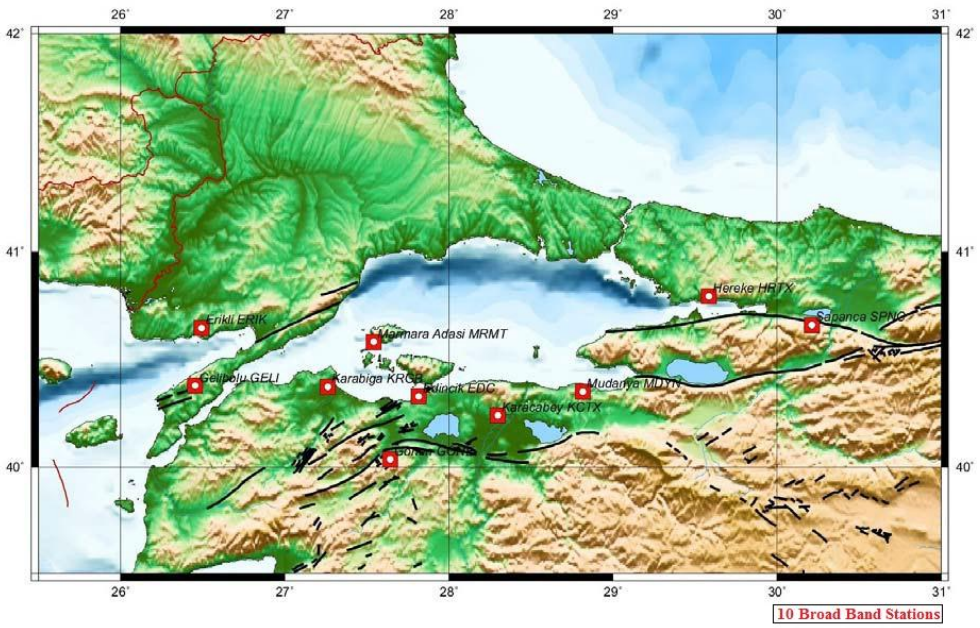


***Figure 2.2.15.*** *The location of 10 Broad Band Land Stations which are installed with the support of Turk Telekom.*

***Figure 2.2.16.*** *An example of a Land Station with satellite system*

*OCEAN BOTTOM STATIONS*

- Cable connected Marmara Sea Ocean Bottom Observatories are the most unique ones in the world, and bring a new dimensions to the studies of seismology and tsunami.
- Real-time data acquisition from OBS to land stations is carried out by fiber optic cables laid in the sea bottom.
- The land stations, equipped with satellite systems, transmit real-time data to KOERI-NEMC (Kandilli Observatory and Earthquake Research Institute National Earthquake Monitoring Centre)

***Table 2.2.5.*** *List of near-fault observatory OBS located around The NAFZ in the Marmara Sea.*

| Station name | Latitude °N | Longitude °E | Elevation m |
|---|---|---|---|
| SBT1 | 40.7042 | 29.1517 | 1260 |
| SBT2 | 40.8783 | 28.5133 | 810 |
| SBT3 | 40.8850 | 27.9783 | 1204 |
| SBT4 | 40.8283 | 27.5350 | 1144 |
| SBT5 | 40.6311 | 28.8804 | 368 |

***Table 2.2.6.*** *Technical specifications of OBS*

| Station code | Sensor type, corner freq.$^{-1}$ | Resolution bit | Sampling rate s$^{-1}$ | Digitizer type | Transmission | Software |
|---|---|---|---|---|---|---|
| SBT1 | 3T | 24 | 1000 | DM24 | Satellite | Scream |
| SBT2 | 3T | 24 | 1000 | DM24 | Satellite | Scream |
| SBT3 | 3T | 24 | 1000 | DM24 | Satellite | Scream |
| SBT4 | 3T | 24 | 1000 | DM24 | Satellite | Scream |
| SBT5 | 3T | 24 | 1000 | DM24 | Satellite | Scream |

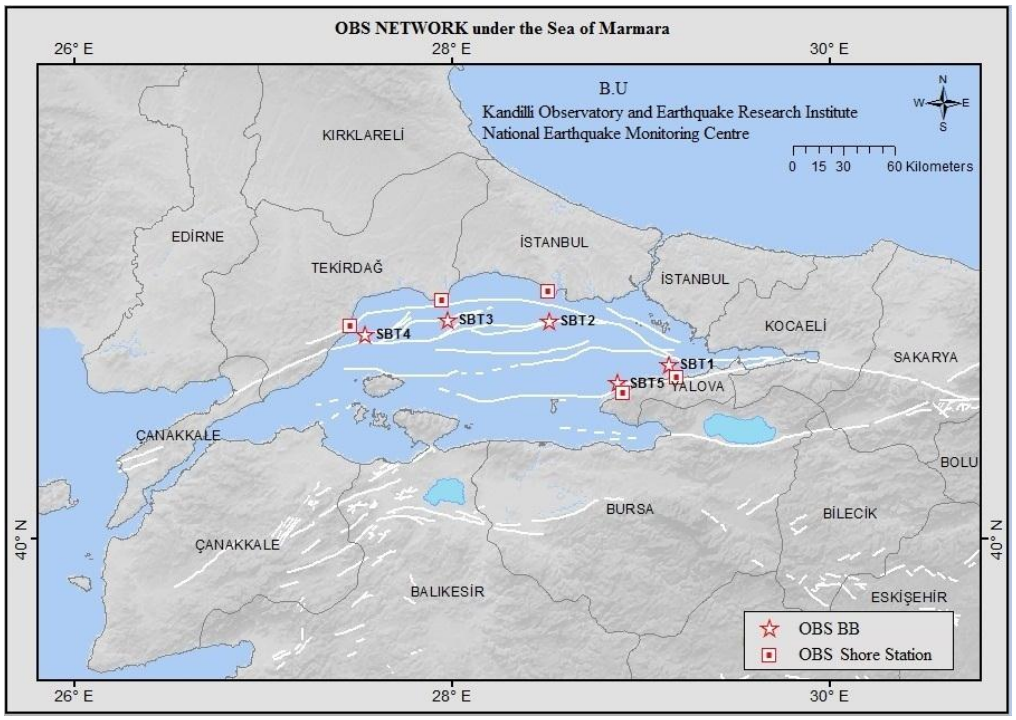


***Figure 2.2.17.*** *Map showing the locations of OBS and OBS shore stations*

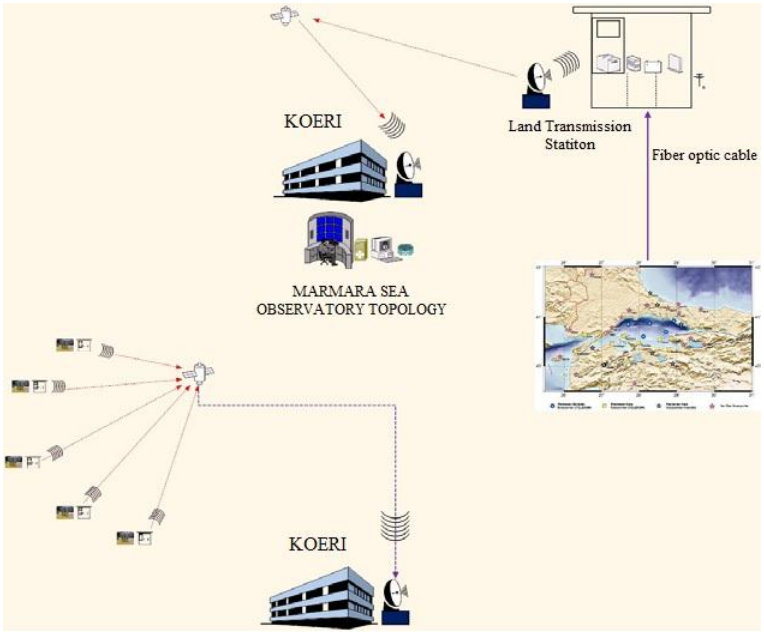


***Figure 2.2.18.*** *Simple graphic of the operation principle of Marmara Sea Observatories*

### *2.2.3.2 Software systems*

A description of some of the general aims of the OBS system is given in chapter 2.2.3.1 above.

### *2.2.3.3 Station installation procedure*

The stations are up to 20km from the coastline at depths of up to 1,300m. The seismometer component is based on Guralp Systems Ltd's industry-leading CMG-3T weak-motion very-broadband force-feedback instruments. Three uniaxial sensor components are each mounted in separate gimbals, with individual levelling control systems. The accelerometer component is based on the CMG-5T compact, high dynamic range, strong motion instrument and also uses a true-orthogonal force-feedback system. In addition to these sensors, each instrument is equipped with a hydrophone, a differential pressure gauge, a precision thermometer, a flux-gate magnetometer, a camera and an inclinometer, effectively providing a complete, sub-sea, multi-disciplinary observatory (URL 2).

The following pictures show the installation process of SBT5 OBS station step by step.(KOERI).

***Figure 2.2.19.*** *The general outlook of Ocean Bottom Observatory system*

***Figure 2.2.20.*** *The main components of the system (current and pressure meter) and protection container*


***Figure 2.2.21.*** *The Fiber optic link connecter of the system and lopping system*


***Figure 2.2.22.*** *Launching the system into the sea*


***Figure 2.2.23.*** *Cable laying operation*


***Figure 2.2.24.*** *The landing stage of the cable and laying operation*

***Figure 2.2.25.*** *Stringing out the cable to the Shore Transmission station*

***Figure 2.2.26.*** *Steel plate equipment*

***Figure 2.2.27.*** *The process of burying the fiber optic cable*

***Figure 2.2.28.*** *Transportation of the fiber optic cable protection equipments*

***Figure 2.2.29.*** *Inner view of the OBS Shore station*

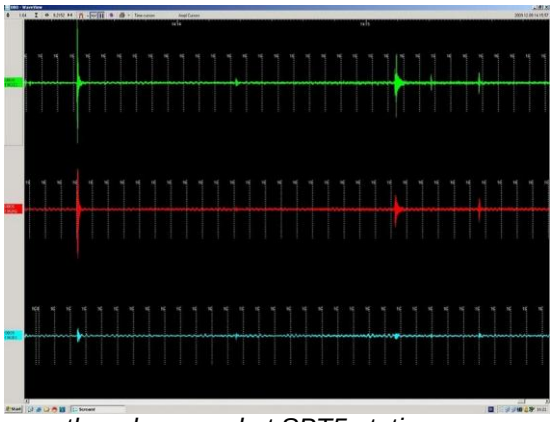

***Figure 2.2.30.*** *The first micro earthquake record at SBT5 station*

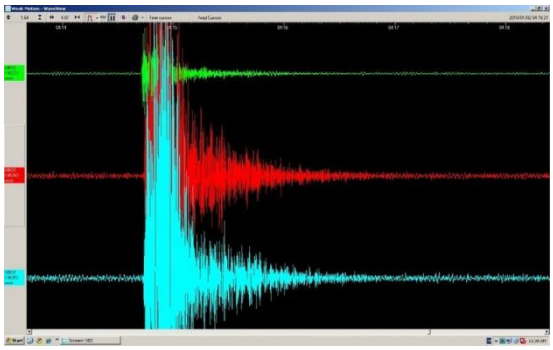

***Figure 2.2.31.*** *The record of 2 January 2010 Tuzla Offshore-Marmara Sea earthquake at SBT5 station (06:14 LT; Ml=3.0)*

## 2.2.4 GPS network

### *2.2.4.1 Network, hardware, and installation*

The Geodesy Department of KOERI started research activities in 1987. Within the scientific research projects conducted by the department over 20 years, crustal deformation monitoring, strain and seismic hazard analysis, deformation monitoring of engineering structures, Geographical Information Systems (GIS), and InSAR studies are carried out. By cooperating with national/international institutions, the department installs and runs GPS networks and performs observations periodically in order to determine crustal deformation in various regions of Turkey (Marmara, Aegean, Eastern Anatolia) where seismic hazard is very high. Fieldwork by GPS and conventional (terrestrial) geodetic techniques is carried out on a

regular basis (about 6 times a year) within the scope of national/international ongoing projects.
In 1989, three microgeodetic networks at Iznik (10 $km^2$ with 10 points), at Sapanca (30$km^2$ with 7 points), and at Akyazi (50$km^2$ with 10 points) on the North Anatolian Fault Zone (NAFZ) were established in order to monitor crustal displacements. The networks were established by by the Geodesy Department of Kandilli Observatory and Earthquake Research Institute (KOERI) of Bogazici University (Ozener, 2000)

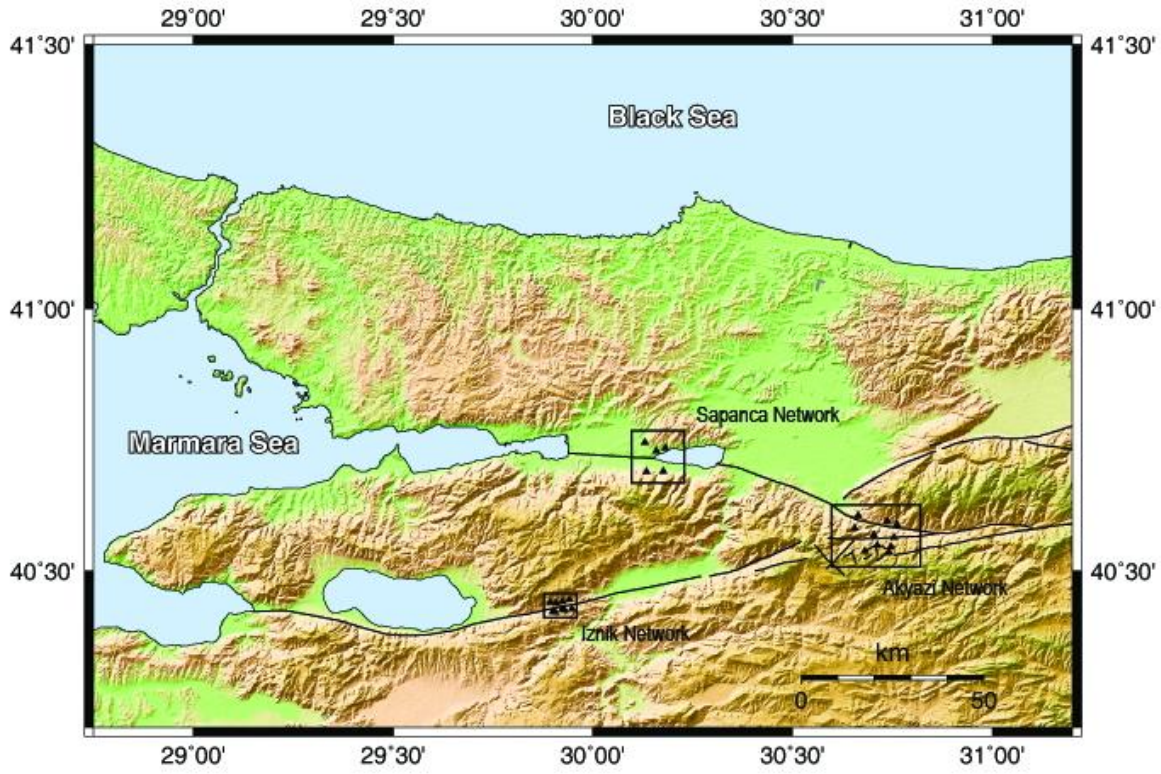


***Figure 2.2.32.*** *Three micro-geodetic network installed eastern Marmara (western NAFZ)*

Each station point of the networks is monumented on bedrock with a well designed concrete pillar by a geologist and a civil engineer. The place of the pillar is dug as deep as possible and the base concreted. The iron construction is connected to the base with iron sticks. The standard ground mark of the point consists of three levels. At the bottom; a foundation and column steel work (120cm x 120cm x 30cm), then a moulding system as a second level (50cm x 50cm x 60cm) and a pillar on the top (35 cm diameter, 120 cm height). The pillars are constructed from 400 dosage concrete. Stainless pillar heads are used on the top which are capable of carrying the instrument, the prisms and the antennas for GPS measurements. Pillars are covered using asbestos pipe in order to protect them from vandalism and bad weather conditions. To enable high accuracy replacement of the antennas, a geodetic monument is also installed. GPS antenna are secured to a stainless steel pin which is anchored within the top of the pillar (Figure 2.2.35).


***Figure 2.2.33.*** *The pillar*

Since 1994, the GPS technique has been carried out at the temporary and permanent points in the area. Campaign mode (also known as episodic or survey mode) of data collection (10-hour/day) is realized using Trimble 4000 SSI, 4000 SSE and 5700 receivers with following parameters:
*elevation mask: +10º*
*logging interval: 15.0 sec*
*minimum num of svs: 1*

In order to avoid antenna-specific systematic effects, the sites are occupied with the same antenna. The campaigns are organised yearly about the same time of the year to avoid seasonal effects. Solar panels and batteries are used to provide power.

Data from two GPS networks located in different geographical regions in Turkey (30x50km$^2$ with 15 points, Izmir-Aegean; 200x350km$^2$ with 16 points, East Anatolian) are also contributing to the KOERI data bank. These networks were also installed and have been operated in survey-mode for geodynamic pruposes. For these networks, stainless-steel monument pins on the ground are used instead of concrete pillars since they are inexpensive and have short installation time. By using a standard tripod with tribrach and optical plummet, the sites can be occupied with a wide variety of antenna mounts (Figure 2.2.36). Table 2.2.7 gives the coordinates of GPS stations established by the Geodesy Department. Figure 2.2.37 shows all the GPS points, spread over Turkey, which have been observed since 1994 by KOERI Geodesy Department.

***Figure 2.2.34.*** *Tripod with GPS antenna at mountain station KCMZ at eastern NAFZ.*

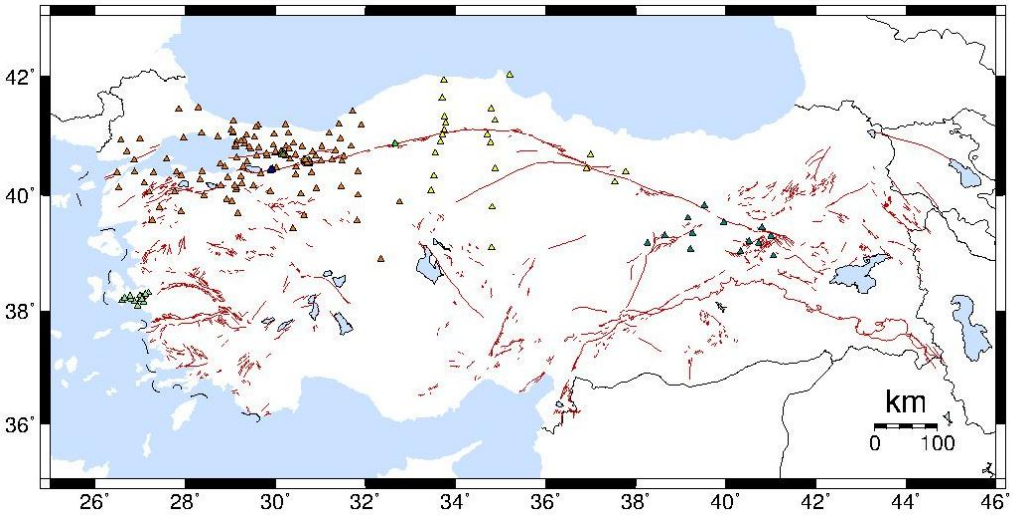


***Figure 2.2.35.*** *GPS stations observed periodically by the Geodesy Department.*

***Table 2.2.7.*** *List of GPS stations (installed by the Department) contributing data to KOERI.*

| Station ID | Latitude °N | Longitude °E | Network |
|---|---|---|---|
| IHIS | 40,445750 | 29,941666 | IZNIK_MARMARA |
| IBES | 40,441166 | 29,923472 | IZNIK_MARMARA |
| IUCK | 40,424750 | 29,928944 | IZNIK_MARMARA |
| ICER | 40,427138 | 29,947027 | IZNIK_MARMARA |
| IYUM | 40,426388 | 29,923277 | IZNIK_MARMARA |
| IGZL | 40,438027 | 29,908000 | IZNIK_MARMARA |
| IMUN | 40,421583 | 29,899111 | IZNIK_MARMARA |
| IYPN | 40,440111 | 29,893333 | IZNIK_MARMARA |
| IGAZ | 40,421555 | 29,906083 | IZNIK_MARMARA |
| SESM | 30,181272 | 40,734938 | SAPANCA_MARMARA |
| SISL | 30,130330 | 40,745338 | SAPANCA_MARMARA |
| SMAS | 30,134088 | 40,689716 | SAPANCA_MARMARA |
| SYNK | 30,176072 | 40,690800 | SAPANCA_MARMARA |
| SASK | 30,158983 | 40,730483 | SAPANCA_MARMARA |
| ABAL | 40,581966 | 30,654811 | AKYAZI_MARMARA |
| ABOZ | 40,569061 | 30,703252 | AKYAZI_MARMARA |
| ACV1 | 40,546502 | 30,746141 | AKYAZI_MARMARA |
| ACV2 | 40,535950 | 30,741366 | AKYAZI_MARMARA |
| AGOK | 40,588872 | 30,761086 | AKYAZI_MARMARA |
| AGUV | 40,563608 | 30,754038 | AKYAZI_MARMARA |
| AGUZ | 40,538344 | 30,680366 | AKYAZI_MARMARA |
| AGYK | 40,596013 | 30,736375 | AKYAZI_MARMARA |
| AKRT | 40,548716 | 30,712272 | AKYAZI_MARMARA |
| ATOP | 40,605538 | 30,663936 | AKYAZI_MARMARA |
| SOLH | 38,959000 | 41,057000 | EASTERN_TR |
| KRPR | 39,182000 | 40,733000 | EASTERN_TR |
| GENC | 38,758000 | 40,575000 | EASTERN_TR |
| ATAP | 39,215000 | 40,515000 | EASTERN_TR |
| USVT | 39,039000 | 40,330000 | EASTERN_TR |
| KLKY | 38,949000 | 40,105000 | EASTERN_TR |
| KAKO | 38,963000 | 40,052000 | EASTERN_TR |
| BLYM | 39,430000 | 40,038000 | EASTERN_TR |
| KTAS | 39,538000 | 39,957000 | EASTERN_TR |
| SRYB | 38,737000 | 39,910000 | EASTERN_TR |
| KCMZ | 39,824000 | 39,524000 | EASTERN_TR |
| KLKT | 40,151000 | 39,420000 | EASTERN_TR |
| SRTS | 39,350000 | 39,258000 | EASTERN_TR |
| HZAT | 39,074000 | 39,217000 | EASTERN_TR |
| KMAH | 39,613000 | 39,164000 | EASTERN_TR |
| CMG1 | 39,026000 | 38,931000 | EASTERN_TR |

| | | | |
|---|---|---|---|
| DBAS | 39,310000 | 38,645000 | EASTERN_TR |
| ILIC | 38,987000 | 40,673000 | EASTERN_TR |
| DIVR | 39,178000 | 38,264000 | EASTERN_TR |
| ASKE | 38,174166 | 26,866666 | IZMIR_AEGEAN |
| CTAL | 38,257222 | 27,041388 | IZMIR_AEGEAN |
| ESEN | 38,155833 | 27,083611 | IZMIR_AEGEAN |
| GEMR | 38,318888 | 27,185833 | IZMIR_AEGEAN |
| GORC | 38,295833 | 27,116666 | IZMIR_AEGEAN |
| HZUR | 38,067777 | 26,900277 | IZMIR_AEGEAN |
| KOKR | 38,183055 | 26,599444 | IZMIR_AEGEAN |
| KPLC | 38,085277 | 26,907500 | IZMIR_AEGEAN |
| PTKV | 38,209166 | 27,012500 | IZMIR_AEGEAN |
| SFRH | 38,215555 | 26,797222 | IZMIR_AEGEAN |
| TRAZ | 38,267777 | 26,781388 | IZMIR_AEGEAN |
| TURG | 38,265000 | 26,781388 | IZMIR_AEGEAN |
| URKM | 38,092500 | 26,948611 | IZMIR_AEGEAN |
| YACI | 38,229166 | 26,657777 | IZMIR_AEGEAN |
| YKOY | 38,215833 | 27,036111 | IZMIR_AEGEAN |

#### *2.2.4.2 Software and processing*

The data is acquired and stored by the GPS receivers on site. In order to check the quality of measurements Trimble Geomatics Office software is used on site for the preliminary evaluation of GPS data (URL 3). Precise ephemeris is used for post-processing. After data acquisition, the data is downloaded for the processing software. The conversion to rinex format is done using the TEQC software (URL 4).
The processing of the GPS data is performed with the GAMIT / GLOBK (Herring et al., 2010) software package using the International Terrestrial Reference Frame ITRF2005. Twelwe IGS stations are included in the process to calculate Earth Rotation Parameters more precisely and to associate the local network with the global network. Precise final orbits by the International GNSS Service (IGS) are obtained in SP3 (Standard Product 3) format from SOPAC (Scripps Orbit and Permanent Array Center). Earth Rotation Parameters (ERP) come from USNO_bull_b (United States Naval Observatory_bulletin_b). The 9-parameter Berne model is used for the effects of radiation and the pressure. The Scherneck model is used for the solid earth tide and the ocean tide loading effects. Zenith Delay unknowns are computed based on the Saastamoinen a priori standard troposphere model with 2-h intervals. Iono-free LC (L3) linear combination of L1 and L2 carrier phases is used. Loosely constrained daily solutions obtained from GAMIT are included in the ITRF2005 reference frame by a 7 parameters (3 offset–3 rotation–1 scale) transformation with 16 global IGS stations. Station velocities are obtained from trend analysis by time series which formed by daily precise coordinates combined with Kalman analysis.
Quality control is done as a part of the analyses procedures. Stations with high RMS values and little data are deleted from the processing. The data is archived in rinex format and the final processed data are copied to a server wich is access controlled.

## 2.3 The Alto tiBerina fault ObservatOry – TABOO
### [43.1- 43.6N; 12.1-12.8E]

### Tectonic setting and observatory overview

The Alto Tiberina fault (ATF) is one of the rare worldwide examples of an active low angle (NE-dipping at 15°) normal fault (LANF), [Chiaraluce et al., 2007]. This NW-trending fault is located in the Northern Apennines of Italy (Figure 2.3.1), along a sector of the chain undergoing a NE-trending extension rate of 2-3 mm/yr.

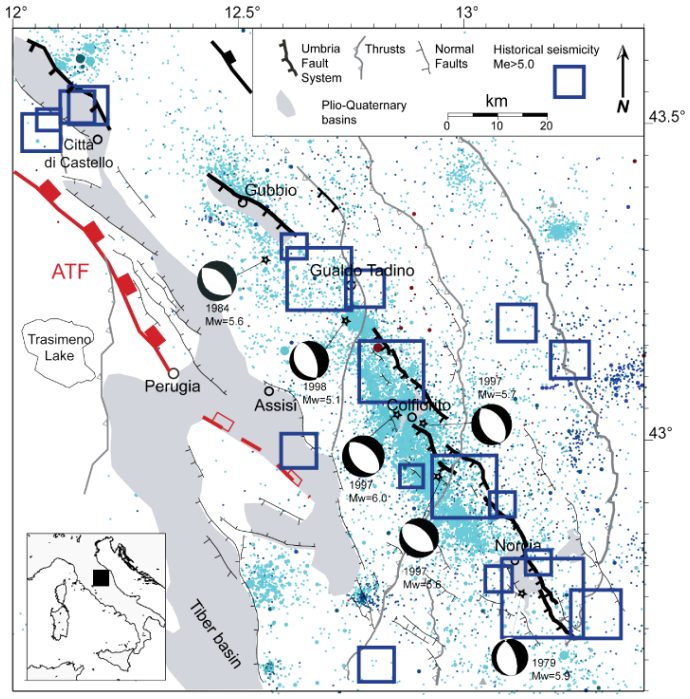


***Figure 2.3.1*** *– Map view of the study area. The seismicity (blue points) is reported together with the focal mechanisms of the largest events that have occurred in the area in the past 20 years. The (dark blue) squares are the historical earthquakes. The red line defines the Alto Tiberina fault trace projected to the surface.*

The possibility that moderate-to-large earthquakes nucleate on low-angle normal faults (LANF, i.e., normal faults dipping less than 30°), accommodating extension of continental crust, is widely debated in the published literature [Wernicke, 1995, and reference therein]. Anderson-Byerlee frictional fault mechanics [e.g., Sibson, 1985] predict no slip on normal faults dipping less than 30° in an extensional tectonic setting characterized by a vertical $\sigma_1$, if faults have a friction coefficient ($\mu_s$) ranging between 0.6 and 0.85 [Byerlee, 1978]. This should mean that mechanically it is easier to form a new fault instead of reactivating a severely misoriented low-angle structure. This hypothesis is supported by the observation that no moderate-to-large earthquake ruptures have been documented on LANF using positively discriminated focal mechanisms [Jackson and White, 1989; Collettini and Sibson, 2001]. Therefore LANF are believed to be unimportant structures in terms of seismic hazard and in the accommodation of regionally significant amounts of crustal extension.

Therefore, the *Alto Tiberina Fault Observatory* (hereinafter TABOO), actually composed of a set of seismic and GPS stations, has been built by the INGV to study the deformation processes active along this 40 km long structure that has accumulated 2 km of displacement over the past 2 Ma in a densely populated area. The availability of high resolution data, besides being a fundamental requirement to understand the physics of faulting, is a prerequisite to evaluate the seismic hazard generated by the ATF.

## Network descriptions

## 2.3.1 Seismic network, including borehole sensors.

### *2.3.1.1 Network and hardware*

The TABOO seismic network is a uniform 24-bit, set of 25 stations equipped with three component, both short period and semi-broad band seismometers (see stations location in Table 2.3.1 and technical details in Table 2.3.2). This scientific infrastructure (see Figure 2.3.2) was developed during the past four years in the framework of the AIRPLANE project, funded by both the National Institute of Geophysics and Volcanology (INGV) and the Minister of the University and Research (MIUR). The final configuration of the network was completed and complemented in 2011 with the installation of strong motion stations at 6 sites, while in the near future a set of three shallow boreholes (around 250 deep) will be instrumented with short period sensors. We point out here that the GPS stations are primarily co-located at the sites of semi-broadband stations.

***Table 2.3.1.*** *List of seismic stations contributing data to the TABOO near-fault observatory.*

| Station name | Latitude °N | Longitude °E | Elevation m | Sensor Depth m |
|---|---|---|---|---|
| ATBU | 43.47571 | 12.54828 | 1000 | 1 |
| ATCA | 43.56589 | 12.26614 | 688 | 1 |
| ATCC | 43.18514 | 12.63994 | 557 | 1 |
| ATFO | 43.36660 | 12.57150 | 960 | 1 |
| ATLO | 43.31516 | 12.40726 | 584 | 1 |
| ATMC | 43.44685 | 12.19280 | 740 | 1 |
| ATMI | 43.33419 | 12.26801 | 581 | 1 |
| ATPC | 43.48070 | 12.45700 | 810 | 1 |
| ATPI | 43.45068 | 12.40222 | 694 | 1 |
| ATTE | 43.19790 | 12.35360 | 929 | 1 |
| ATVA | 43.27860 | 12.28531 | 605 | 1 |
| ATVO | 43.38211 | 12.40663 | 638 | 1 |
| SSP9 | 43.57387 | 12.13136 | 324 | 117 |
| NARO | 43.61082 | 12.58058 | 272 | 1 |
| FRON | 43.51777 | 12.72572 | 515 | 1 |
| BADI | 43.50967 | 12.24433 | 430 | 1 |
| PIEI | 43.53567 | 12.53500 | 665 | 0 |
| SSFR | 43.43628 | 12.78225 | 750 | 1 |
| CDCA | 43.45840 | 12.23360 | 50 | 146 |
| MURB | 43.26300 | 12.52460 | 845 | 1 |
| CPGN | 43,80117 | 12,32050 | 1400 | 1 |
| MPAG | 43,62917 | 12,75950 | 930 | 1 |
| PARC | 43,64867 | 12,23867 | 580 | 1 |
| CAFI | 43,32917 | 11,96633 | 547 | 1 |
| CRE | 43,61883 | 11,95167 | 1215 | 1 |
| BAT1[1)] | 43.381567 | 12.435667 | 643 | 0 and 210 |
| BAT2[1)] | 43.370417 | 12.409367 | 691 | 0 and 210 |
| BAT3[1)] | 43.401340 | 12.410340 | 580 | 0, 50, 150, 250 |

[1)]Borehole stations with vertical sensor arrays; part of the IV net.

Today, all the stations are integrated into the INGV National Network real-time data acquisition system, providing feasibility for real-time continuous data archiving in standard formats, data dissemination for scientific purposes, strict interaction with existing procedures devoted to quality check, and instrumental parameters and meta-data collection. Of course the availability of data coming from additional stations causes a significant reduction in the threshold magnitude for earthquake detection in a large portion of the Northern Apennines, between the Marche, Umbria and Toscana regions.

***Table 2.3.2.*** *Technical specifications of stations in the TABOO observatory.*

| Station Name | SP Type Corner freq.$^{-1}$ | BB Type Corner freq. $^{-1}$ | SM Type | Sensor sensitivity V/m/s | Sensor sensitivity V/m/s$^2$ | Digitizer Type | Digitizer gain μV/bit | Transmission | Power | Data | Sampling rate $s^{-1}$ |
|---|---|---|---|---|---|---|---|---|---|---|---|
| ATBU | LE3D-5S | | | 400 | | GAIA2-FS-10-VPP | 1258290 | WIFI | Solar | C | 100 |
| ATCA | | TRILLIUM-40S | | 1553 | | GAIA2-FS-16-VPP | 786432 | Modem UMTS | AC | C | 100 |
| ATCC | LE3D-5S | | | 400 | | GAIA2-FS-10-VPP | 1258290 | WIFI | Solar | C | 100 |
| ATFO | | TRILLIUM-40S | | 1500 | | GAIA2-FS-16-VPP | 786432 | WIFI | Solar | C | 100 |
| ATLO | LE3D-5S | | | 400 | | GAIA2-FS-10-VPP | 1258290 | WIFI | Solar | C | 100 |
| ATMC | LE3D-5S | | | 400 | | GAIA2-FS-10-VPP | 1258290 | WIFI | AC | C | 100 |
| ATMI | | TRILLIUM-40S | | 1500 | | GAIA2-FS-16-VPP | 786432 | WIFI | Solar | C | 100 |
| ATPC | | TRILLIUM-40S | | 1500 | | GAIA2-FS-16-VPP | 786432 | WIFI | Solar | C | 100 |
| | | | EpiSensor FBA ES-T | | 1.0197 | GAIA2-FS-40-VPP | 314573 | WIFI | Solar | C | 200 |
| ATPI | LE3D-5S | | | 400 | | GAIA2-FS-10-VPP | 1258290 | Internet | Solar | C | 100 |
| ATTE | | TRILLIUM-40S | | 1500 | | GAIA2-FS-16-VPP | 786432 | WIFI | Solar | C | 100 |
| ATVA | LE3D-5S | | | 400 | | GAIA2-FS-10-VPP | 1258290 | WIFI | Solar | C | 100 |
| ATVO | | TRILLIUM-40S | | 1500 | | GAIA2-FS-16-VPP | 786432 | WIFI | Solar | C | 100 |
| SSP9 | LE3D-1S | | | 400 | | GAIA2-FS-10-VPP | 1258290 | Modem UMTS | AC | C | 100 |
| NARO | | TRILLIUM-40S | | 1553 | | GAIA2-FS-16-VPP | 786432 | Modem UMTS | Solar | C | 100 |
| FRON | LE3D-5S | | | 400 | | GAIA2-FS-10-VPP | 1258290 | Modem UMTS | AC | C | 100 |
| BADI | LE3D-5S | | | 400 | | GAIA2-FS-10-VPP | 1258290 | Rupa | AC | C | 100 |
| PIEI | | TRILLIUM-40S | | 1500 | | GAIA2-FS-16-VPP | 786432 | Rupa | AC | C | 100 |
| SSFR | | TRILLIUM-40S | | 1500 | | GAIA2-FS-16-VPP | 786432 | Internet | AC | C | 100 |
| CDCA | LE3D-1S | | | 400 | | GAIA2-FS-10-VPP | 1258290 | Rupa | AC | C | 100 |
| | | | EpiSensor FBA ES-T | | 1.0197 | GAIA2-FS-40-VPP | 314573 | Rupa | AC | C | 200 |
| MURB | | TRILLIUM-40S | | 1500 | | GAIA2-FS-16-VPP | 786432 | WIFI | AC | C | 100 |
| | | | EpiSensor FBA ES-T | | 1.0197 | GAIA2-FS-40-VPP | 314573 | WIFI | AC | C | 200 |
| CPGN | LE3D-1S | | | 400 | | GAIA2-FS-10-VPP | 1258290 | WIFI | AC | C | 100 |
| | | | EpiSensor FBA ES-T | | 1,0197 | GAIA2-FS-40-VPP | 314573 | WIFI | AC | C | 200 |
| MPAG | LE3D-5S | | | 400 | | GAIA2-FS-10-VPP | 1258290 | WIFI | AC | C | 100 |
| | | | EpiSensor FBA ES-T | | 1,0197 | GAIA2-FS-40-VPP | 314573 | WIFI | AC | C | 200 |
| PARC | | TRILLIUM-40S | | 1500 | | GAIA2-FS-16-VPP | 786432 | WIFI | AC | C | 100 |
| CAFI | | TRILLIUM-40S | | 1500 | | TRIDENT-FS-16-VPP-SG-1 | 1000000 | Sat. HellasSat | Solar | C | 100 |
| | | | EpiSensor FBA ES-T | | 1,0197 | Trident -FS-40-VPP | 400000 | Sat. HellasSat | Solar | C | 100 |
| CRE | | TRILLIUM-40S | | 1500 | | GAIA2-FS-16-VPP | 786432 | Rupa | AC | C | 100 |
| BAT1[1)] | 0.5S | | | | | RefTek 130 | | | | C | 500 |
| BAT2[1)] | 0.5S | | | | | RefTek 130 | | | | C | 500 |
| BAT3[1)] | 0.5S | | | | | RefTek 130 | | | | C | 500 |

[1)]Borehole stations with vertical sensor arrays; part of the IV net.

### *2.3.1.2 Software systems*

*Acquisition, detection and transmission software*

The basic structure of the TABOO acquisition system is the same as that of the INGV National Network. It is based on the ***SeedLink*** protocol implemented in the ***SeisComP*** free software package (Geofon, GFZ). The Seismological Communication Processor (SeisComP) is widely adopted for seismological data acquisition and real- time data exchange over the internet, including tools to gather, distribute and archive waveform data. It has proven to be a reliable and robust product. SeedLink clients connect to the server using a TCP/IP application level protocol (SeedLink protocol). The data source of a SeedLink server can be anything which is supported by a SeedLink plugin - a small program that sends data to the SeedLink server.

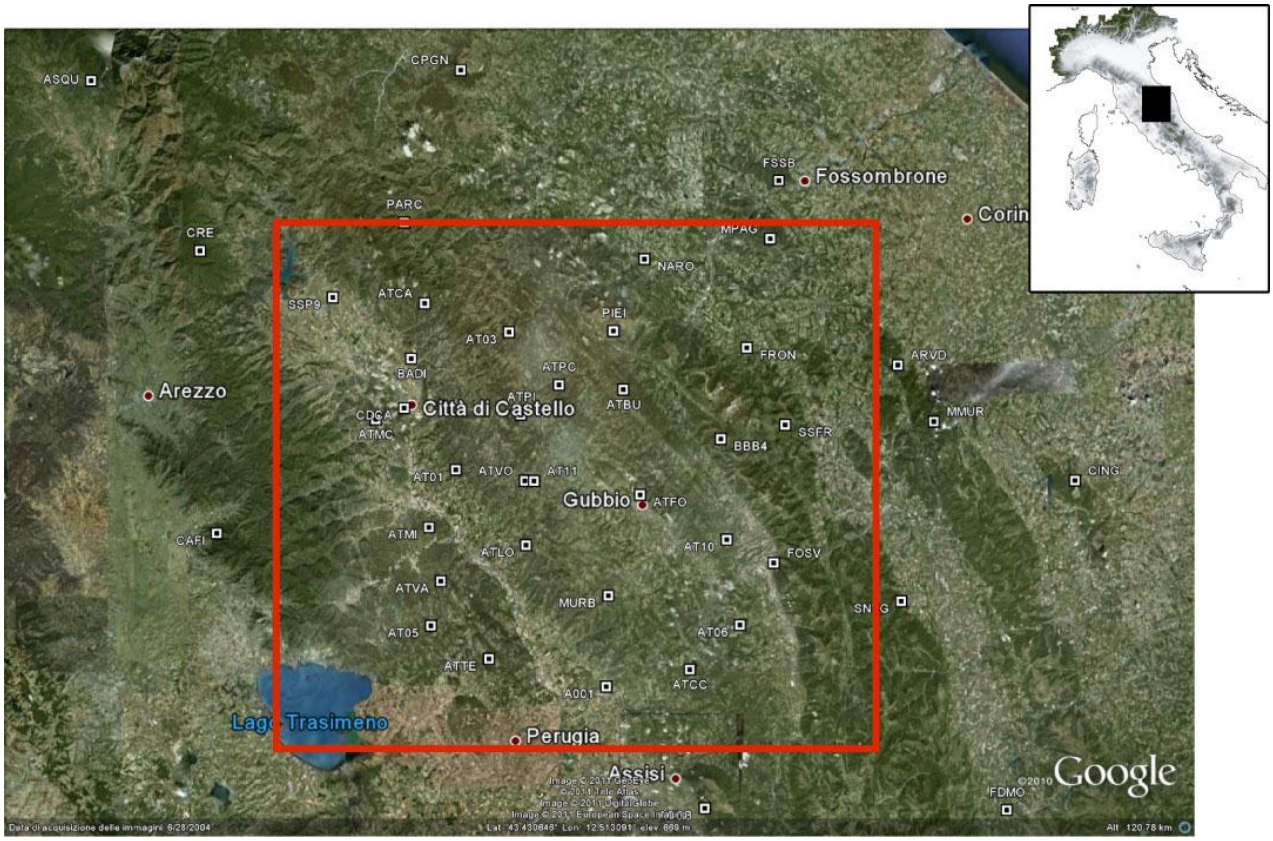


***Figure 2.3.2*** *Map of the TABOO network. The white squares represent the seismic and GPS stations.*

Data supplied by a plugin can be in the form of Mini-SEED packets or just raw integer samples with accompanying timing information. The TABOO network uses mainly one type of digitizer named GAIA_II (see Table 2.3.2), which is an INGV homemade digitizers with *SeedLink* server on-board, but also Nanometrics digitizers, for which a plugin (***nmxptool***) is needed to get and archive data in miniSEED format.

Real time seismic data recordings are collected and archived in a Storage Area Network with a SEED Data Structure, while station information is organized in a MySQL database. ***ArcLink*** (SeedLink companion protocol, available in the latest distribution of SeisComP 3.0) complements SeedLink, in providing access to archived data and station information. *ArcLink* is based on TCP and uses simple ASCII coded commands for requesting all waveforms and metadata available in specified time windows. Moreover ArcLink supports distributed archives. With this feature the data bank has a highly scalable architecture. Waveform output is in SEED or MiniSEED format, while metadata output is in XML or dataless SEED (response information only).In addition, using the ArcLink protocol all partner station information and data are integrated in one virtual data bank: the European Integrated Data Archive (EIDA).

The remote stations transmit data through a HiperLAN link to a radio backbone, installed in the ATF area for the collection of the multi-parametric data recorded by the network where the different instruments are installed. This backbone is connected to a main backbone in SDH technology, called MarcheWay and owned by the Civil Protection Department of the Marche region. This network is used by the whole monitoring system of the Marche region, centralized in the control center in Passo Varano (Ancona). Here the seismic signals are acquired by SeisComP servers, locally stored and transmitted through a dedicated ADSL connection, to the main INGV acquisition center located in Rome.

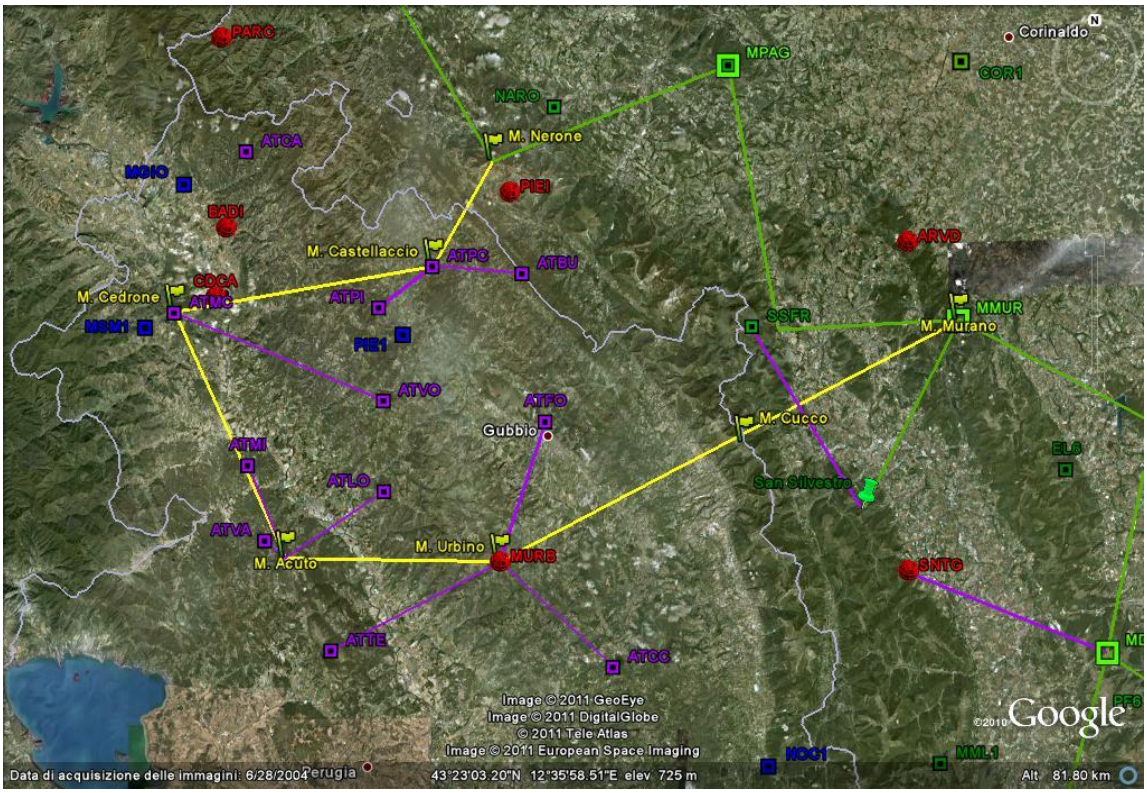


***Figure 2.3.3*** *Map of the TABOO network with the radio links configuration connecting the sub-centers to the acquisition center (yellow lines) and the remote stations to the sub-centers (purple lines).*

The status of the radio links (see Figure 2.3.3) is continuously monitored by means of dedicated software (*Netscout*). The state of health of the remote stations (power supply, synchronization, continuity of recording) is also continuously checked by means of purposely developed software. The quality of the seismic signal is routinely controlled by means of the PQLX software, which allows monitoring of the spectral characteristics of the recorded data.

*Manual analysis software*

During the time devoted to the building of the infrastructure a team of scientists implemented a modular procedure, composed of different codes to perform a series of basic analysis in near real time, including event detection (triggering; see Figure 2.3.4), P- and S-wave arrival-time reading (see Figure 2.3.5), phase association, magnitude, focal mechanism and so on. The availability of these data will allow us to map and monitor the behaviour of a large number of parameters with time (e.g. seismicity rate, b-value, Poisson ratio).

Once the waveforms related to single events have been collected we can perform analysis devoted to the measurements of the main anisotropic parameters (e.g. delay time and fast/slow polarization). While on the continuous recordings we are able to monitor the minimum magnitude detection of the seismic network, and analyze of the frequency content of the signal, in order to look for different types of transient signals, such as low frequency earthquakes and non-volcanic tremor.

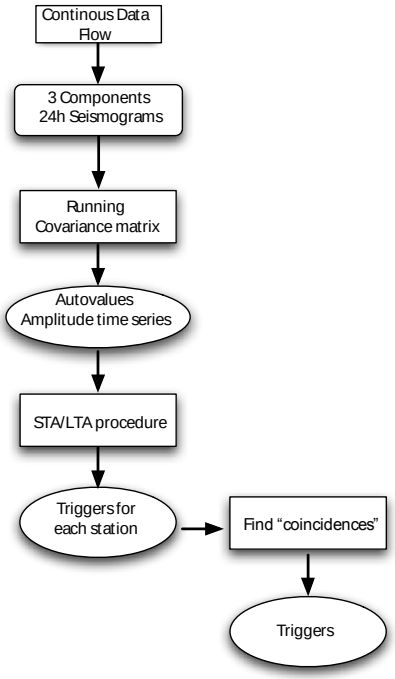


***Figure 2.3.4*** *Workflow of the triggering procedure.*

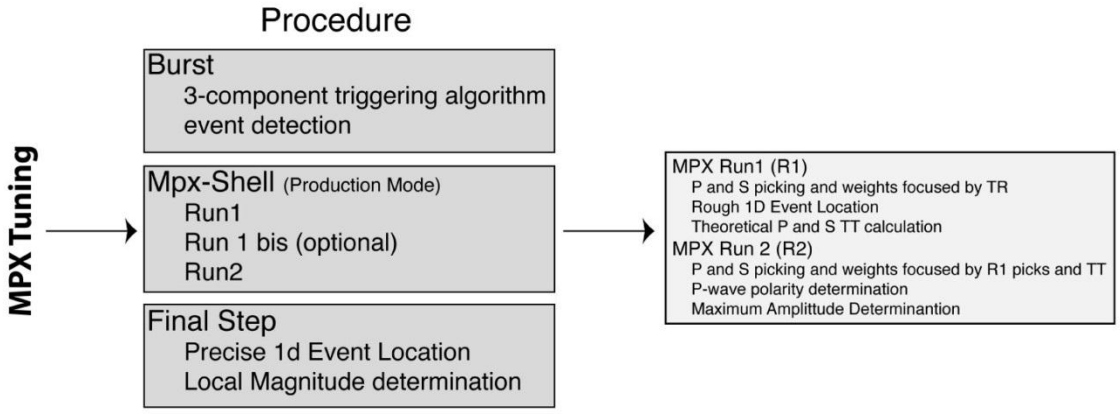


***Figure 2.3.5 –*** *Workflow of the automatic procedure for P- and S-wave arrival time pickings.*

The main codes integrated in the analysis modular procedure are defined below.

***Module 1****: Devoted to event detection from the continuous data recordings and evaluation of the network minimum detection.*

| | Name | Characteristics |
|---|---|---|
| 1.1 | EveyPosseCut | Get 24h continuous recording seismic data form the ArcLink server and convert the data to SAC format. |
| 1.2 | Burst | Triggering algorithm based STA-LTA. |
| 1.3 | Burst2Coinc-Checkdoub | Associate the triggers to one single event. |
| 1.4 | EGE_AL | Get single event waveforms from the ArcLink server writing a rough P arrival time in the SAC file. This information is the basis for the automatic picker described in module 2. |
| 1.5 | MinDet | Compute minimum detection of the network based on amplitude spectra computed from the background noise. |

***Module 2**: Devoted to the automatic evaluation of P- and S-wave arrival times, first motion polarity, earthquake locations, magnitude and focal mechanisms.*

| | Name | Characteristics |
|---|---|---|
| 2.1 | TriggerPosse | Compute refined triggers for P- and S-waves. |
| 2.2 | MannekenPix | Automatic evaluation of P- and S-wave arrival times and related weighting scheme. |
| 2.3 | HypoEllipse | Earthquake location based on 1D velocity model (linear inversion; Lahr, 1989). |
| 2.3 | NonLinLoc | Earthquake location based on 1D and 3D velocity model (non-linear inversion; Lomax et al., 2000). |
| 2.4 | Arc2Sac | Compute P- and S-wave theoretical arrival times and write them in the header SAC file. |
| 2.5 | Mpx2Mag CalculateML | Compute ML of the events based on the waveform amplitude. |

***Module 3**: High resolution earthquake location and 3D velocity model computation.*

| | Name | Characteristics |
|---|---|---|
| 3.1 | Correl8 | Compute differential arrival times at a single station for similar waveforms based on cross correlation analysis. |
| 3.2 | HypoDD | Compute relative earthquake locations (Waldhauser, 2001). |
| 3.3 | SimulPS14 | Tomographic inversion procedure (e.g. Thurber, 1983). |

***Module 4**: Data analysis and interpretation.*

| | Name | Characteristics |
|---|---|---|
| 4.1 | FPFIT | Compute focal mechanisms based on first motion polarity data (Reasenberg and Oppenheimer, 1985). |
| 4.2 | Anisomat+ | Compute anisotropic parameters of the medium (fast polarization direction and delay time) from 3-component waveforms of a single event. |
| 4.3 | Vipis | Compute $V_P/V_S$ at a single station versus time. |
| 4.4 | R-T plot | Generate space-time diagrams for computing diffusivity values. |
| 4.5 | Mc2B | Compute completeness magnitude and b-value versus time. |
| 4.6 | SPEK-RMS | Compute spectrograms on 24h time windows. |
| 4.7 | MakePlots | Automatic procedures to visualise results. |
| 4.8 | Auto_RFC | Perform receiver function analysis on teleseismic data. |

#### *2.3.1.3 Station Installation Procedures*

Examples of seismic and GPS station installations are shown below (Figure 2.3.6), which in terms of the site construction are quite standard.


*ATPC station showing the radio antenna and the power system composed by a set of solar panel.*

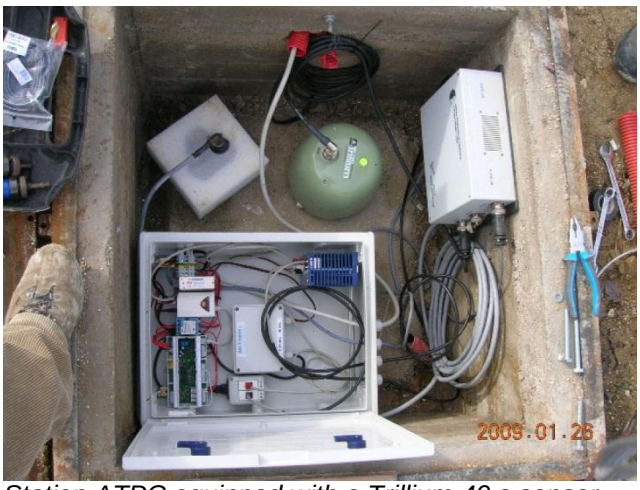


*Station ATPC equipped with a Trillium 40 s sensor, strong motion Episensor and Gaia-II digitizer.*

*Details of the ATPC antenna.*

*Antenna and radio link at MURB station.*


*ATFO seismic (green box) and GPS station (antenna in the background).*

*ATFO station equipped with a Trillium 40 s and batteries for power supply.*


*Example of a node (ATMC) with details of the power system.*

*Mt. Nerone node in winter time.*


*ATPI station showing the GPS antenna located at about 30 m distance from the seismic station.*


*Details of the ATPI station showing the short period sensor (Lennartz 5 s), the seismic digitizer (GAIA-II) and power supply.*

***Figure 2.3.6.*** *Station installation procedures.*

## 2.3.2 Strong motion network

### *2.3.2.1 Network, hardware and software systems*

In Table 2.3.2 are listed the selected sites where strong motions sensors were added. In terms of acquisition system, data trasmission and quality control software, the same architecture was adopted as that used for the short period stations.

#### *2.3.2.2 Station installation procedures*

The only difference between short period and strong motion sensor installation procedure is that the latter ones are fixed with screws to the cement bed (see photos reported in the previous paragraph showing the strong motion installed at station ATFO).

### 2.3.3 GPS Network

#### *2.3.3.1 Network and hardware*

Ten GPS stations have been installed in the Alto Tiberina Valley region in the frame of a densification project of the INGV National GPS Network RING (http://ring.gm.ingv.it). The stations were installed to increase the resolution of crustal deformation, by decreasing the ~25-50 km, mean station spacing of the RING network to ~5-10km. This densification allows resolution of the strain rate distribution on a wavelength scale of 5-10 km, as well as enabling resolution of the strain accumulation on the individual tectonic structures mapped in the area. The increased resolution of crustal deformation now enables tackling important scientific problems, such as the presence of creeping faults and aseismic release of tectonic loading. Site locations and technical specifications of the GPS network are listed in Tables 2.3.3 and 2.3.4.

***Table 2.3.3.*** *List of GPS stations contributing data to the TABOO near-fault observatory*

| Station name | Latitude °N | Longitude °E | Elevation m |
|---|---|---|---|
| CSSB | 43.2093 | 12.2454 | 753.6 |
| VALC | 43.2790 | 12.2848 | 664.1 |
| UMBE | 43.3112 | 12.3286 | 306.7 |
| MVAL | 43.3821 | 12.4066 | 639.4 |
| PIET | 43.4507 | 12.4019 | 746.5 |
| ATFO | 43.3701 | 12.5671 | 1021.5 |
| ATLO | 43.3151 | 12.4071 | 653.5 |
| ATTE | 43.1996 | 12.3506 | 967 |
| ATBU | 43.4757 | 12.5483 | 999 |
| ATMI | 43.3342 | 12.2680 | 581.3 |

***Table 2.3.4.*** *Technical specifications of GPS stations in the TABOO observatory*

| Station | Receiver Type and Model | Antenna Type | Antenna Height (DELTA H/E/N) m | Transmission | Power | Data | Sampling rate $s^{-1}$ (Hz) |
|---|---|---|---|---|---|---|---|
| CSSB | LEICA GRX1200PRO | LEIAT504 SCIT | 0.0083/0.0000 /0.0000 | Router UMTS | Solar | Rinex | 10 |
| VALC | LEICA GRX1200GGPRO | LEIAT504 SCIT | 0.0083/0.0000 /0.0000 | WIFI | Solar | Rinex | 10 |
| UMBE | LEICA GRX1200GGPRO | LEIAT504 SCIT | 0.0083/0.0000 /0.0000 | Internet | AC/DC power supply | Rinex | 10 |
| MVAL | LEICA GRX1200GGPRO | LEIAT504 SCIT | 0.0083/0.0000 /0.0000 | WIFI | Solar | Rinex | 10 |
| PIET | LEICA GRX1200GGPRO | LEIAT504 SCIT | 0.0083/0.0000 /0.0000 | WIFI | Solar | Rinex | 10 |
| ATFO | LEICA GRX1200GGPRO | LEIAT504 SCIT | 0.0083/0.0000 /0.0000 | WIFI | Solar | Rinex | 10 |
| ATLO | LEICA GRX1200GGPRO | LEIAT504 SCIT | 0.0083/0.0000 /0.0000 | WIFI | Solar | Rinex | 10 |
| ATTE | LEICA GRX1200GGPRO | LEIAT504 SCIT | 0.0083/0.0000 /0.0000 | WIFI | Solar | Rinex | 10 |
| ATBU | LEICA GRX1200GGPRO | LEIAT504 SCIT | 0.0083/0.0000 /0.0000 | WIFI | Solar | Rinex | 10 |
| ATMI | LEICA GRX1200GGPRO | LEIAT504 SCIT | 0.0083/0.0000 /0.0000 | WIFI | Solar | Rinex | 10 |

#### *2.3.3.2 Software systems*

*Acquisition, detection and transmission software*

Data from GPS stations are collected using WIFI transmission (details in section 2.3.1.2) and managed by the Ancona operational centre. There the data are collected transmitted and archived with the Leica-Geosystems GNSS-SPIDER software, which sends the data to the additional archiving and processing centers (Roma, Grottaminarda). At the Grottaminarda data center the observation files, and metadata of the RING, are managed by a Knowledge Management (KM) infrastructure, complete to web sharing management (*bancadati*).The process model associated with KM consists of well-defined layers, handling: data, software and web services (Presentation).

In the first layer (Data Sources Layer) the data sources are made up of a file system to manage raw data and rinex, and of a relational database with Oracle technology, which manages information about sites and instruments (log files, monographies etc). The second layer (Knowledge Management Layer) contains analysis and development software, and data mining tools. Finally, the querying, management and sharing of all the data sources are under control of the web portal (Knowledge Presentation Layer).

These services were created with the intent to support data, information and exchange of know-how in the internal structure, based on the principle that the greater source of an organization is the knowledge common to the people working there.

*Automatic and Manual analysis software*

GPS code and phase data are processed with the Gipsy-Oasis II software using the precise point positioning (PPP) strategy (Zumberge et al., 1997) and JPL products from ftp://sideshow.jpl.nasa.gov. Integer ambiguity resolution is then applied using *Ambizap* (Blewitt, 2008). This processing algorithm uses a fixed point theorem to identify linear combinations of network parameters that are theoretically invariant under ambiguity resolution, and produce a unique, self-consistent daily ambiguity-fixed solution for the entire network. The resulting daily solutions are aligned to the ITRF2005 reference frame using a seven-parameter transformation. The ITRF2005 realization is obtained using daily precise-point-positioning solutions of 67 sites in Eurasia, Nubia and Central Mediterranean and daily coordinate transformation parameters to ITRF2005 from JPL (x-files). A no-net rotation constraint is applied using a subset of 32 sites within the stable Eurasian continent that were deemed to be sufficiently far (Noquet et al., 2005) from tectonic and horizontal glacial isostatic adjustments effects. The RMS of the horizontal residual velocities of these 32 sites after application of the no-net rotation constraint are 0.40 and 0.36 mm/yr for the East and North components respectively. Temporal variation of positions thus represent crustal motion relative to the stable Eurasian plate in the north (latitude), east (longitude) and up (vertical) components. The time series are then cleaned of outliers and analyzed using the CATS software (Williams, 2007) for their noise properties, linear velocities, periodic signals and antenna jumps. The model parameters (linear terms, antenna offsets, and annual and semi-annual periodic signals) are estimated using a white+flicker noise error model (Williams, 2007). Each graph shows the cleaned time series (red dots), the antenna offsets (yellow dashed lines), the model time series (green lines), WRMS and linear velocity uncertainties for each component.

*Quality control processes*

The Data Mining Software, Clinic checks Rinex Files and produces new information stored in the database. The first check is for: file type, file length, and file name. If it is positive, the next step will be TEQC check, otherwise the RINEX file will be put in quarantine. The TEQC software checks: marker name, hours, percent, cycle slips, gaps, first and last epoch, sessions. If the results are positive, then the RINEX file is put in the outgoing directory and the information is stored in the relational database (bancadati). The front-end version of Clinic allows production of charts about functioning parameters of the GPS Stations (i.e. Mp1, Mp2, SLPS, GAP, ...).

*Data formats, accessible data bases and available data*

Data from GPS stations are distributed within INGV by a centralized archive. Rinex files, with 30-seconds-sampling, are collected daily from all the core- and densification sites of the RING network.

#### *2.3.3.3 Station installation procedures*

The installation of the GPS monuments follows the procedure illustrated in the RING web page (http://ring.gm.ingv.it/monuments.php). In particular the majority of GPS stations use a SCIGN-type tripod project, which ensures the maximum coupling between the antenna and the crust.

### 2.3.4 Deep Drilling

#### *2.3.4.1 Description and purpose of deep bore hole*

The Alto Tiberina fault has been declared a potentially interesting site for a deep drilling project of an active fault by the International Continental Drilling Program (ICDP; http://www.icdp-online.org/contenido/icdp/front_content.php?idcat=1038). Within this context TABOO is a basic activity for achieving high resolution information to elaborate a rational project for drilling.

### 2.3.5 Future Goals and Developments of the TABOO Observatory

The plan for the near future is to instrument a set of three shallow boreholes (250 m deep) with 3-component, passive, short-period sensors within the GLASS EU project.

## 2.4 Corinth Rift Laboratory Seismic Zone

### [38.15N – 38.48N; 21.7E – 22.36E]

### Tectonic setting and observatory overview

The western rift of Corinth (western Greece) is the seismic area with the largest strain rate ($10^{-6}$/yr) and densest swarm activity of the Euro-Mediterranean area (10 000 events located every year). It experienced large historical earthquakes in the 18th and 19th century, occurring on a complex system of en-echelon normal faults. Most of these faults are dipping to the north, rooting around 6 to 8 km in depth within a seismically active layer, 1 to 2 km thick, gently dipping towards the north, which is interpreted by Rigo et al. (1996) as a possible detachment fault. The 1995 Aigion earthquake, magnitude 6.2, struck the eastern edge of the target zone (Bernard et al. 1997). Most of the large faults of the target area are probably in the latest part of their seismic cycle, owing to geodetic, historical, archaeological, and paleohistorical data. In particular, the opening rate from GPS is 1.5 cm/year, and the last historical earthquakes with magnitude above 6 occurred in 1861 and 1888 in the central zone, and no large historical earthquakes are reported for 3 centuries in the western zone near Patras. One or more earthquakes with magnitudes above 6 are thus expected in the coming decades, depending on the ability for a single rupture to break across multiple fault segments.

Since year 2000, a dense array monitoring has produced an exceptional data base (seismology, GPS, strain meters) (see the instrumentation for the Corinth Rift Laboratory, **http://crlab.eu**). Many earthquakes swarms are well documented, showing strong, unexplained pulsations of activity at various times and spatial scales, located at 5-10 km in depth at the root of the locked, major normal faults. Their slow migration with time suggests pore pressure diffusion. A slow event equivalent to a magnitude 5 earthquake was recorded on a borehole strain meter in 2002, during a large seismic swarm (Bernard et al., 2006). The Psathopyrogos fault system (20 km long), in the western rift of Corinth, deserves a specific attention, as it is subject to major, episodic seismic swarms, and shows transient episodes of creep on a time scale of hours, weeks, decades, and centuries (Bernard et al., 2010). It is presently in a state of accelerated strain and is a serious threat, although yet not quantified, for the Patras city (pop. 300 000), less than 5 km from its south-western end.

The continuously monitoring arrays of CRL have evolved since the first permanent installation in 2000, the total number of sites having increased, but some sites having been suppressed. This evolution has followed the evolution of the main targets of these arrays, and the evolution in the priorities given to specific measurements.

Initially designed to monitor the fault system in an area less than 10 km around the Aigion fault, focussing on the 1 km deep AIG10 drilling site which crossed the Aigion fault at depth, the arrays progressively extended more towards the west, including the Rio-Antirio area at the western end of the rift, and allowing a better view of the seismicity close to or under the city of Patras.

The AIG10 monitoring systems (hydrophones and pore pressure at depth), started in June 2007 and stopped in February 2008 due to instrumental problems. Also, shallow borehole measurements of groundwater (level, temperature, geochemistry), initiated in the early 2000, have progressively stopped, as evidence for an almost exclusive signature of meteorological water of the shallowest kilometres of the crust became clear. Only 2 sites are presently maintained by INGV, outside the frame of CRL.

For the CRL instruments, the installation and routine operations (maintenance, telemetry), are under the responsibility of the owning Institution (NKUA, UPSL, CNRS), as is the

organization of the corresponding, specific data bases. However, for most of the seismic stations, there is an integration of the real-time telemetered data from different Institutions, which is sent to NKUA in Athens and made accessible to the other partners through *SeedLink*.

## Network descriptions

## 2.4.1 Seismic networks

### *2.4.1.1 Network and hardware*

***Table 2.4.1.*** *List of seismic stations contributing data to the CRL near-fault observatory*.

| Station name | Latitude °N | Longitude °E | Elevation m | Sensor Depth m | Operator |
|---|---|---|---|---|---|
| AIO | 38° 11.63‘ | 22° 03.52‘ | 198 | 130 | CNRS |
| KOU* | 38° 13.91‘ | 22° 04.52‘ | 133 | 66 | CNRS |
| TEM | 38° 13.90‘ | 22° 07.09‘ | 54 | 71 | CNRS |
| DIM | 38° 14.81‘ | 22° 02.62‘ | 152 | 80 | CNRS |
| AGE | 38° 15.99‘ | 22° 03.80‘ | 17 | 135 | CNRS |
| ALI | 38° 15.63‘ | 22° 06.68‘ | 37 | 70 | CNRS |
| PSA | 38° 19.92‘ | 22° 10.51‘ | 117 | 0 | CNRS |
| TRZ | 38°21.93‘ | 22° 04.36‘ | 57 | 2 | CNRS |
| TRI | 38°21.94‘ | 22° 04.35‘ | 64 | 0 | CNRS |
| TRX | 38° 21.94‘ | 22° 04.35‘ | 64 | 0 | CNRS |
| PYR | 38° 24.61‘ | 22° 01.01‘ | 596 | 0 | CNRS |
| PAN | 38° 22.41‘ | 22° 14.99‘ | 149 | 0 | CNRS |
| ROD | 38.308 | 21.892 | 448 | 0 | CNRS |
| ZIRI | 38.309 | 21.953 | 479 | 0 | CNRS |
| TRAZ | 38.168 | 22.212 | 668 | 0 | NKUA |
| LAKA | 38° 14.40‘ | 21° 58.80‘ | 500 | 0 | NKUA |
| KALE | 38° 23.46‘ | 22° 08.39‘ | 789 | 0 | NKUA |
| SERG | 38.4133 | 22.0566 | 480 | 0 | UPSL/CUP |
| UPR | 38.2836 | 21.7864 | 138 | 0 | UPSL |
| VVK | 38.4222 | 21.8115 | 651 | 0 | UPSL |
| EFP | 38.4270 | 21.9058 | 175 | 0 | UPSL |
| ANX | 38.5933 | 21.9209 | 1020 | 0 | UPSL/HP |

* : station closed on june 2011.

***Table 2.4.2.*** *Technical specifications of stations in the CRL observatory.*

| Station Name | SP Type Corner freq. | BB Type Corner freq. $^{-1}$ | SM Type | Sensor sensitivity V/m/s | Sensor sensitivity V/m/s$^2$ | Digitizer Type | Digitizer gain µV/bit | Transmission | Power | Data | Sampling rate $s^{-1}$ |
|---|---|---|---|---|---|---|---|---|---|---|---|
| AIO | L22 - 2 | | | 83 | | Taurus Nanometrics | 1 | none | solar | C | 100 |
| KOU* | L22- 2 | | | 83 | | Taurus Nanometrics | 1 | none | mains | C | 100 |
| TEM | L22 - 2 | | | 83 | | R130 Reftek | 1.9 | gprs | mains | C | 100 |
| DIM | L22 - 2 | | | 83 | | Taurus Nanometrics | 1 | gprs | mains | C | 100 |
| AGE | L22 - 2 | | | 83 | | Kephren Agecodagis | 1 | adsl | mains | C | 125 |
| ALI | L22 - 2 | | | 83 | | Taurus Nanometrics | 1 | gprs | mains | C | 100 |
| PSA | L22 - 2 | | | 155 | | R130 Reftek | 1.5 | gprs | mains | C | 100 |
| TRIZ | | STS2 120 s | | 1500 | | R130 Reftek | 1.6 | gprs | mains+solar | C | 100 |
| TRIZ | | | Episensor Kinemetrics | | 2 | R130 Reftek | 1.6 | Gprs (local) | mains+solar | C | 20 (100) |
| PYR | L22- 2 | | | 155 | | R130 Reftek | 1.5 | gprs | solar | C | 100 |
| PAN | L22-2 | | | 155 | | R130 Reftek | 1.5 | gprs | mains | C | 100 |
| ROD | L22-2 | CMG40 60 s | | 800 | | R130 Reftek | 1.5 | gprs | mains | C | 100 |
| ZIRI | L22- | | | 2000 | | R130 Reftek | 1.5 | gprs | solar | C | 100 |
| TRAZ | | CMG40 30 s | | 800 | | 72A Reftek | 1.9 | gprs | | C | 100 |
| LAKA | | CMG3T 120 s | | 6000 | | CMG-DM24 | 3 | | | C | 100 |
| KALE | | CMG40 60 s | | 800 | | R130 Reftek | 1.5 | | | C | 100 |
| SERG | | CMG-3T 120 s | CMG-5T | 3000 | 2.04 | Guralp DM24 | 0.78 | GPRS | mains | C | 100 |
| UPR | SIG-1Hz | | | 1000 | | Trident | 1 | Ethernet | Mains | C | 100 |
| VVK | S100-0.5Hz | | | 1000 | | SR-24 | 1.192 | GPRS | Mains | C | 100 |
| EFP | | Trillium - 40s | | 1500 | | Trident | 1 | Satellite | mains | C | 100 |
| ANX | | CMG-3T 120 s | CMG-5T | 750 | 2.04 | Guralp DM24 | 0.78 | GPRS | mains | C | 100 |

SP: Short period BB: Broad band SM: Strong motion
C: Continuous data recording; E: Event based recording

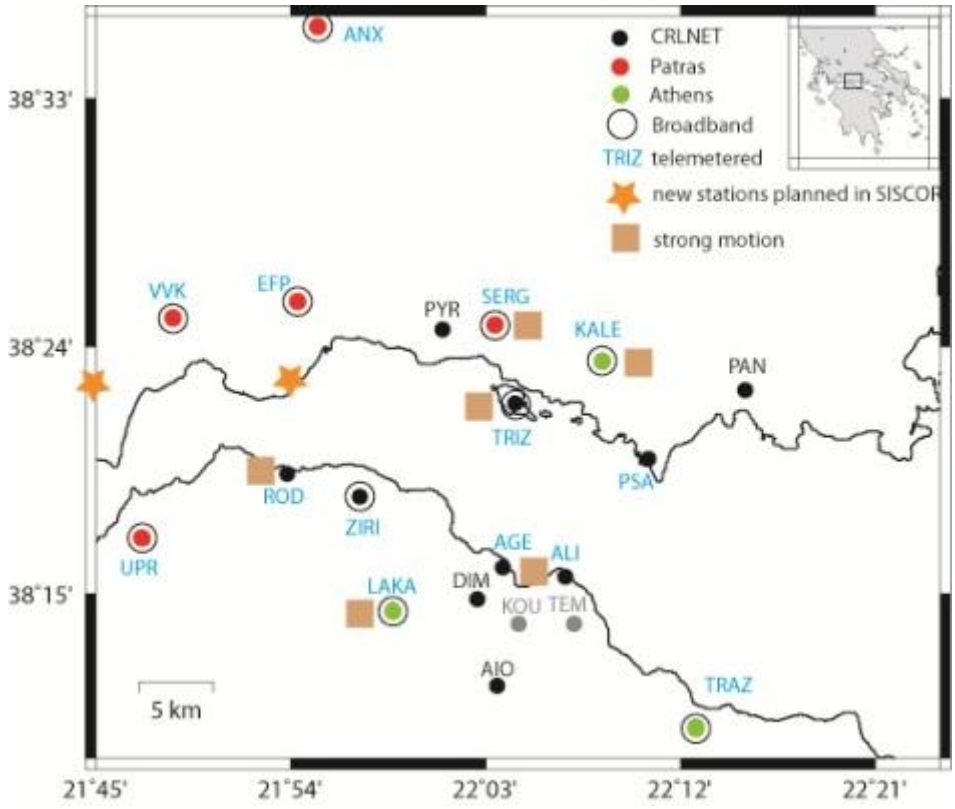


***Figure 2.4.1*** *Seismological sites of the CRL array (from CRL website www.crlab.eu).*

### *2.4.1.2 Software systems*

***CNRS/CRL systems***

*Acquisition, detection and transmission at the CNRS/CRL stations*

All recorders of CRL-net are in continuous mode, at 100 Hz sampling rate. Most of them are telemetered in real-time through GPRS directly to the NKUA CRL data server. One station (AGE) uses ADSL lines to feed the NKUA server. A few stations are still stand alone.
All telemetered data (CNRS, NKUA and UPS) are received at ENS through seedlink and are archived in miniseed format.
All stations (telemetered or not) are visited once every 3 to 4 months for a complete download of their memory storage.

*Automatic analysis at the CNRS/CRL data center*

Earthworm combined with an automatic picking algorithm developped for CRL, allows real-time analysis and location of the seismicity (http:/ephesite.ens.fr/~eworm)

*Manual analysis at CNRS/CRL stations*

Manual analysis is not done routinely but occasionaly by researchers looking at specific datasets.

*Quality control processes for CNRS/CRL*

A basic quality control of the data is done by filling gaps in the real-time data. The complete seismological data set of one year is processed to include non-real-time data and to obtain a more complete yearly catalogue.

*Data formats, accessible data bases and available data for CNRS/CRL*

Event data are open and available at http://bdsis.u-strasbg.fr/BDsis. Continuous data can be obtain by request.

***NKUA/CRL systems***

*Acquisition, detection and transmission at the NKUA/CRL stations*

The signals of all the continuously recording seismographs of the remote NKUA stations are transmitted in real time through GPRS, to the central server of the University of Athens, with a sampling rate equal to 100Hz. In addition, the CRL data are received by the NKUA servers and retransmitted to the CNRS/CRL data center. The two main acquisition systems, i.e. the **NAQS** and **SEISCOMP** servers, receive the data from the remote stations. These software perform management and real-time display of waveforms and the state of health, on a daily basis. Furthermore, real-time event detection and automatic daily backup take place.

*Automatic analysis at the NKUA/CRL data center*

An automatic procedure for the detection and location of seismic events is applied. The obtained source parameters are published in real-time on the webpage of the Seismological Laboratory of the University of Athens: www.geophysics.geol.uoa.gr.

*Manual analysis at NKUA/CRL stations*

Manual analysis includes the determination of source parameters, i.e. hypocenter location and magnitude determination. For moderate and strong events, a moment tensor inversion is applied to obtain the seismic moment and the fault plane solution. These are published both on the webpage of the Seismological Laboratory of the University of Athens and on the EMSC website.

***UPSL/CRL systems***

*Acquisition, detection and transmission at the UPSL/CRL stations*

Remote stations transmit data, (continuous records with a 100Hz sampling rate) through a satellite system to a central Hub, which is located on the University of Patras campus. The central Hub receives data packets and then forwards them, through a local network, to the **NAQS** server acquisition software. This is an acquisition and data handling software package that performs the following tasks: data storage in ring buffer files, state of health data storage, real time display of waveforms and state of health, data error handling and re-transmission requests, triggering of events and access to ring buffer data for clients, like e.g.

picking software. Ring-buffer files store continuous data and are copied on backup disks once per day.

*Automatic analysis at the UPSL/CRL data center*

For automatic detection and location of the seismic events the **Hydra** system is used. Hydra receives real time data from the Naqs server and identifies, locates, and measures earthquakes. Thus, epicenter locations and seismic magnitudes ($M_L$, $M_{wp}$, $m_b$, $M_s$ etc), as well as moment tensors are calculated automatically. All solutions, automatic and manual ones, are stored in a **MySQL** database and can be accessed using a Web interface.

*Manual analysis at UPSL/CRL*

The Nanometrics **Atlas** software is used for manual data processing. This means phase picking, epicenter location and magnitude determination. Results are stored in a **MySQL** database and are accessible through the Internet. The **Hypoinverse** program is used by Atlas for the determination of epicenter and the calculation of event magnitude. Moment tensor solutions are calculated in the case of an event with M>4.0, using the **ISOLA-GUI** code (Sokos and Zahradnik 2008). The location and moment tensor results of the manual analysis are posted immediately on the EMSC web page, and in case of strong events a small report is also prepared.

### *2.4.1.3 Station installation procedures*

***CNRS/CRL stations***

Most stations located on the Southwestern coast have been installed in boreholes, 70 to 100 m deep. The steel casing on the boreholes stops one or a-few-meters above the bottom of the hole. The 3 component, passive 2 Hz seismometers were emplaced below the casing level and sand was poured from the surface to lock the seismometer in a nearly vertical position, and to allow a stable coupling to the rock. However, for a few components, slow strain in the sand has caused mechanical drift (tilt) of the instrument and finally the loss of signal.

The surface stations are of two main types:

- outside buildings, seismometers are buried in a small hole, 40 to 50 cm deep, blocked directly with compact earth filling the hole.
- inside small buildings (one-story), the seismometers are put directly on the cement floor.

***NKUA/CRL stations***

The remote stations of NKUA are installed in buildings. The broadband seismometers are buried in holes or vaults about 0.5 m deep.

***UPSL/CRL stations***

The UPSL/CRL stations are installed:

- in small houses; the sensor is buried in a small hole outside the house (station VVK),
- in small buildings; the sensor is put on the cement floor of the building (station ANX),
- as surface installations; in small vaults (stations EFP, UPR),
- in deep vaults (3m) with thermal protection (station SERG).

## 2.4.2 Other strong motion networks

**RASMON (NKUA)**

The RASMON strong motion network is operated around the area of the Gulf of Corinth (W. Greece) since 1991, to assist in the investigation of the complex seismotectonic regime of the area, as well as to provide the basis for strong ground motion attenuation and site effect studies. Specifically, it consists of 14 digital (18- or 24-bit) accelerograps.


***Figure 2.4.2.*** *Map of RASMON and CORSSA accelerometric arrays*

Most of the RASMON stations communicate via GPRS modems or ADSL connections with the Seismological Laboratory of NKUA, in order to retrieve the data and perform regular state of health controls remotely. For the remaining stations, data are retrieved by regular visits. Data from all RASMON stations are inserted in a databank and are analysed for instrument response, baseline correction and for USGS V1/V2/V3 data format.

**CORSSA (NKUA/AUTH/IRSN)**

The CORSSA array (COrinth Rift Soft Soil Array) is located in the Aigion harbour and consists of four borehole broad-band acceleration sensors and one surface broadband accelerometer. The data from the CORSSA array are retrieved through ADSL lines and are regularly corrected for instrument response.

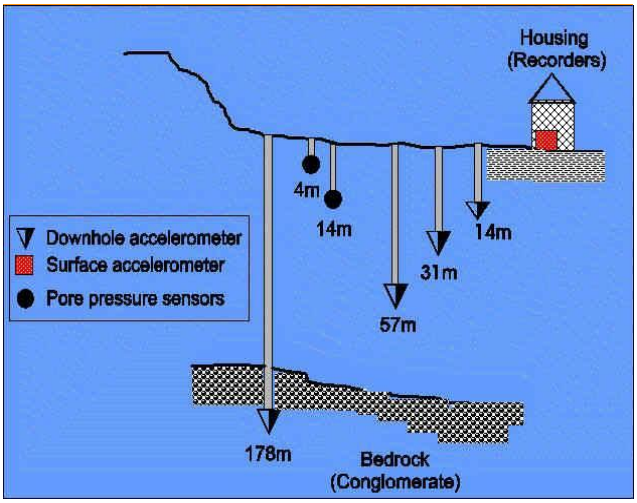


***Figure 2.4.3.*** *CORSSA configuration*

**Accelerometer of Charles University/UPSL:**

Already described in Table 2.4.2 above for "Seismic Networks" - see also http://seis30.karlov.mff.cuni.cz/

***Table 2.4.3.*** *List of other strong motion stations contributing data to CRL (CORSSA and RASMON).*

| Station name | Latitude °N | Longitude °E | Elevation m | Sensor depth m | Operator |
|---|---|---|---|---|---|
| SER | 38° 24.834'N | 22° 3.432'E | 497 | 0 | NKUA |
| GLX | 38° 22.200'N | 22° 23.667'E | 72 | 0 | NKUA |
| TRI | 38° 22.254'N | 22° 4.674'E | 35 | 0 | NKUA |
| MAN | 38° 23.394'N | 21° 53.394'E | 58 | 0 | NKUA |
| ANT | 38° 21.833'N | 22° 37.958'E | 50 | 0 | NKUA |
| ROD | 38° 19.374'N | 21° 53.826'E | 117 | 0 | NKUA |
| LAK | 38° 14.428'N | 21° 58.878'E | 500 | 0 | NKUA |
| AIG | 38° 15.018'N | 22° 5.268'E | 99 | 0 | NKUA |
| AKR | 38° 9.783'N | 22° 20.006'E | 119 | 0 | NKUA |
| XYL | 38° 4.132'N | 22° 37.443'E | 87 | 0 | NKUA |
| KIA | 37° 59.250'N | 22° 45.258'E | 76 | 0 | NKUA |
| LOU | 37° 58.530'N | 22° 58.618'E | 5 | 0 | NKUA |
| TRAZ | 38° 10'6.6"N | 22° 12' 43.56"E | 668 | 0 | NKUA |
| EPID | 37° 36'51.84"N | 23° 7' 8.04"E | 444 | 0 | NKUA |
| CORSSA ARRAY (SSA) | 38° 15.360'N | 22° 4.500'E | 1 | 0<br>14m<br>31m<br>57m<br>178m | NKUA |

**Table 2.4.4.** Technical specifications of other strong motion stations contributing to CRL.

| Station Name | SM Type | Sensor sensitivity $V/m/s^2$ | Digitizer Type | Digitizer gain µV/bit | Transmission | Power | Data | Sampling rate $s^{-1}$ |
|---|---|---|---|---|---|---|---|---|
| SER | ETNA | | Kinemetrics | | REM | mains | E | 200 |
| GLX | K2 | | Kinemetrics | | REM | mains | E | 200 |
| TRI | K2 | | Kinemetrics | | REM | mains | E | 200 |
| MAN | K2 | | Kinemetrics | | REM | mains | E | 200 |

| | | | | | | | | |
|---|---|---|---|---|---|---|---|---|
| ANT | ETNA | | Kinemetrics | | REM | mains | E | 200 |
| ROD | ETNA | | Kinemetrics | | GPRS | mains | E | 200 |
| LAK | ETNA | | Kinemetrics | | GPRS | mains | E | 200 |
| AIG | ETNA | | Kinemetrics | | ADSL | mains | E | 200 |
| AKR | ETNA | | Kinemetrics | | REM | mains | E | 200 |
| XYL | ETNA | | Kinemetrics | | ADSL | mains | E | 200 |
| KIA | ETNA | | Kinemetrics | | ADSL | mains | E | 200 |
| LOU | ETNA | | Kinemetrics | | ADSL | mains | E | 200 |
| TRAZ | ETNA | | Kinemetrics | | GPRS | mains | E | 200 |
| EPID | ETNA | | Kinemetrics | | GPRS | mains | E | 200 |
| CORSSA ARRAY (SSA) | MTW | | Kinemetrics | | ADSL | mains | E | 200 |

C: Continuous data E: event data

## 2.4.3 GPS network

### *2.4.3.1 Network and hardware*

For complete information on the network and stations see the CRL portal (http://crlab.eu) and the CRL page on the GPSCOPE portal (https://gpscope.dt.insu.cnrs.fr/chantiers/corinthe/). For the campaign networks see the CRL web site.

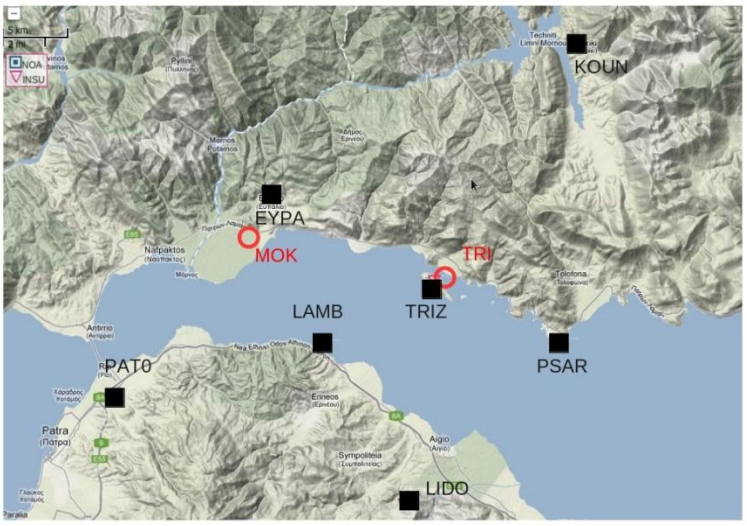


***Figure 2.4.4.*** *Location of Continuous GPS (black squares) and borehole strainmeters (red circles) CRL sites.*

***Table 2.4.5.*** *List of the permanent GPS stations contributing data to CRL.*

| Station name | Latitude °N | Longitude °E | Elevation m |
|---|---|---|---|
| EYRA | 38° 25' 26" | 21° 55 '42" | 197 |
| KOUN | 38° 12' 34" | 22° 02' 45" | 595 |
| TRIZ | 38° 21' 55" | 22° 04' 22" | 57 |
| LIDO | 38° 31' 44" | 22° 12' 04" | 594 |
| PSAR | 38° 19' 18" | 22° 11' 03" | 89 |
| ARIO | 38° 20' 02" | 21° 45' 59" | 20 |
| RIO0 | 38° 18' 40" | 21° 46' 58" | 15 |
| PAT0 | 38° 17' 01" | 21° 47' 12" | 121 |
| LAMB | 38° 19' 14" | 21° 58' 23" | 20 |

***Table 2.4.6.*** *Technical specifications of GPS stations in the CRL*

| Station | Receiver Type and Model | Antenna Type | Height of Antenna m | Transmission | Power | DATA | Sampling interval s |
|---|---|---|---|---|---|---|---|
| EYRA | TOPCON GB1000 | JAVAD Legant | 0.300 | No | AC | 1 TPS file/day | 30 |
| KOUN | TOPCON GB1000 | JAVAD Legant | 0.300 | No | AC/solar | 1 TPS file/day | 30 |
| TRIZ | TOPCON GB1000 | JAVAD Legant | 0.300 | IP (with seismic station) | AC | 1 TPS file/day | 30 |
| LIDO | TOPCON GB1000 | JAVAD Legant | 0.300 | No | AC | 1 TPS file/day | 30 |
| PSAR | TOPCON GB1000 | TOPCON PG-A1 | 0.300 | No | AC | 1 TPS file/day | 30 |
| ARIO | TOPCON GB1000 | TOPCON PG-A1 | 0.000 | IP (Gefyra intranet) | AC | 1 TPS file/day | 30 |
| RIO0 | TOPCON GB1000 | TOPCON PG-A1 | 0.000 | No | AC | 1 TPS file/day | 30 |
| PAT0 | TOPCON GB1000 | Choke-Ring | 0.000 | IP (UPAT seismolab) | AC | 1 TPS file/day & 1 TPS file/hour (1s) | 30 & 1 |
| LAMB | TOPCON GB1000 | TOPCON PG-A1 | 0.3000 | No | AC | 1 TPS file/day | 30 |

C: Continuous data

### *2.4.3.2 Software systems*

*Acquisition software*

Topcon firmware on board of the Topcon receivers – Produces TPS files (1 file/day and 1 file/hour at PAT0).

*Automatic analysis software*

Data is processed on a daily basis at the GPSCOPE data centre (DT INSU Meudon) using GAMIT.

*Manual analysis software*

Manual analysis performed at ENS using GIPSY/OASIS (also used for processing of campaign data).

*Quality control processes*

Quality control performed during the data processing. Extra quality control for PAT0 (EUREF station).

*Data formats and accessible data bases*

Data in RINEX format available on line on the GPSCOPE web portal.

### *2.4.3.3 Station installation procedures*

The crucial aspects concern the antennas:

Two stations (KOUN, EYPA) are installed on a water tank. After nine year of operation, according to the time series, they appear particularly stable.

Four stations (PSAR, PATO, LAMB) are installed in small (one storey) buildings. They also appear stable in the time series.

RIO0 is a new station installed on a 1 m high pillar, and ARIO is on a tall building (3 storeys). Their time series are too short to assess the stability.

TRIZ is on a tall pillar (>3m) and the time series exhibits an annual oscillation of more than a cm. After several years of recording, it is now possible to remove this annual oscillation.

All stations have electricity, and TRIZ has an additional solar panel supply. All receivers have internal batteries that allow a few hours of autonomy, in case of short power failure (most common case). Three stations (TRIZ, KOUN,) are exposed to the risk of power shut down by local people, but the network operators take care to regularly remind them to leave the connection on.

## 2.4.4 Borehole strain meters

### *2.4.4.1 Network and hardware*

***Table 2.4.7.*** *List of strain stations contributing data to CRL.*

| Station name | Latitude °N | Longitude °E | Elevation m | Sensor Depth m |
|---|---|---|---|---|
| TRI | 38.370315 | 2.073826 | 0 | 150 |
| MOK | 38.403326 | 21.925101 | 5 | 150 |

***Table 2.4.8.*** *Technical specifications of strain stations in CRL.*

| Station name | Strain Sensor Type | Recorder Type | Transmission | Power | Data | Sampling rate $s^{-1}$ |
|---|---|---|---|---|---|---|
| TRI | Sacks-Evertson | R130 | none | mains | C (E) | 5 ( 50) |
| MOK | Sacks-Evertson | SOC-box | none | mains | C | 50 |

C: Continuous data E: event data

### *2.4.4.2 Software systems*

*Acquisition software*

The TRI station has a Reftek R130 recorder, with 4 channels and 3 data streams. Channel 1 for the DT1 signal (high resolution aerial strain/stress); channel 2 for the DT2 signal (low resolution strain when valves are open for a large strain event; temperature otherwise, when valves are closed). Channel 3 and 4 are for tide-guage and barometric pressure. Data stream 1 is continuous recording of channel 1 and 2, at a sampling rate of 5 Hz. Data stream 2 is trigerred recording of channel 1 and 2, at a sampling rate of 50 Hz. Stream 3 is continuous recording of channels 1, 2, 3 and 4, at 1 Hz sampling rate. The data is stored locally on a flash card and dowloaded manually every 3 months. The native format is segy.

The MOK station has a recorder manufactured by the Carnegie Institution of Washington. It continuously records all three 3 components of the strainmeter (horizontal stress in 3 directions 120° apart) at a sampling rate of 50 Hz, and provides the barometric pressure and temperature at a 1 Hz sample rate. Data records at 1 s and 1 minute intervals are also automatically generated. Data is stored on a Nano-usb stick, and dowloaded manually every 3 months. The data format is SAC.

*Manual analysis and quality control*

Quality control is done by visual inspection of the daily and monthly records. In particular the response to earth tides, atmospheric pressure, and earthquakes.

At TRI, inspection of data records revealed a change in the transfert function in November 2009. More recent data suffer from a reduction in low frequency content, possibly due to small leaking of valves, physically mixing signals from DT1 and DT2. The stability of the new transfert function is being investigated.

At MOK, inspection of the data records revealed very frequent automatic resetting of pressure (valve opening to reduce the pressure) during the first years of operation. This has progressively been corrected with adjustments of the control system, and also thanks to the natural reduction in the strain drift rate, due to the borehole stabilization. Since 2010, the strainmeter does not suffer from undue resetting.

*Data formats and accessible data bases*

At TRI and MOK, the data is converted to SAC format. Data records are not presently accessible on-line, but they are available on request.

#### *2.4.4.3 Station installation procedures*

For both strainmeters, the borehole is first drilled (10 cm diameter inner casing) and logged below the casing, from about 120 to 155 m. The bottom, open part of the borehole is then cemented, and drilled again, for a better stabilization of the rock walls. On the installation phase, a first load of cement is downloaded with a bailer ( a 6 m long tube, which opens when hitting the bottom, pouring out the cement. Then, within about 15 minutes, the strainmeter (4 m long) is downloaded and immersed within the cement filling the bottom of the hole, and hanged at the proper depth while the cement is setting hard.

For TRI, the second load of cement was poured 2 month afterwards, when it appeared that the strainmeter was only partially coupled. But the analysis of records showed that this second cementation did not succeed into a complete solid coupling to the rock. Only about 40% (+-10%) of the instrumnent is well coupled to the rock through solid cement; the remaining part senses pore pressure of the borehole. The TRI dilatometer thus measures a combination of aerial strain and the confined pore pressure.

For MOK, the day after the installation of the instrument, a second load of cement was poured down through a long pipe reaching 5 m above the strainmeter, for securing the proper coupling of the instrument to the rock in its top part. Analysis of records show that the cementation was globally successfull.

### 2.4.5 Geochemical monitoring

A few automatic geochemical stations have been installed in the area by INGV, within EC projects related to CRL, in order to monitor and track fluid transients from deep crustal sources related to earthquake activity. Two stations are still in operation near villages on the southern coast; Neratzes (borehole equipped with complete geochemical station) and

Psathopyrgos (roman well monitored for water level, temperature, conductivity). For more information, contact the P.I. Luca Pizzino: *pizzino@ingv*.it

### 2.4.6 Water level gauges in boreholes

A water level gauge is installed in the same borehole as the MOK strainmeter. The small device (6 cm long and 2 cm diameter) is hung in the borehole, at the depth of about 2 m below the mean water table level.

***Table 2.4.9.*** *List of borehole water level stations contributing data to CRL.*

| Station name | Latitude °N | Longitude °E | Elevation m | Sensor Depth m |
|---|---|---|---|---|
| MOK | 38.403326 | 21.925101 | 5 | 4 |

***Table 2.4.10.*** *Technical specifications of water level stations in CRL.*

| Station name | Water level Sensor Type | Recorder Type | Transmission | Power | Data | Sample interval s |
|---|---|---|---|---|---|---|
| MOK | DIVER-CETRA | | none | battery | C | 600 |

### 2.4.7 Tide gauges

The Tide gauge is installed in a narrow, vertical PVC tube, fixed to the dock of the Marina, at about 2 m below the mean sea level. It is located 30 m east to the TRI borehole dilatometer.

***Table 2.4.11.*** *List of borehole tide-gauge stations contributing data to CRL.*

| Station name | Latitude °N | Longitude °E | Elevation m | Sensor Depth m |
|---|---|---|---|---|
| TRI | 38.3703 | 2.0738 | 0 | 2 |

***Table 2.4.12.*** *Technical specifications of tide-gauge stations in CRL.*

| Station name | Water level Sensor Type | Recorder Type | Transmission | Power | Data | Sampling rate $s^{-1}$ |
|---|---|---|---|---|---|---|
| TRI | PDCR1830 Campbell | R130 | none | mains | C | 1 |

### 2.4.8 Deep drilling

In 2002-2003 a 1-km-deep borehole, AIG10, was drilled in the area, within the CRL project. The borehole cut the Aigion fault at a depth of about 780 m. The borehole was instrumented at various depths; by geophones (at 745 m, 2000 Hz s.r.), hydrophones (at 250 and 500 m, 2000 Hz s.r.), and with a high resolution pore pressure sensor (at 700 m, 1pt/12s s.r.). However, due to fluid overpressure, the installation failed and after repair and reinstallation, the data acquisition only worked fully and correctly between mid-June and mid-October 2007. After that, part of the data is missing, until the final stop of the system, in February 2008. The AIG10 monitoring systems are now stopped, and there is no plan to repair or restart the system in the CRL in the coming years.

Data will be made available in 2012 through the BDSIS database of EOST in Strasbourg. For more information on sensors and data, contact the P.I. François Cornet: *Cornet@eost.u-strasbg.fr.*

### 2.4.9 Magnetic and other EM sensors

Independently from the CRL installations, magnetic and electrotelluric sensors have been installed in the same area as the ground-based segment of the DEMETER experiment.

More information on instrument type and location, as well as on data availability, can be retrieved on the DEMETER website.

For more information on sensors and data availability, contact the P.I. Jacques Zlonicki: jacques.zlotnicki@opgc.univ-bpclermont.fr.

### 2.4.10 Future Goals and Developments of the CRL Observatory

The monitoring system of CRL is evolving in order to expand the research area to the west, to better understand the activity of the faults systems connected in the NW to the Trichonis rift, and in the SW to the Rio-Patras strike-slip fault system. The latter is of particular importance as it crosses Patras city, with potential earthquakes possibly above M=6. A specific target is the Psathopyrgos fault, the westernmost normal-fault of the Corinth rift, which is the place of frequent seismic swarms and possible slow slip transients, and has the potential for a significant earthquake within the next decades.

For this purpose, the installation of a few more seismic stations is planned to the west of the present arrays (SISCOR French ANR project). In addition, a few more continuous GPS stations will be installed, to better map the locked and slipping areas of the active faults (SISCOR French ANR project). Tiltmeters and one more strainmeter will be installed for quantifying the aseismic strain signature of seismic swarms (REAKT EC project). Finally, installation of a small scale, dense array of seismometers is planned the, in order to apply antenna techniques for better locations of swarms of events and to detect and locate possible tremors and/or non-impulsive seismic sources (REAKT EC project). All these installations should be completed in 2012.

## 2.5 The Irpinia Fault System

**[40.23N – 41.23N; 14.74E – 15.99E]**

### Tectonic setting and observatory overview

The Irpinia Seismic Network (ISNet) is displaced over an area of approximately *100 km × 70 km* in the Irpinia-Basilicata area, an Appenninic region located in Southern Italy which experienced several large earthquakes (M>6) in the last century. During the last century the region was struck by 3 events of magnitude larger than 6: the 1930, M=6.7 Irpinia earthquake (Emolo et al., 2004, Pino et al. 2008) the 1962, M=6.2, Irpinia earthquake (Westaway, 1987) and the 1980, M=6.9, Irpinia-Basilicata earthquake (Westaway and Jackson, 1987; Bernard and Zollo, 1989; Pantosti and Valensise, 1990). Most of the largest historical events occurred on NW-SE oriented normal faults, with a few of them having a strike-slip component. The 1980 event however, occurred on a complex fault system, with at least three main structures activated during the faulting process. Since then, the area has begun to be monitored by the accelerometric network RAN (Rete Accelerometrica Nazionale), held by the National Civil Protection and the broad-band INGV network. During the monitoring period, the regional networks recorded 6 events of magnitude ranging between 4 and 5.5 and several events of magnitude larger than 3. Since the recent installation of *ISNet*, the largest events in the region have not exceed magnitude 3.7, with few hundreds of events detected by the network, mainly located along Appenninic/sub-Appenninic structures which generated the 1980 earthquake. Some are clustered along the right-lateral, strike-slip Potenza fault, which was responsible for the 1990-1991 sequence, characterized by two main events of magnitude 5.7 and 5.2 and a maximum VII-MCS intensity (Tertulliani et al., 1992). For this reason, the characterization of the size of small events, within its location, is fundamental to detect space and time variations of the seismicity, as indicators of changes in the tectonic state of the area.

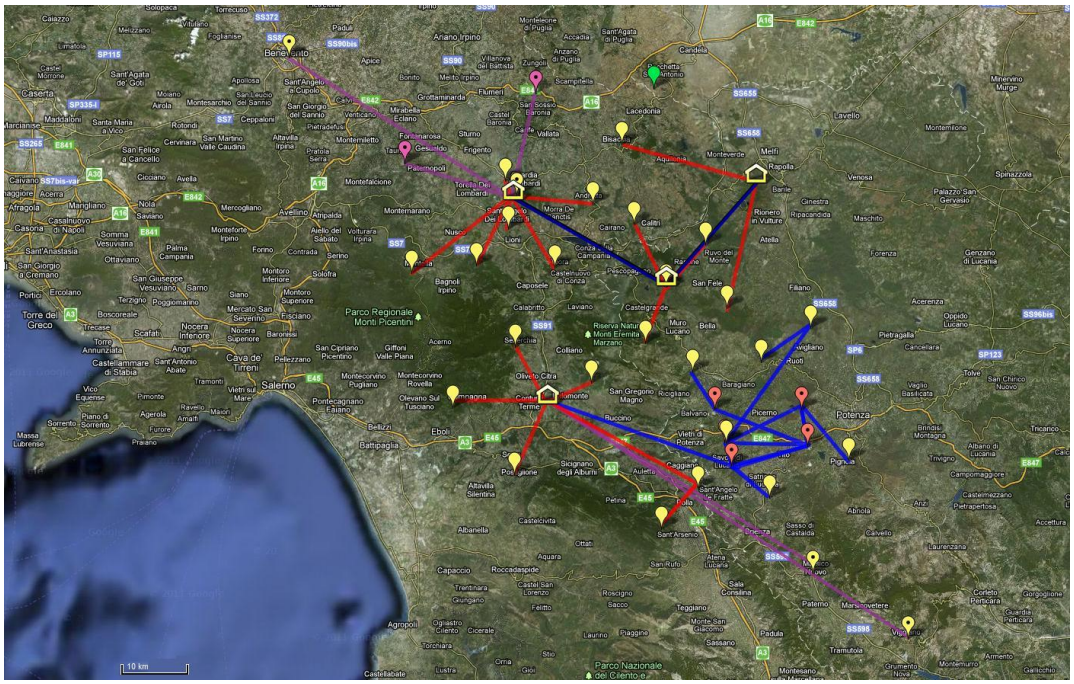


***Figure 2.5.1.*** *ISNet location in southern Italy. Lines represent Wifi or ADSL (violet lines) connections. Data from the stations are collected by the LCCs, represented here by houses.*

## Network descriptions

## 2.5.1 Seismic and strong motion networks

### *2.5.1.1 Network and hardware*

***ISNet*** is constituted by 31 stations and covers an area of about 100 × 70 $km^2$. Each site is equipped with an accelerometer (p-p: ±1g) and a short-period velocimeter. Furthermore, five sites are equipped with broad-band sensors instead of short period velocimeters. There is olso one station (AND3) that has a second accelerometer with a full scale of ¼g. Data acquisition at the seismic stations is performed by the Osiris-6 data-logger produced by Agecodagis. This has a Σ-Δ 24-bit A/D converter, a 100-MHz ARM® processor with embedded Linux and open-source software, onsite data storage, serial and TCP/IP connectivity, global positioning system (GPS) time tagging, an integrated SeedLink server, and simple/flexible configuration via a Web interface (HTTP).

***Table 2.5.1*** *List of seismic stations contributing data to the ISNet near-fault observatory.*

| Station name | Latitude °N | Longitude °E | Elevation m | Sensor Depth m |
|---|---|---|---|---|
| AND3 | 15.3331 | 40.9298 | 905 | 0 |
| AVG3 | 15.7251 | 40.7619 | 1213 | 0 |
| BEL3 | 15.6369 | 40.7153 | 758 | 0 |
| BENI | 14.7716 | 41.1298 | 75 | 0 |
| BSC3 | 15.3852 | 41.012 | 980 | 0 |
| CGG3 | 15.5225 | 40.542 | 1067 | 0 |
| CLT3 | 15.4043 | 40.903 | 525 | 0 |
| CMP3 | 15.0802 | 40.6519 | 958 | 0 |
| COL3 | 15.3304 | 40.6871 | 1026 | 0 |
| CSG3 | 15.4633 | 40.8181 | 1253 | 0 |
| LGS3 | 14.9906 | 40.9865 | 413 | 0 |
| LIO3 | 15.1804 | 40.8969 | 737 | 0 |
| MNT3 | 15.0067 | 40.837 | 866 | 0 |
| MRN3 | 15.7296 | 40.4256 | 772 | 0 |
| NAPI | 14.18 | 40.84 | 120 | 0 |
| NSC3 | 15.1222 | 40.8468 | 1300 | 0 |
| PGN3 | 15.7967 | 40.5722 | 882 | 0 |
| PST3 | 15.2433 | 40.5609 | 762 | 0 |
| RDM3 | 15.5361 | 40.8755 | 784 | 0 |
| RSF3 | 15.176 | 40.9643 | 865 | 0 |
| SALI | 15.18 | 40.93 | 872 | 0 |
| SCL3 | 15.5114 | 40.6951 | 744 | 0 |
| SFL3 | 15.5782 | 40.7889 | 1062 | 0 |
| SNR3 | 15.1927 | 40.7357 | 1009 | 0 |
| SRN3 | 15.458 | 40.4861 | 1067 | 0 |
| SSB3 | 15.2292 | 41.0785 | 724 | 0 |
| STN3 | 15.6515 | 40.53 | 832 | 0 |
| TEO3 | 15.2633 | 40.8447 | 870 | 0 |
| VDP3 | 15.5721 | 40.6052 | 959 | 0 |
| VDS3 | 15.427 | 40.7408 | 1154 | 0 |
| VGG3 | 15.901 | 40.336 | 882 | 0 |

***Table 2.5.2*** *Technical specifications of stations in the ISNet observatory.*

| Station Name | SP Type Corner freq. $^{-1}$ | BB Type Corner freq.$^{-1}$ | SM Type | Sensor sensitivity V/m/s | Sensor sensitivity V/m/s$^2$ | Digitizer Type | Digitizer gain μV/bit | Transmission | Power | Data | Sampling rate s$^{-1}$ |
|---|---|---|---|---|---|---|---|---|---|---|---|
| AND3 | | | CMG-5T | | 0.509 (p-p: ± 1g) | OSIRIS6 | 1 | WiFi | Solar | Cont. | 125 |
| | | | EPISENSOR | | 1.019 (p-p: ± ¼g) | | | | | | |
| AVG3 | | | CMG-5T | | 0.509 (p-p: ± 1g) | OSIRIS6 | 1 | WiFi | Solar | Cont. | 125 |
| BEL3 | S13J (1s) | | CMG-5T | 340 | 0.509 (p-p: ± 1g) | OSIRIS6 | 1 | WiFi | Solar | Cont. | 125 |
| BENI | | | EPISENSOR | | 1.019 (p-p: ± ¼g) | OSIRIS6 | 1 | LAN | Mains | Cont. | 125 |
| BSC3 | | | CMG-5T | | 0.509 (p-p: ± 1g) | OSIRIS6 | 1 | WiFi | Solar | Cont. | 125 |
| CGG3 | S13J (1s) | | CMG-5T | 340 | 0.509 (p-p: ± 1g) | OSIRIS6 | 1 | WiFi | Solar | Cont. | 125 |
| CLT3 | S13J (1s) | | CMG-5T | 340 | 0.509 (p-p: ± 1g) | OSIRIS6 | 1 | WiFi | Solar | Cont. | 125 |
| CMP3 | S13J (1s) | | CMG-5T | 340 | 0.509 (p-p: ± 1g) | OSIRIS6 | 1 | WiFi | Solar | Cont. | 125 |
| COL3 | | TRILLIUM (40s) | CMG-5T | 1500 | 0.509 (p-p: ± 1g) | OSIRIS6 | 1 | WiFi | Solar | Cont. | 250 |
| CSG3 | | | CMG-5T | | 0.509 (p-p: ± 1g) | OSIRIS6 | 1 | WiFi | Mains | Cont. | 125 |
| LGS3 | | | CMG-5T | | 0.509 (p-p: ± 1g) | OSIRIS6 | 1 | UMTS | Mains | Cont. | 125 |
| LIO3 | | TRILLIUM (40s) | CMG-5T | 1500 | 0.509 (p-p: ± 1g) | OSIRIS6 | 1 | WiFi | Solar | Cont. | 125 |
| MNT3 | Lennartz LE3D (5s) | | CMG-5T | 400 | 0.509 (p-p: ± 1g) | OSIRIS6 | 1 | WiFi | Solar | Cont. | 125 |
| MRN3 | | | CMG-5T | | 0.509 (p-p: ± 1g) | OSIRIS6 | 1 | ADSL | Mains | Cont. | 125 |
| NAPI | | | CMG-5T | | 0.509 (p-p: ± 1g) | MYKERINOS | 1 | LAN | Mains | Cont. | 125 |
| NSC3 | S13J (1s) | | CMG-5T | 340 | 0.509 (p-p: ± 1g) | OSIRIS6 | 1 | WiFi | Solar | Cont. | 125 |
| PGN3 | | TRILLIUM (40s) | CMG-5T | 1500 | 0.509 (p-p: ± 1g) | OSIRIS6 | 1 | WiFi | Solar | Cont. | 125 |
| PST3 | S13J (1s) | | CMG-5T | 340 | 0.509 (p-p: ± 1g) | OSIRIS6 | 1 | WiFi | Solar | Cont. | 125 |

| | | | | | | | | | | | |
|---|---|---|---|---|---|---|---|---|---|---|---|
| RDM3 | | TRILLIUM (40s) | CMG-5T | 1500 | 0.509 (p-p: ± 1g) | OSIRIS6 | 1 | WiFi | Solar | Cont. | 125 |
| RSF3 | | TRILLIUM (40s) | CMG-5T | 1500 | 0.509 (p-p: ± 1g) | OSIRIS6 | 1 | WiFi | Solar | Cont. | 125 |
| SALI | | | EPISENSOR | | 1.019 (p-p: ± ¼g) | SAGE3 | 1 | ADSL | Mains | Cont. | 125 |
| SCL3 | S13J (1s) | | CMG-5T | 340 | 0.509 (p-p: ± 1g) | OSIRIS6 | 1 | WiFi | Solar | Cont. | 125 |
| SFL3 | S13J (1s) | | CMG-5T | 340 | 0.509 (p-p: ± 1g) | OSIRIS6 | 1 | WiFi | Solar | Cont. | 125 |
| SNR3 | S13J (1s) | | CMG-5T | 340 | 0.509 (p-p: ± 1g) | OSIRIS6 | 1 | WiFi | Solar | Cont. | 250 |
| SRN3 | | CMG-40T (flat band 60s - 50Hz) | CMG-5T | 800 | 0.509 (p-p: ± 1g) | OSIRIS6 | 1 | WiFi | Solar | Cont. | 125 |
| SSB3 | | | CMG-5T | | 0.509 (p-p: ± 1g) | OSIRIS6 | 1 | UMTS | Mains | Cont. | 125 |
| STN3 | S13J (1s) | | CMG-5T | 340 | 0.509 (p-p: ± 1g) | OSIRIS6 | 1 | WiFi | Solar | Cont. | 125 |
| TEO3 | | | CMG-5T | | 0.509 (p-p: ± 1g) | OSIRIS6 | 1 | WiFi | Solar | Cont. | 125 |
| VDP3 | | | CMG-5T | | 0.509 (p-p: ± 1g) | OSIRIS6 | 1 | WiFi | Solar | Cont. | 125 |
| VDS3 | S13J (1s) | | CMG-5T | 340 | 0.509 (p-p: ± 1g) | OSIRIS6 | 1 | WiFi | Solar | Cont. | 125 |
| VGG3 | | | CMG-5T | | 0.509 (p-p: ± 1g) | OSIRIS6 | 1 | ADSL | Mains | Cont. | 125 |

***ISNet*** is organized in “sub-nets”, each of them composed of a maximum of nine seismic stations and managed by a Local Control Center (LCC ). Most of the stations are connected to the LCC via WiFi antennas. When optical visibility does not allow direct connection of the site to the LCC, then the site is connected via ADSL or UMTS. Due to the design characteristics, i.e., the wide dynamic range and the high density of stations, the ISNet is expected to be able to estimate, in real-time the earthquake location and magnitude of low- to high-magnitude events, and to provide ground-motion parameter values. Moreover, the availability of high-quality data allows studying of the source processes related to the seismogenetic structures in the area. The development of the seismic network started in 2005 with the financial support of the local Government of the Campania Region.

### *2.5.1.2 Software systems*

The infrastructure for the system management and data analysis is mainly based on different modules and software packages, distributed on two different levels (LCC and NCC) as shown in Figure 2.5.2.

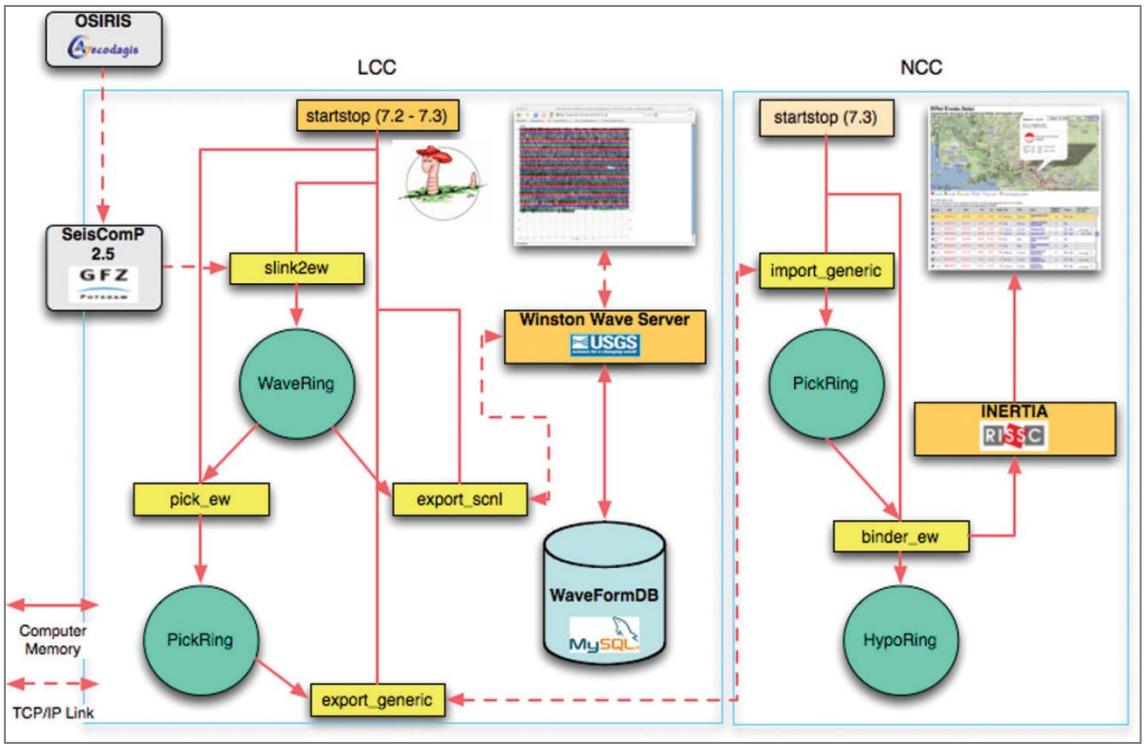


***Figure 2.5.2.*** *Data flow in a LCC and in a NCC of ISNet within the main modules of the software infrastructure (SeisComP, Earthworm’s modules, Winston Wave server and INERTIA)*

*Acquisition and data storage software*

The data transmission from data loggers to LCC is managed by a ***SeedLink*** server, running on *ISNet*’s LCCs SeedLink, and associated with the software ***SeisComP2.X*** (developed and maintained by the GEOFON software development group at GFZ Potsdam), also installed on the LCC server. The data are acquiree from the ISNet digitizers and data acquisition systems by use of the ***acquisition*** sub-package that includes the ***SeedLink*** server and plugins. Also included is a ***slarchive–SeedLink client*** for archiving data on local hard-disk using ***SeisComP Data Structure*** (SDS).

For data storage on disk, the standard ***Earthworm*** module (***WaveServerV***) was replaced with a separate ***Winston*** software (http://www.avo.alaska.edu/Software/winston/W_Manual_TOC.html). This software package overcomes some of the limitations of the ***Earthworm*** module, such as the maximum size of data records on disk. It also offers additional features, such as compressed data retrieval and data display facilities. The ***Winston*** installation imports the data from ***Earthworm*** and stores them on disk (this program also implements the ***Winston Wave Server***, replacing the standard ***Earthworm Wave Server*** module, which provides the recorded data to client applications).

*Real-time automatic analysis software*

The data analysis is performed by several modules of the ***Earthworm7.X*** automatic processing system developed by the USGS and ISTI and mainly written in *C* and *C++*. The processing modules used are:

- ***pick_ew***, for the picking of P-first arrivals. The picks times are calculated using an algorithm developed by Rex Allen (1978,1982). The module reads the real-time wave_ring waveform format *TRACEBUF*, picks independently each vertical components, and produces pick messages, which are sent to an *Earthworm* transport ring ( http://folkworm.ceri.memphis.edu/ew-doc/ovr/pick_ew_ovr.html)
- ***binder_ew*** associates the automatically picked P-arrivals into events. The *binder_ew* phase association module (Dietz, 2002) is based on a grid search for the most likely common hypocenter that explains a set of arrival times from different stations. (http://folkworm.ceri.memphis.edu/ew-doc/ovr/binder_setup.html)
- ***hyp2000*** is the stand-alone version of the *hypoinverse* earthquake location program, written and maintained by Fred Klein at USGS, Menlo Park. ( http://folkworm.ceri.memphis.edu/ew-doc/ovr/hyp2000_ovr.html)
- ***localmag*** calculates the local magnitude. As a standalone program, *localmag* is run one or more times for each declared event. The module fetches SAC traces from wave_servers. Then it converts the original amplitudes to Wood-Anderson amplitudes by a frequency domain convolution to remove the original instrument response and replace it with the Wood-Anderson response. In addition to the peak amplitude values from the Wood-Anderson traces, *localmag* corrects for attenuation with station-hypocenter distance. The used attenuation law has been specifically computed for Southern Italy, in the area monitored by *ISNet* (Bobbio et al. 2009). (http://folkworm.ceri.memphis.edu/ew-doc/ovr/localmag_ovr.html)

*Near real-time automatic analysis and manual software*

After the determination of local magnitude of the event, the ***eventpostproc*** bash shell script measures the *PGA* and *PGV* from raw SAC traces saved by ***localmag*** at all stations and reports via mail, the earthquake location (coordinates and toponym), the magnitude and the computed peak ground values.

At this point an analysis chain called ***INERTIA*** (Isnet NEar Real TIme Analisys) starts. It is composed of different modules used to compute the source parameters, the moment magnitude, the shake map and other parameters of the detected event. In this chain, each module starts only when the previous-one has finished its analysis. Several modules have been written for manual review of recorded events (for adjusting and adding phase-arrival picks and polarities of P and S waves, and for relocating seismic events) or for inserting events not associated by the binder. All modules are currently implemented as *Linux* Bash

shells and several modules use internally SAC macros, *awk* scripts, and/or ad hoc developed *Fortran* codes.

The main modules of the ***INERTIA*** chain are:

- ***Get Traces:*** downloads (via ***GetWave***) the 6-component waveforms for stations bound to automatic events. Stores them is SAC format with full header (picks and source parameters);
- ***Get Full Traces:*** retrieves waveforms from stations not associated by the binder;
- ***Rev. Checkin:*** Finds the toponym of the event location and plots the waveforms for the bulletin;
- ***Get Rev Traces:*** downloads waveforms from revised events with no revised waveforms (e.g. teleseisms);
- ***Spectra:*** computes S-wave displacement spectra. Spectra are then modeled to compute seismic moment, corner frequency, stress drop and source radius. At this time an Update mail is sent if the moment magnitude is different from the previous estimation based on the local magnitude value;
- ***GRS Map:*** computes the ground shaking map and the estimated instrumental intensity map;
- ***Mag Rev:*** computes local magnitude using ***ISNet*** algorithm;
- ***Foc. Mec.:*** computes the focal mechanisms;
- ***ShakeMap:*** computes the ground shaking maps using USGS' ShakeMap software.

*Early-Warning system software*

***PRESTo*** (PRobabilistic and Evolutionary early warning SysTem) is a software platform for regional earthquake early warning that integrates algorithms for real-time earthquake location and magnitude estimation into a highly configurable and easily portable package. ***PRESTo*** follows a regional approach, i.e. it relies on the information coming from a seismic network deployed in the epicentral area to rapidly estimate source parameters (location and size) of a potentially destructive earthquake and to predict the ground motion at distant targets (Figure 2.5.3). The following algorithms are implemented in the current system:

- ***FilterPicker*****:** designed so that it operates stably on continuous, real-time, broad-band signals, avoids excessive picking during large events, and produces a realistic time uncertainty on the pick (Lomax et al., 2011);
- ***Threshold-based alert level*** issued independently by each station. Based on peak displacement and predominant P-waves period measured over a few-second-long window following the first arrival (Zollo et al., 2010);
- ***RTLoc:*** evolutionary location technique based on an equal differential time (EDT) formulation and a probabilistic approach for describing the hypocenter estimation (Satriano et. al., 2008). Both triggered and not-yet-triggered stations are used
- ***RTMag:*** magnitude estimation based on 2/4 second windows of signal following the automatically picked P-waves arrival and predicted S-waves arrival (Lancieri et al., 2008);
- The ***continuous, real-time updating*** of eqk location, Pd and τc, allows the determination of the extent of the Potential Damage Zone, defined as the area within which the Instrumental intensity is expected to be greater the VII (Colombelli et al., 2011).

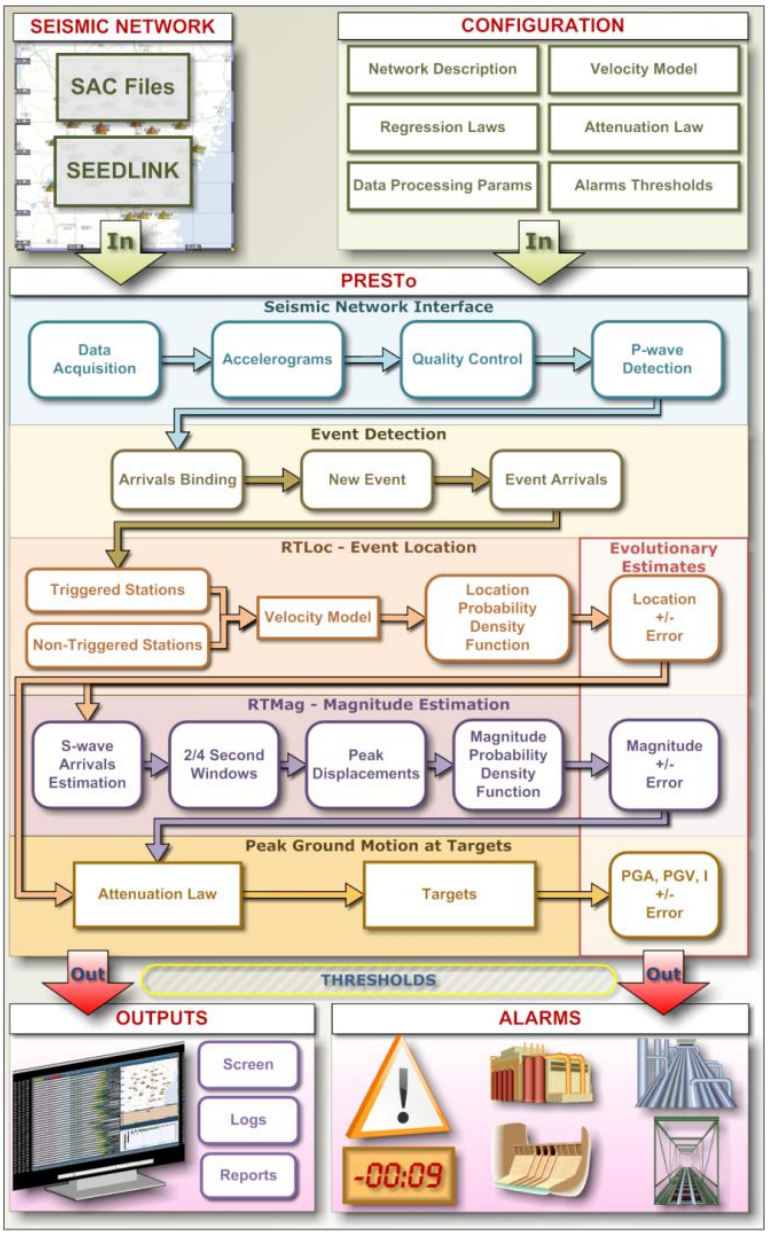


***Figure 2.5.3.*** *Diagram of the data flow within the building blocks of PRESTo. At the top are the inputs, i.e. the ground motion data (as files or real-time streams) and the end-user configuration data (including the seismic network description and velocity model). The vertical components of the data streams are continually analyzed to detect P-wave arrivals. After arrivals at different stations have triggered a new event, a chain of modules produces a probability density function for hypocenter and magnitude. Each target site is promptly informed of the most likely hypocenter and magnitude (and related uncertainties) and, most importantly, of the expected peak ground motion it will experience in a few seconds (if above the target specific threshold)*.

*Quality control processes*

An automatic routine for the quality control processes is applied to the recordings of ***ISNet*** velocimeters. The routine is a Bash script shell that works on each LCC and every day:

1. downloads 24 hours of data from the three components of associated velocimeters;
2. divides the traces into one-hour waveform segments of continuous, non-overlapping data;
3. converts the amplitudes into m/s;

4. removes the mean value and the linear trends and applies to the resulting traces a 10% cosine taper;
5. computes the Power Spectral Density for each processed one-hour waveform segment.

All the computed PSD curves and the related figures are stored at the NCC and are available by a web interface, which allows a quick way to access the results, with the option to select the station and the day of interest.

#### *2.5.1.3 Station installation procedures*

Most of the sites (about 85%) record in stand-alone mode to reduce as much as possible the cultural noise. The seismic stations are located in 2m × 2m × 2m shelters that are installed inside 6m × 4m fenced areas. Each station is supplied with two solar panels (120W peak, with 480Wh/day), two 115Ah gel cell batteries (which avoids possible freezing damage). With this configuration, 72h autonomy is ensured for the seismic and radio communication equipment.

To transmit waveforms in real time from the seismic sites to the LCC's, two out-door 1310 Cisco Wireless local area network (LAN) bridges that operate in the 2.4 GHz band are used for each link. For particular conditions and distances, a different technology operating in the 5 GHz band allowes connection over more than 20km.

Inside each seismic site, the sensors are installed on a $1m^3$ reinforced concrete base, at least 0.8 m below the surface of the soil. To ensure a high dynamic range, each station is equipped with two types of three-component sensors: strong-motion accelerometers and velocity instruments.

***Figure 2.5.4.*** *Top left : a typical shelter hosting the seismic instrumentation. It is equipped with solar panels and an antenna for wi-fi connection. Top right: Inside the shelter the instruments are installed on a concrete block, which is deconnected from the shelter. Bottom: the local control center, connecting data from a set of stations.*

### 2.5.2 Future Goals and Developments of the Irpinia Observatory

ISNet objectives are two-pronged: on the one hand is it aimed at monitoring the micro-seismicity of the area with the use of both velocimetic and accelerometric sensors; on the other hand, it is devoted to issue an early warning during the occurrence of a moderate to large earthquake in the area. Along the first axis, the main future goal is to improve earthquake location by the use of a 3D velocity model and accurate picking based on waveform cross-correlation, and source characterization by automatic estimation of seismic moment, stress drop and radiated energy, from both spectral amplitudes and empirical Green's function analysis. Special attention will be paid to the characterization of sequences as indicators of mechanical processes occurring along the monitored fault system (fluid migration, cracklings, etc.). With this aim, future development will concern the installation of instrumentation at depth and/or of small-size arrays to increase the signal-to¬-noise ratio at high-frequency and the detection threshold of the network. Future development of the early warning monitoring system will consist instead into the deployment of a large number of low-cost accelerometers, directly connected to internet (via UMTS or ADSL). They will constrain the peak-ground acceleration during the main shock and will better define the potential damaged zone associated with the occurrence of a significant earthquake in the area.

## 2.6 The Valais Area (VA)

**[45.8N – 46.5N; 6.8W – 8.2W]**

### Tectonic setting and observatory overview

The Valais region in general, and specifically the area of Visp, as well as the Visper and Matter valleys, has been selected as a test bed due to its high seismic hazard. In the past, the Valais has experienced a magnitude 6 or larger event every 100 years, with the last magnitude 5.8 earthquake in 1946 occurring close to Sion and Sierre. The region of Visp is affected by damaging earthquakes on average every 40 years (Intensity VI-VIII), with the last nearby event in 1960 reaching a macroseismic intensity of VII (Fäh et al., 2011a) (Figure 2.6.1). During all large events in the Valais, significant damage is produced from not only the ground motion but also from various kinds of secondary phenomena such as liquefaction in the Rhone plain, slope instabilities and extended rock fall (Fritsche et al., 2011). The probability of observing a major earthquake in the next 40 years is high, and the Swiss Seismological Service (SED) is preparing for such an occurrence by installing the dense multi-sensor network for detailed monitoring and scientific analysis. Project COGEAR "Coupled seismogenic Geohazards in Alpine Regions" (COGEAR, 2008-2012; http://www.cogear.ethz.ch) was launched to focus on the Valais area, and to involve the scientific community in research activities (Fäh et al., 2011b). The project adds two new elements to the ongoing surveillance and seismic hazard assessment in Switzerland: 1) interdisciplinary investigation and monitoring of short and long-term earthquake preparation processes at a regional scale, and 2) the study of complex non-linear surface effects induced by seismic strong ground motion at a local scale. The interest is in tectonic processes and the related variability of seismicity in space and time, earthquake forecasting and observation of possible short-term precursors, and modeling and observation of weak and strong ground motion as a result of complex source and path effects. For soils and rock, we study non-linear wave propagation phenomena and liquefaction, the long-term impacts of repeated earthquakes on slope stability through rock-mass strength degradation, and the triggering of landslides and snow avalanches. The integrated approach includes detailed field investigations with new field techniques, the development and application of numerical modeling techniques, and the installation of prototype multi-sensor monitoring systems. The multi-sensor monitoring system and a central database are the key elements supporting the research activities. The monitoring system is planned to be operational for several decades, with a high probability that it will monitor the next damaging earthquake in Valais. It includes a local densification of the existing national continuous GPS and seismic networks, a test installation with magnetic and geo-chemical sensors for observing earthquake precursors, and different borehole installations to study site-effects and non-linear phenomena in two test areas.

The Valais is the most seismically active area in Switzerland. Earthquake epicenters in northern Valais follow a more or less ENE-WSW trending alignment situated north of and parallel to the Rhone Valley, while in the southern Valais (Switzerland) and in Haute Savoie (France) seismicity is more scattered (Figure 2.6.2, top). The area is composed of two main tectonic units – the Helvetic domain in northern Valais and in most of the Haute Savoie, and the Penninic domain in southern Valais. In the northern Valais and Haute Savoie, earthquake focal mechanisms are predominantly strike-slip with P-axes orientations mainly NW-SE, while in the southern Valais they show normal faulting with T-axes oriented in a N-S direction. Active fault planes could be identified for 12 different earthquake sequences (Mauvoisin, two sequences of Anzère, Gd. Bornand, Leukerbad, Annecy, Samoëns, Martigny, Glarey, Derborence, Vallorcine and Sierre) (Fäh et al., 2011b) by applying a precise relative location procedure (e.g. Maurer and Deichmann, 1995; Maurer *et al.*, 1997; Fréchet *et al.*, 2011) (Figure 2.6.2, bottom).

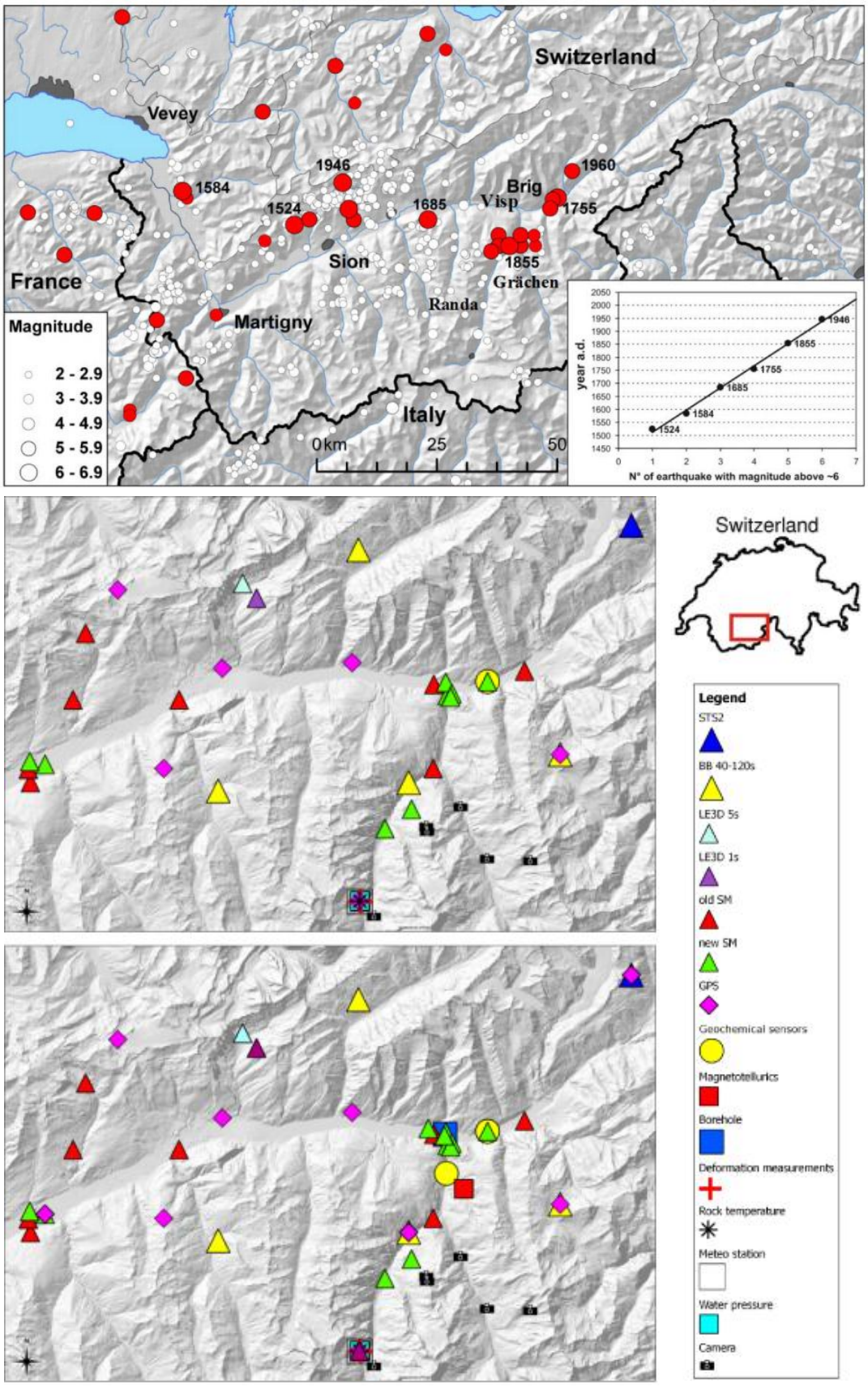


***Figure 2.6.1.*** *Top: Seismicity in the Valais. Below: present status of sensors and plan for the full system in 2012.*

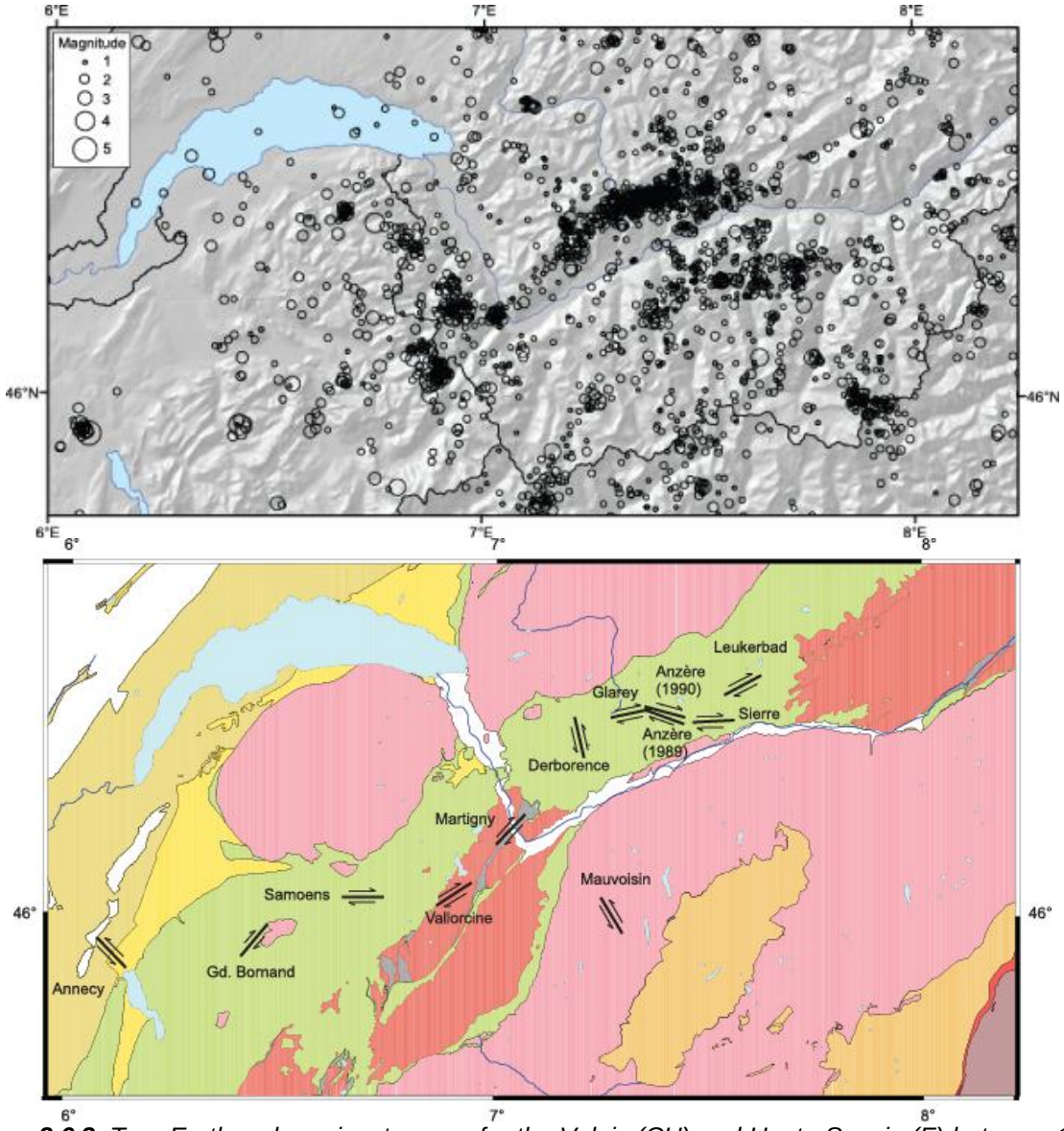


***Figure 2.6.2.*** *Top: Earthquake epicenter map for the Valais (CH) and Haute Savoie (F) between 1984 and 2010 with $M_L \geq 1.0$. Bottom: Tectonic map of the Valais (CH) and Haute Savoie (F) and orientation and slip of those active focal mechanism fault planes identified from precise relocations of earthquake sequences. Note that the dimensions of the fault planes are not to scale (from Fäh et al. (2011b)).*

At first glance, the orientations of active fault planes identified in the Helvetic domain and in the Aiguilles Rouges Massif seem unsystematic. However, on a regional scale they are compatible with a rotation of the direction of maximum compression from E-W oriented compression south of the Lake of Geneva to NW-SE oriented compression in the Helvetic domain of northern Valais. On a local scale, this would mean that some of the identified fault planes are unfavorably oriented for rupture. Comprehensive analysis of the state of stress in the region based on focal mechanisms available up to 1998 was published by Kastrup *et al.* (2004). An update of this analysis incorporating newer data is currently underway.

When possible, GPS sites have been co-located with seismic stations. For velocity estimation with reasonable accuracy, observations must be recorded for several years to precisely determine and reduce seasonal effects and increase the reliability of the obtained results. Preliminary results of an interpolated velocity field are shown in Figure 2.6.3. When velocities from all sites are available, local deformation will be better constrained and detailed comparisons with earthquake focal mechanisms possible.

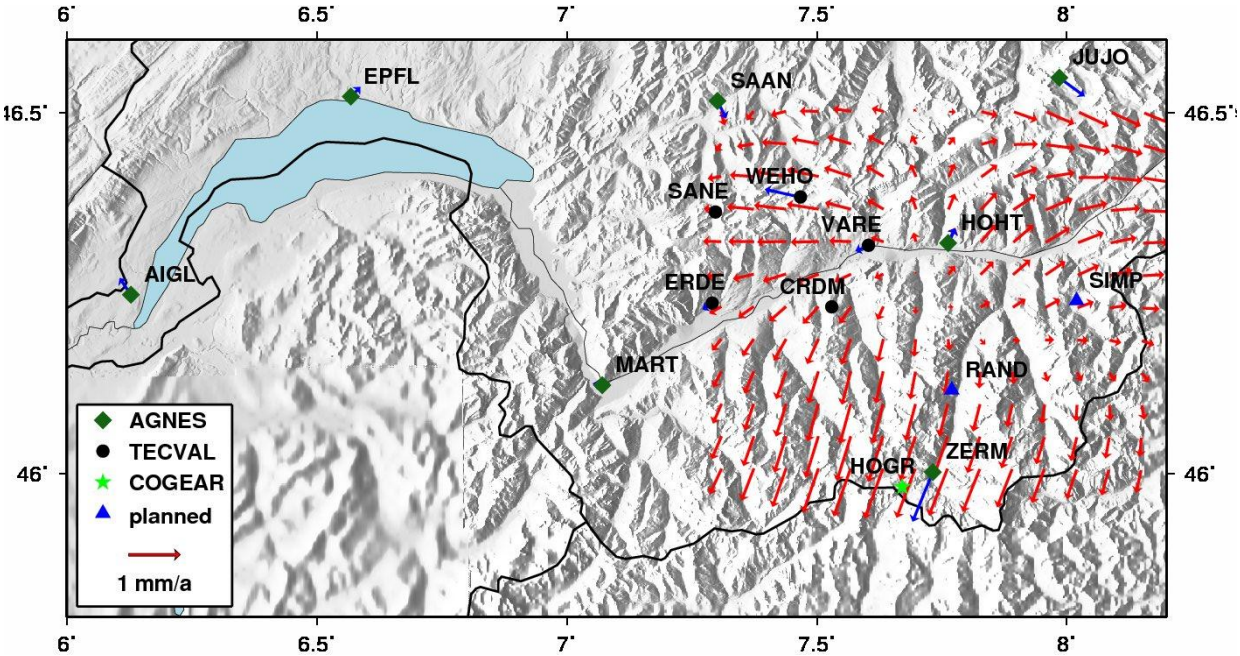


***Figure 2.6.3.*** *Preliminary velocity field (red arrows) derived from velocities calculated by Swisstopo (blue arrows). Stations CRDM and SANE are not included in the interpolation. Existing and planned continuous GNSS stations: project AGNES (diamond), TECVAL (circle), COGEAR (star), and planned (triangle). (from Fäh et al., 2011b).*

## Network descriptions

Networks of modern seismic and GPS stations have been operational in the Valais area for more than a decade. The instrumentation described focuses on new and existing parts of the national networks located in the epicentral areas of the 1755 and 1855 earthquakes, including the Rhone river plain at Visp and the Alpine valley at St. Niklaus. The present instrumental network status and plan for the final network is shown in Figure 2.6.1.

## 2.6.1 Seismic and strong motion networks, including borehole sensors

### *2.6.1.1 Network and hardware*

**Seismic network:**

The seismic network in Switzerland migrated to a uniformly 24-bit, predominantly broadband set of 30 stations from 1999-2002. As part of this scheme, 5 STS-2 (EMV, AIGLE, SENIN, DIX, MMK) and 4 short period (GRYON, SALAN, LKBD, LKDB2) stations were installed in the Valais. As shown in Figure 2.6.4, the majority of these stations were located in the lower Valais. In the framework of the COGAER project, a densification of the seismic network in the Upper Valais, with four semi-broadband and one broadband station in the region was completed in 2010. The stations completed in 2009 were Fiescheralp (FIESA), Val d'Anniviers (VANNI), Embd (EMBD) and Simplon Pass (SIMPL), and in 2010 the station at Lauchneralp (LAUCH). The stations are complemented with the network of new strong motion stations in Visp and the Matter valley, described in the next section, this new dense network will be used to test ground motion prediction models. Some of the planned GPS stations will be co-located at some of the sites of semi-broadband stations. By the end of 2010 all new stations were fully integrated into the Swiss Digital Seismic Network (SDSNet), with real time continuous communication. This provides a significant reduction in the

threshold magnitude for earthquake detection throughout the upper Valais region. Future seismic events occurring in the target region of Visp/St. Niklaus will have excellent azimuthal station coverage at close distances to produce extremely reliable event locations and depths.

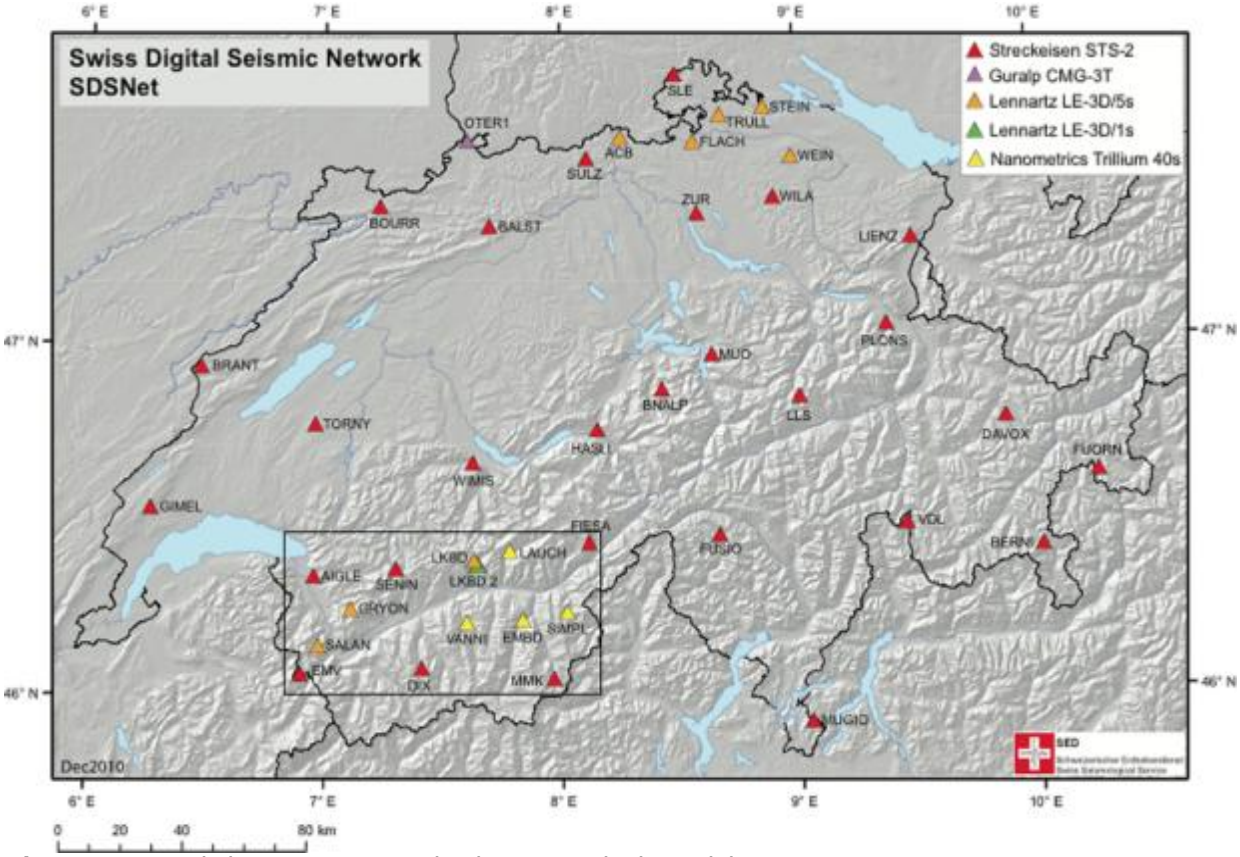


***Figure 2.6.4.*** *Existing permanent seismic sensors in the Valais.*

***Table 2.6.1*** *List of seismic stations contributing data to the VA near-fault observatory.*

| Station name | Latitude °N | Longitude °E | Elevation m | Sensor Depth m |
|---|---|---|---|---|
| AIGLE | 46.34161 | 6.95336 | 800 | (-) |
| BIBA | 46.30255 | 7.93038 | 660 | (-) |
| DIX | 46.08007 | 7.40815 | 2410 | (-) |
| EMBD | 46.21652 | 7.83223 | 1180 | (-) |
| EMV | 46.06318 | 6.89883 | 2210 | (-) |
| FIESA | 46.43527 | 8.11043 | 2338 | (-) |
| GRYON | 46.25053 | 7.11106 | 1300 | (-) |
| LAUCH | 46.41554 | 7.77166 | 2160 | (-) |
| LKBD | 46.38703 | 7.62714 | 1550 | (-) |
| LKBD2 | 46.37455 | 7.64433 | 2128 | (-) |
| MMK | 46.05053 | 7.96399 | 2210 | (-) |
| SALAN | 46.1441 | 6.973 | 1885 | (-) |
| SALT | 46.2173 | 7.3645 | 702 | (-) |

| | | | | |
|---|---|---|---|---|
| SAYF | 46.288 | 7.4171 | 1081 | (-) |
| SBRG | 46.311 | 7.9763 | 721 | (-) |
| SDI1[(1)] | 46.081 | 7.4009 | 2406 | (-) |
| SDI2[(1)] | 46.0805 | 7.4035 | 2406 | (-) |
| SDI3[(1)] | 46.0801 | 7.4061 | 2406 | (-) |
| SDI4[(1)] | 46.0805 | 7.4035 | 2144 | (-) |
| SDI5[(1)] | 46.0817 | 7.4037 | 2144 | (-) |
| SDIF | 46.0841 | 7.4018 | 2222 | (-) |
| SEM1[(1)] | 46.0677 | 6.9346 | 1979 | (-) |
| SEM2[(1)] | 46.0678 | 6.9332 | 1979 | (-) |
| SEM3[(1)] | 46.0675 | 6.9319 | 1979 | (-) |
| SEM4[(1)] | 46.0675 | 6.9319 | 1824 | (-) |
| SENIN | 46.36335 | 7.2993 | 2035 | (-) |
| SGRA | 46.193636 | 7.835612 | 1591 | 0.7[(2)] |
| SIES | 46.2877 | 7.54854 | 504 | (-) |
| SIMPL | 46.23962 | 8.01958 | 1930 | (-) |
| SIOM | 46.2289 | 7.3618 | 552 | 0.7[(2)] |
| SIOO | 46.2328 | 7.3832 | 495 | (-) |
| SIOV | 46.2351 | 7.36423 | 560 | 0.7[(2)] |
| SMA1[(1)] | 46.0491 | 7.9599 | 2256 | (-) |
| SMA2[(1)] | 46.0501 | 7.9641 | 2256 | (-) |
| SMA3[(1)] | 46.0491 | 7.9599 | 2147 | (-) |
| SMAF | 46.0567 | 7.9546 | 2127 | (-) |
| SMAR | 46.2079 | 6.9949 | 662 | (-) |
| SMAV | 46.1002 | 7.0878 | 527 | (-) |
| SMUK | 46.2863 | 6.9406 | 388 | (-) |
| SMUR | 46.2772 | 6.9205 | 480 | (-) |
| SNIB | 46.177142 | 7.802367 | 1110 | 0.7[(2)] |
| STAM | 46.2288 | 7.8625 | 921 | (-) |
| STSW | 46.3451 | 7.4325 | 1826 | (-) |
| SVIL | 46.29225 | 7.88653 | 647 | 0.7[(2)] |
| SVIO | 46.2908 | 7.88033 | 650 | 0.7[(2)] |
| SVIP | 46.3002 | 7.8636 | 697 | (-) |
| SVIT | 46.289679 | 7.884962 | 651.9 | 0.7[(2)] |
| VANNI | 46.21006 | 7.59678 | 1520 | (-) |

[(1)] dam-related station
[(2)] average embedment of new Swiss strong-motion vaults

***Table 2.6.2*** *Technical specifications of seismic stations in the VA observatory.*

| Station Name | SP Type Corner freq.$^{-1}$ | BB Type Corner freq.$^{-1}$ | SM Type | Sensor sensitivity V/m/s | Sensor sensitivity V/m/s$^2$ | Digitizer Type | Digitizer gain µV/bit | Transmission | Power | Data | Sampling rate s$^{-1}$ |
|---|---|---|---|---|---|---|---|---|---|---|---|
| AIGLE | (-) | STS-2, 120 s | (-) | 1500 | (-) | HRD-24 | 2.36 | ADSL | Mains | C | 120 |
| BIBA | (-) | (-) | Episensor ES-T | (-) | 1.019 | Taurus | 2.5 | ADSL | Mains | C | 250 |
| DIX | (-) | STS-2, 120 s | Episensor ES-T | 1500 | 1.019 | HRD-24 | 2.36 | ADSL | Mains | C | 120 |
| EMBD | (-) | Trillium, 40 s | (-) | 1553 | (-) | Taurus | 2.5 | ADSL | Mains | C | 120 |
| EMV | (-) | STS-2, 120 s | Episensor ES-T | 1500 | 1.019 | HRD-24 | 2.36 | ADSL | Mains | C | 120 |
| FIESA | (-) | STS-2, 120 s | (-) | (-) | (-) | Trident | 2.5 | ADSL | Mains | C | 120 |
| GRYON | Lennartz 3D, 5s | (-) | (-) | 400 | (-) | HRD-24 | 2.36 | ADSL | Mains | C | 120 |
| LAUCH | (-) | Trillium, 40 s | (-) | 1553 | (-) | Taurus | 2.5 | ADSL | Mains | C | 120 |
| LKBD | Lennartz 3D, 5s | (-) | (-) | 400 | (-) | HRD-24 | 2.36 | ADSL | Mains | C | 120 |
| LKBD2 | (-) | (-) | (-) | 400 | (-) | (-) | (-) | (-) | Mains | C | 120 |
| MMK | (-) | STS-2, 120 s | Episensor ES-T | 1500 | 1.019 | HRD-24 | 2.36 | ADSL | Mains | C | 120 |
| SALAN | Lennartz 3D, 5s | (-) | (-) | 400 | (-) | HRD-24 | 2.36 | ADSL | Mains | C | 120 |
| SALT | (-) | (-) | AC23 | (-) | | SMACH SM-2 12 bit | 408.163 * | Modem | Mains | E | 128 |
| SAYF | (-) | (-) | AC23 | (-) | | SMACH SM-2 12 bit | 408.163 * | Modem | Mains | E | 128 |
| SBRG | (-) | (-) | AC23 | (-) | | SMACH SM-2 12 bit | 408.163 * | Modem | Mains | E | 128 |
| SDI1 | (-) | (-) | MS2002 | (-) | | Syscom MR-2002 12bit | 418.409 * | Modem | Mains | E | 200 |
| SDI2 | (-) | (-) | MS2002 | (-) | | Syscom MR-2002 12bit | 418.409 * | Modem | Mains | E | 200 |
| SDI3 | (-) | (-) | MS2002 | (-) | | Syscom MR-2002 12bit | 418.409 * | Modem | Mains | E | 200 |
| SDI4 | (-) | (-) | MS2002 | (-) | | Syscom MR-2002 12bit | 418.409 * | Modem | Mains | E | 200 |
| SDI5 | (-) | (-) | MS2002 | (-) | | Syscom MR-2002 12bit | 418.409 * | Modem | Mains | E | 200 |
| SDIF | (-) | (-) | MS2002 | (-) | | Syscom MR-2002 12bit | 418.409 * | Modem | Mains | E | 200 |
| SEM1 | (-) | (-) | MS2002 | (-) | | Syscom MR-2002 12bit | 418.409 * | Modem | Mains | E | 200 |
| SEM2 | (-) | (-) | MS2002 | (-) | | Syscom MR-2002 12bit | 418.409 * | Modem | Mains | E | 200 |

| | | | | | | | | | | | |
|---|---|---|---|---|---|---|---|---|---|---|---|
| SEM3 | (-) | (-) | MS2002 | (-) | | Syscom MR-2002 12bit | 418.409 * | Modem | Mains | E | 200 |
| SEM4 | (-) | (-) | MS2002 | (-) | | Syscom MR-2002 12bit | 418.409 * | Modem | Mains | E | 200 |
| SENIN | (-) | STS-2, 120 s | Episensor ES-T | 1500 | 1.019 | HRD-24 | 2.36 | ADSL | Mains | C | 120 |
| SGRA | (-) | (-) | Episensor ES-T | (-) | 1.019 | Taurus | 2.5 | ADSL | Mains | C | 250 |
| SIES | (-) | (-) | AC63 | (-) | | SMACH SM-2 12 bit | 204.082 * | Modem | Mains | E | 250 |
| SIMPL | (-) | Trillium, 40 s | (-) | 1553 | (-) | Taurus | 2.5 | ADSL | Mains | C | 120 |
| SIOM | (-) | (-) | Episensor ES-T | (-) | 1.019 | Taurus | 2.5 | ADSL | Mains | C | 250 |
| SIOO | (-) | (-) | Episensor ES-T | (-) | 1.019 | Taurus | 2.5 | ADSL | Mains | C | 250 |
| SIOV | (-) | (-) | Episensor ES-T | (-) | 1.019 | Taurus | 2.5 | ADSL | Mains | C | 250 |
| SMA1 | (-) | (-) | MS2002 | (-) | | Syscom MR-2002 12bit | 418.409 * | Modem | Mains | E | 200 |
| SMA2 | (-) | (-) | MS2002 | (-) | | Syscom MR-2002 12bit | 418.409 * | Modem | Mains | E | 200 |
| SMA3 | (-) | (-) | MS2002 | (-) | | Syscom MR-2002 12bit | 418.409 * | Modem | Mains | E | 200 |
| SMAF | (-) | (-) | MS2002 | (-) | | Syscom MR-2002 12bit | 418.409 * | Modem | Mains | E | 200 |
| SMAR | (-) | (-) | SMACH SM-2 12 bit | (-) | | SMACH SM-2 12 bit | 408.163 * | Modem | Mains | E | 256 |
| SMAV | (-) | (-) | SMACH SM-2 12 bit | (-) | | SMACH SM-2 12 bit | 204.082 * | Modem | Mains | E | 256 |
| SMUK | (-) | (-) | Episensor ES-T | (-) | 1.019 | Taurus | 2.5 | ADSL | Mains | C | 250 |
| SMUR | (-) | (-) | Episensor ES-T | (-) | 1.019 | Taurus | 2.5 | ADSL | Mains | C | 250 |
| SNIB | (-) | (-) | Episensor ES-T | (-) | 1.019 | Taurus | 2.5 | ADSL | Mains | C | 250 |
| STAM | (-) | (-) | AC23 | (-) | | SMACH SM-2 12 bit | 5102.04 * | Modem | Mains | E | 200 |
| STSW | (-) | (-) | AC23 | (-) | | SMACH SM-2 16 bit | 408.163 * | Modem | Mains | E | 128 |
| SVIL | (-) | (-) | Episensor ES-T | (-) | 1.019 | Taurus | 2.5 | ADSL | Mains | C | 250 |
| SVIO | (-) | (-) | Episensor ES-T | (-) | 1.019 | Taurus | 2.5 | ADSL | Mains | C | 250 |
| SVIP | (-) | (-) | AC23 | (-) | (-) | SMACH SM-2 12 bit | 408.163 * | Modem | Mains | E | 256 |
| SVIT | (-) | (-) | Episensor ES-T | (-) | 1.019 | Taurus | 2.5 | ADSL | Mains | C | 250 |
| VANNI | (-) | Trillium, 40 s | (-) | 1553 | (-) | Taurus | 2.5 | ADSL | Mains | C | 120 |

(*) overall station sensitivity in count/(m/s$^2$)

***Strong motion network:***

In the early 1990's, 70 triggered, 12/16-bit accelerometers were installed across Switzerland in the original strong motion network; in the Valais, 9 stations were located in urban areas, and 4 arrays were located in key reservoir dams. In the past decade, new high quality, 24-bit real-time continuous strong motion stations were added in the region, at 4 sites co-located with the broadband sensors (EMV, MMK, SENIN, DIX), and 4 sites in Alpine valley sediments (SMUK, SIOV, SIOO) or slopes (SMUR) (Figure 2.6.5). As part of the COGEAR project, 4 new accelerometer stations and a borehole are being installed in Visp to better understand the amplification in the Rhone sediments and at the basin edges. Three new permanent strong motion stations were installed in 2010: the Visp Obere Stapfengasse (SVIO) station, a reference rock site station in the old city centre, the Visp Terbinerstrasse (SVIT) station on the alluvial fan under the hospital of Visp and the Visp Litterna (SVIL) station, on the Rhone sediments in the centre of the city.

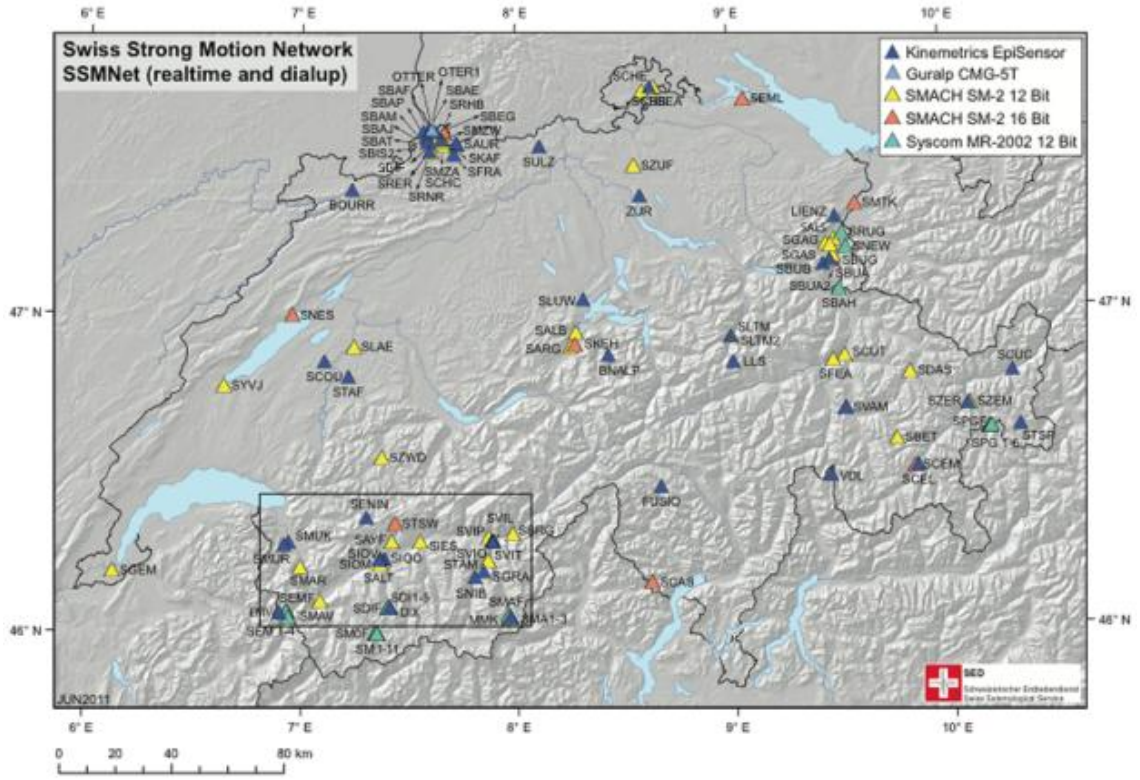


***Figure 2.6.5.*** *Existing permanent strong motion sensors in the Valais (SW Switzerland).*

The strong motion network is in the process of a renewal program, where by 2012 the old network will be replaced by 30 real-time, continuous 24bit accelerometer stations. As part of this project, the old SSM station SVIP in the middle of the Rhone valley to the West of Visp will be upgraded. Other new or upgraded strong motion stations part of the renewal project in the region are SNIB (St-Niklaus, installed 2010), SGRA (Grächen, installed 2010) and SIOM (Sion, installed 2011).

A borehole site has been selected in Visp, with 3 strong-motion sensors located at different depths alongside deformation devices being installed during 2012. Additional

sensors will include pore water pressure transducers distributed over depth as well as a SAA (Shape Accel Array) which measures 3 components of acceleration and deformation, every 30cm-1m over depth.

#### *2.6.1.2 Software systems*

Although the currently official software system is described in the following Subsections, the Seismic Network is transitioning to the new ***SeisComP3*** software system. ***SeisComP3*** is a comprehensive community software which includes waveform acquisition, automated earthquake detection and source location and quantification, manual event relocation; event alerting; and waveform archiving and dissemination. *SeisComP3* is based on a coherent software base and a ***QuakeMl*** compliant database structure. *SeisComP3* is a development of GFZ and gempa GmbH, and was conceived to rapidly detect and quantify large potentially tsunamigenic events in Indonesia. The current operational system is based on ***Nanometrics NAQS*** acquisition and homegrown scripts using GSE2 format data. The *SeisComP3* is based on **SeedLink and ArcLink** for data exchange and access using continuous miniSEED data. The transition to the new system will take place in 2012, though already certain components of the existing system are being replaced by relevant *SeisComP3* systems (for example, data dissemination is via *ArcLink*)

For both systems, great effort is made to homogenize the two high gain and low gain networks. Acquisition, processing and archival paths are essentially identical for both broadband and strong motion stations.

*Acquisition, detection and transmission software*

All seismic sensors (broadband, short period and strong motion) are digitised locally on *Nanometrics* dataloggers. Data transfer from the field to the processing facility in Zurich is primarily via ADSL using a mix of high bandwidth military, goverment, commercial and power company lines. Real time data is collected in Zurich using a suite of fully redundent, duplicated ***NAQS*** servers at separate locations on the two ETH Zurich campuses. Gaps/missing packets are requested via retransmit requests. All data is transfered at high sample rates (120 sps for broadband, 250 sps for strong motion).

Real time data streams are also made available in ***SeedLink*** from the ***NAQS*** via ***nmxptool***. These streams are used for data sharing with other agencies, for rapid mSEED archival, and for ***SeisComp3*** processing.

*Automatic analysis software*

Earthquake Detection, Location and Quantification:

STA/LTA triggers are performed within the **NAQS software**. STA/LTA are computed in programmable frequency bands. Post picking using the ***Baer*** **picker** is performed, and events are detection-based on coincidence criteria of triggers/picks. Only the high gain channels are used for automatic locations. Automatic locations are made using a grid search using a 1-D Swiss model. Local Richter magnitudes are computed using a Wood-

Anderson filter on the horizontal components. The attenuation relation used is derived for the greater Swiss region. Locations are assigned a quality and if a high quality is reached, the location is automatically distributed to the scientific community, local authorities, public and media via ***qwids***, SMS, email, FTP as well as the SED website. Automatic solutions are available and distributed within 2 minutes for all Swiss events.

Once a location is computed, spectral moment magnitude and, if the event is large enough, moment-tensor-inversion producing focal mechanism and moment magnitude, are automatically invoked. Solutions are avialable within 10 minutes.

Other Products:

USGS ***ShakeMaps*** are also available typically within 6 minutes of an event, using both strong motion and broadband data. The SED produces automatic aftershock probabilities but these are not made available externally yet. The SED participates in the Early Warning prototype project in California, and the ***Virtual Seismologist System*** is implemented locally, but results are only distributed internally. The SED website solicits felt reports for larger events, and this information is collected and summarized internally.

*Manual analysis software*

The current manual analysis package used is called ***SNAP***. It is an internally developed software. In addition to the standard grid-search solutions, manual relocations are possible using ***NonLinLoc***, a probabilistic location software, using Swiss specific local 1D- and 3D-velocity models. Strong motion data is included for these locations and magnitudes where relevant.

These same features are currently being developed for the ***SeisComp3*** relocation software GUI called ***scolv***. Final, catalogue-quality relocated solutions are typically available within 30 minutes to 1hour after a large event.

*Quality control processes*

***Hobbit*** is used to monitor data completeness, network latency, connection to the stations as well as internal seismic network software and hardware. ***PQLX*** is used routinely on all seismic data to evaluate data quality, with nightly updates. Alerts are sent via ***Hobbit*** notifying of any sensor or system failures, loss of connections to the stations, or degradation of waveform quality from normal performance.

*Data formats, accessible data bases and available data*

The native Nanometrics/Syscom/Kinemetrics data formats are routinely converted to the standard ***GSE2*** format used by the SED and to *miniSEED* for data dissemination to the public. The continuous waveforms are archived permanently on *NAS*, maintained by the Informatik Department at the ETH. This continuous archive is complete and dates back to the first acquisition of the broadband data in 1999. The archive currently runs to about 10TB, roughly a 3$^{rd}$ of this is due to data collected in the Valais.

The continuous seismic data are available within ten minutes through SED's ***AutoDRM*** and ***Arclink@SED*** (arclink.ethz.ch). Swiss Data is made available in real-time to neighboring Seismic Networks (LED, BGR, INGV, ZAMG, Grenoble…) as well as European and Global Agencies (ORFEUS, GFZ, IRIS). Event and continuous data can be accessed via *Arclink@SED*, along with basic event and station metadata. Data from dial-up strong motion station are typically added to the waveform archive within a few hours after the event.

As part of the SED transition to *SeisComP3*, the SED now runs ***ArcLink***, a software product from GFZ, which allows open access via both scripting and web requests, to the entire continuous archives, making high-quality waveforms available to the seismological and engineering community. A project has been completed to migrate also all the triggered data into suitable standard format to be added to this dataset. All strong motion and weak motion data is available over this platform. Visit *arclink.ethz.ch*.

### *2.6.1.3 Station installation procedure*

***Seismic sensors***

Station Selection: Continuous seismic noise measurements are typically taken over a period of at least four days at potential installation sites. The noise spectra are then compared to the low noise earth model. In the Alpine foreland where the sedimentary layers are substantially thicker than in the more alpine regions, higher noise levels are accepted at the lower frequencies due to the oceanic microseisms as well as at higher frequencies due to greater noise from civilization. Noise spectra, updated daily, are available for all continuously monitored stations in the SDSNet and SSMNet networks in the *PQLX webpages*. Seismic stations are normally installed in declassified former military bunkers or caverns, which are usually cut into solid rock and exhibit excellent infrastructure.

***Figure 2.6.6.*** *Semi-broadband station LAUCH installed at Laucheralp in 2010.*

Station installation: In hard rock sites inside tunnels or bunkers, the sensor is typically placed directly on rock and protected by insulation and in some cases a brick wall. If needed, on sloping ground, a thin concrete plinth is made. On soil sites or outside, the sensor is installed inside a 'pot' designed for the strong motion stations. If possible, the pot is deep enough to directly contact the rock. Whether connected to rock or soil, the pot is coupled to the ground using deep steel rods.

***Strong-motion sensors***

Consistent with the SED Seismic Network approach to seamlessly handle accelerometer and broadband data with identical real-time acquisition, processing and continuous data archiving, site selection is emphasized to minimize local noise as much as possible, even in urban/industrialized locations. This includes research on site effects and data quality constraints, in order to maximize usage of the collected data. It is therefore critical to gather test data at potential new sites, and the acquired data is analyzed through seismological community tools (e.g. *PQLX*) and compared with both world-wide and local noise models.

As a part of the renewal project of the whole strong-motion network of Switzerland, a new housing solution has been designed, drawing some inspiration from the Japanese and Italian experiences, allowing free-field installations, thus minimizing the effects of anthropic and electrical noise and is notably suitable for systematic relocation of the existing stations inside transformer houses. The 'pot' vault consists of a concrete cylinder with a metallic cover, and hosts the sensor. A separate casing with the datalogger and communication systems can be placed either inside the vault, or several meters away from the station. The vault is anchored to the ground via steel bars in order to avoiding ground settlement, relative displacements and rotations. Once installed, the sensor is insulated to minimise long period disturbances. Since 2009, if possible, a site characterization is also performed for new sites, with the main goal of determining the shear-wave velocity profile of the site.


***Figure 2.6.7.*** *Strong motion station SVIL installed in the Visp municipal area in 2010.*

## 2.6.2 GPS network

### *2.6.2.1 Network and hardware*

A dense network of 20 continuous GPS stations is planned for the Valais. Together with the 11 existing stations, the improved network will help to constrain crustal movement in the area with good spatial and temporal resolution. The Federal Office of Topography (swisstopo) is operating most of the stations. It was established in 1988 on its new national first order GPS based Reference Network LV95 (Landesvermessung, 95), and in addition built up an automatic permanent GPS reference network (AGNES) of about 34 stations. Three of the permanent stations are located in the canton Valais (MART, HOHT, ZERM). The institute of Geodesy and Photogrammetry at ETH Zürich has expanded the network during 2005 to 2006 in the frame of project TECVAL. This project investigates the Wildstrubel area (North of the Rhone Valley), where additional sites have been installed. Five new sites with new geodetic GPS instrumentation (Trimble NetRS receiver & Zephyr Antenna) are operated permanently. The data of three stations are transferred to swisstopo and included into the automated analysis of the AGNES network by swisstopo (ERDE, VARE and WEHO). To obtain a better coverage of the area around Visp or the Matter valley, new permanent GNSS sites are planned to be installed with the GPRX1200+ receiver and choke-ring antenna AR25 from Leica. The use of choke-ring antennas will reduce multipath effects and lead to better results, which is vital as the expected relative annual displacements are very small (1 mm range). If possible, GPS sites are co-located with seismic stations.

The GPS network is operated by swisstopo and the institute of Geodesy and Photogrammetry at ETH Zürich. More information is available from their websites: http://www.swisstopo.admin.ch/ and http://www.ggl.baug.ethz.ch/index.

### *2.6.2.2 Software systems*

Information is available from the websites of swisstopo (http://www.swisstopo.admin.ch/) and the institute of Geodesy and Photogrammetry at ETH Zürich (http://www.ggl.baug.ethz.ch/index).

*Data formats, accessible data bases and available data*

GPS data *(continuous and campaign)* are avaliable from the Federal Office of Topography (swisstopo).

### *2.6.2.3 Station installation procedures*

Information is available from the websites of swisstopo (http://www.swisstopo.admin.ch/) and the institute of Geodesy and Photogrammetry at ETH Zürich (http://www.ggl.baug.ethz.ch/index).

### 2.6.3 Strain meters

#### *2.6.3.1 Network and hardware*

For monitoring of unstable rock masses, a new fiber optic strain measurement system installed at the Randa in-situ laboratory has been successfully tested. The sensors are able to measure micro-strain deformations. The system is operated by the Engineering Geology group at ETH Zürich, and specific information is available at the website https://www1.ethz.ch/engineeringgeology/.

#### *2.6.3.2 Software systems*

The system is operated by the Engineering Geology group at ETH Zürich, and specific information is available at the website https://www1.ethz.ch/engineeringgeology/.

#### *2.6.3.3 Station installation procedures*

The system is operated by the Engineering Geology group at ETH Zürich, and specific information is available at the website https://www1.ethz.ch/engineeringgeology/.

### 2.6.4 Geochemical monitoring

#### *2.6.4.1 Nework and hardware*

A specially designed fluorometer is installed at the Brigerbad thermal spring and is now continuously recording. With this instrument the fluorescence is measured in 3 channels of different wavelengths. These channels are named according to the most prominent artificial tracer, which wavelength is within the chosen interval: *Naphthionate* with its interval of fluorescence spectra being most sensitive to humic acids, *Tinopal X*'s interval of the fluorescence spectra being the most sensitive to tectonic caused perturbations of the water fluorescence, and is therefore the most promising for the perception of seismic precursor phenomena, and finally *Uranine*'s spectral interval being already at higher wavelengths than those of interest for the observation of natural variations as seismic precursor signals. As a fourth channel, the turbidity of the water is monitored, because turbidity influences the fluorescence measurements and is used therefore as an internal correction parameter of the fluorometers themselves. Additionally, water temperature, $CO_2$, $CH_4$ and Radon are measured at the same time intervals as the other parameters.

The goal of this installation is to monitor geochemical changes in the spring water, which could be related to intermediate and large earthquakes on an active fault system. The fault system below Brigerbad can be related to the damaging earthquake of 1755 (Mw 5.7). This geochemical installation is part of a permanent multi-sensor instrumentation for the detection of non-seismic, short-term earthquake precursors, including installations of electromagnetic stations and multi-sensor geochemical hot-spring monitoring systems.

***Table 2.6.3*** *Chemical station contributing data to the VA near-fault observatory.*

| Station code | Station name | Latitude °N | Longitude °E | Elevation M | Sensor Depth M |
|---|---|---|---|---|---|
| RQV | Brigerbad thermal well | 46.30294 | 7.93102 | 709 | (-) |

***Table 2.6.4a*** *Technical specifications of the chemical station in the Valais observatory; Gas chemistry instrumentation.*

| Observed property | Sensor architecture | Digitizer/ Logger 1 | Logger 2 | Minimum resolution | Usable dynamic range | Trans-mission | Power | Sampling interval s |
|---|---|---|---|---|---|---|---|---|
| CO2 | dual beam, non-dispersive IR-absorption | Nucfilm M_54 | Tetraédre TRMC5 | 0.01 Vol. % | ~9 bit | GPRS | AC, UPS | 3600 |
| CH4 | dual beam, non-dispersive IR-absorption | Nucfilm M_54 | Tetraédre TRMC5 | 0.01 Vol. % | ~9 bit | GPRS | AC, UPS | 3600 |
| Radon | Lucas cell / photomultiplier | Nucfilm M_54 | Tetraédre TRMC5 | 6,7 Bq/m$^3$ | ~14 bit | GPRS | AC, UPS | 3600 |

***Table 2.6.4b*** *Technical specifications of the chemical station in the Valais observatory; Fluorescence instrumentation.*

| Observed property | Sensor architecture, digitizer | Logger | Minimum resolution | Usable dynamic range | Transmission | Power | Sampling Interval s |
|---|---|---|---|---|---|---|---|
| Fluorescence (Uranine band–514 nm) | Schnegg GGUN-FL30, 24bit | TRMC5 | unknown[1)] | ? | GPRS | AC, UPS | 300 |
| Fluorescence (Rhodamine – 555 nm) | Schnegg GGUN-FL30, 24bit | TRMC5 | unknown[1)] | ? | GPRS | AC, UPS | 300 |
| Fluorescence (Tinopal band – 435 nm) | Schnegg GGUN-FL30, 24bit | TRMC5 | unknown[1)] | ? | GPRS | AC, UPS | 300 |
| Turbidity | Schnegg GGUN-FL30, 24bit | TRMC5 | unknown[1)] | 0.02..400 NTU | GPRS | AC, UPS | 300 |
| Temperature | Schnegg GGUN-FL30 | TRMC5 | 0.1°C | ~9 bit | GPRS | AC, UPS | 300 |

1) Measurement is relative and no calibration/nor resolution can be defined.

### *2.6.4.2 Software systems*

The acquisition of geochemical data involves different pieces of software, and forwards the data to different channels for different purpose:

Primary acquisition is done using the ***TDS software of*** *Tetraédre SA*, the provider of the TRMC-5 logger (http://www.tetraedre.ch/product_view.php?product_id=18). *TDS*

acquires the data from the GPRS connection, dumps it into a *mysql* database as timestamp-value pairs and exposes it to a simple web interface for quick monitoring. The SED *TDS* installation is available at http://multisensor.ethz.ch/visualisation/index.php. The interface, however is password protected.

For data exchange with the Swiss Experiment platform, an integration project for the exchange of sensor data of any type in environmental monitoring (see www.swiss-experiment.ch), the GSN is used (Global Sensor Network, see http://sourceforge.net/projects/gsn/). For data acquisition a virtual instrument wrapper has been implemented, which connects to the *TDS* data repository. The SED GSN instance presents COGEAR hydrochemical data at http://multisensor.ethz.ch:22001/ for streaming and interactive retrieval.

For state-of-health monitoring, event triggering and waveform processing in full integration with the seismic network, a *TDS to SeedLink connector* has been written to stream the data to the SED *SeedLink* servers and miniSEED archives. This will make the data available also via *ArcLink* web at http://arclink.ethz.ch or *ArcLink-fetch*. However, in order to allow for this, a full dataless SEED representation of the sensors is still waiting for completion.

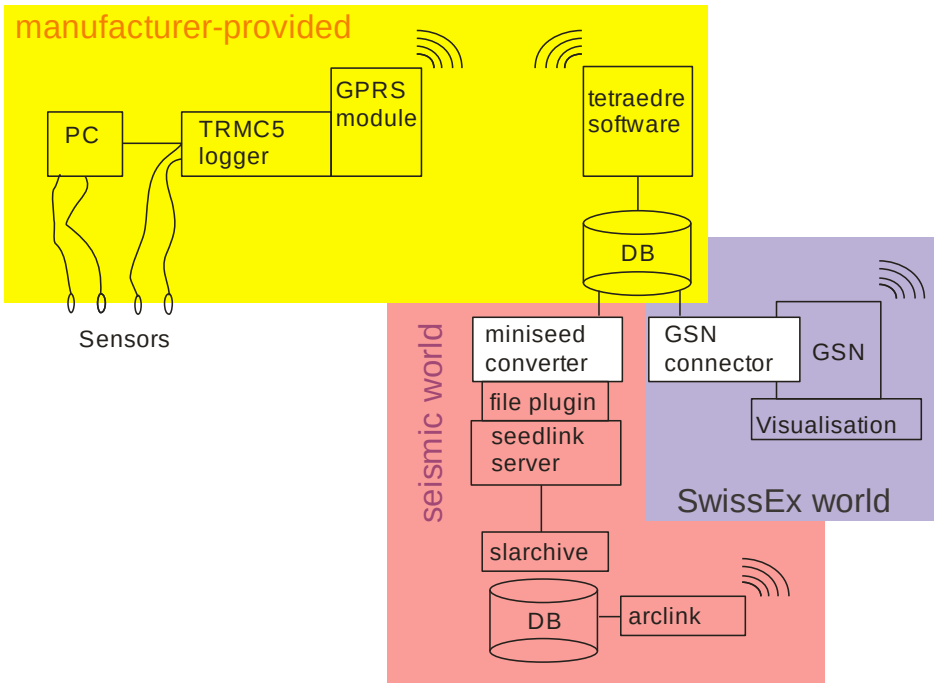


***Figure 2.6.8.*** *COGEAR hydrochemical data is multi-purpose and needs to be integrated with different data standards and streaming environments. However, this can be done with a minimum of custom software (white boxes: miniseed converter and GSN connector); all other components are provider and community standards.*

*Data formats, accessible data bases and available data*

A system to access chemical and pressure data from boreholes is under development.

#### *2.6.4.3 Station installation procedures*

Geochemical sensors need to sample geothermal springs that are not too much influenced by superficial water and anthropogenic effects. The selection of the sites is therefore not easy because most of the springs in the Valais area are in use, and the pumping may “shadow” the possible effects from earthquakes on the geochemical parameters. Some of the key points for a potential site are:

- The site should be easily accessible due to the long-term character of the monitoring system;
- The maintenance of the systems, in terms of instrumentation, data transmission and handling should be minimized;
- There is a need for multi-parametric analysis and different sensors should be placed sufficiently close to each other to sample the same spring water.

### 2.6.5 Magnetic and other EM sensors

#### *2.6.5.1 Network and hardware*

The location of the seismic sensor at EMBD (Table 2.6.1) in an isolated tunnel is a potential site for an off-line, magnetic test-installation starting in 2012, where three magnetic components will be collocated with the semi-broadband seismic instrument. Electric sensors, which are more sensitive to the locally high levels of anthropogenic noise, need more maintenance and are therefore not yet installed. Magnetic coils, rather than other sensors such as fluxgates will be installed. The full magnetic instrumentation (coils and data logger) are *Metronix*, and the instruments are presently being tested in the laboratory.

#### *2.6.5.2 Software systems*

To be developed.

#### *2.6.5.3 Station installation procedures*

Not yet defined.

### 2.6.6 Future Goals and Developments of the Valais Observatory

The main goals of the Valais Observatory is to increase station density in otder to improve the earthquake location accuracy and decrease the magnitude detection threshold. Furthermore to increse the density of magnetic and chemical stations in order to perform multiparameter, almost-real time analysis of data streams.

# 3 Bibliography of Main Research Papers Based on the Observatories

## 3.1 South Iceland Seismic Zone


Antonioli, A., M. E. Belardinelli, A. Bizzari, and K. S. Vogfjord (2006). Evidences of instantaneous triggering during the seismic sequence of year 2000 in south Iceland. J. Geophys. Res., 111, doi:10.1029/2005JB003935.

Ágústsson, K., A. T. Linde, R. Stefánsson, and I. S. Sacks (1999). Strain changes for the 1987 Vatnafjöll earthquake in south Iceland and possible magmatic triggering, J. Geophys. Res. 104, 1151-1161.

Ágústsson, K., A.T. Linde, R. Stefánsson & I.S. Sacks (2000). Borehole strain observations for the February 2000 eruption of Hekla, South Iceland. AGU spring meeting, Washington D.C., USA, May 30 - June 3, 2000.

Árnadóttir, T., S. Hreinsdóttir, G. Guðmundsson, P. Einarsson, M. Heinert, C. Völksen (2001). Crustal deformation measured by GPS in the South Iceland Seismic Zone due to two large earthquakes in June 2000. Geophys. Res. Lett., 28, 4031-4033.

Árnadóttir, T., S. Jónsson, R. Pederssen, and G. B. Guðmundsson (2003). Coulomb stress changes in the South Iceland Seismic Zone due to two large earthquakes in June 2000. Geophys. Res. Lett., 30(5), 1205, doi:10.1029/2002GL016.

Árnadóttir, T., H. Geirsson, and P. Einarsson (2004). Coseismic stress changes and crustal deformation on the Reykjanes Peninsula due to triggered earthquakes on June 17, 2000. J. Geophys. Res., 109, B09307, doi:10.1029/2004JB003130.

Árnadóttir, T., S. Jónsson, F. F. Pollitz,W. Jiang, and K. L. Feigl (2005). Postseismic deformation following the June 2000 earthquakes sequence in the south Iceland seismic zone. J. Geophys. Res., 110, B12309, doi:10.1029/2005JB003701.

Árnadóttir, T., W. Jiang, K. L. Feigl, H. Geirsson, and E. Sturkell, 2006. Kinematic models of plate boundary deformation in southwest Iceland derived from GPS observations. J. Geophys. Res., 111, B07402, doi:10.1029/2005JB003907.

Björnsson, G., Flóvens, Ó.. G., Sæmundsson, K. and Einarsson, E. M. (2001). Pressure changes in Icelandic geothermal reservoirs associated with two earthquakes in June 2000. Stanford University, Stanford, California. Proceedings of the Twenty-Sixth Workshop on Geothermal Reservoir Engineering.

Bödvarsson, R., S. Th. Rögnvaldsson, S. S. Jakobsdóttir, R. Slunga and R. Stefánsson (1996). The SIL Data Acquisition ans Monitoring System. Seism. Res. Lett., 67, 5, 35-46.

Bödvarsson, R., S. Th. Rögnvaldsson, R. Slunga, and E. Kjartansson (1998). The SIL data acquisition system – at present and beyond year 2000. Icelandic Meteorological Office, Rit, VÍ-R98005-JA04.

Clifton, A. E., F. Sigmundsson, K. L. Feigl, G. Guðmundsson, and T. Árnadóttir (2002). Surface effects of faulting and deformation resulting from magma accumulation at the Hengill triple junction, SW Iceland, 1994-1998. Journal of Volcanology and Geothermal Research, 115, 233-255.

Clifton, A. E., C. Pagli, J. F. Jónsdóttir, K. Eythorsdóttir, and K. Vogfjörð, 2003. Surface effects of triggered fault slip on Reykjanes Peninsula, SW Iceland. Tectonophysics, 369, 145-154.

Clifton, A., and P. Einarsson (2005). Styles of surface rupture accompanying the June 17 and 21, 2000 earthquakes in the South Iceland Seismic Zone. Tectonophysics, 396, 141-159.

Decriem, J., Th. Árnadóttir, A. Hooper, H. Geirsson, M. Keiding, B.G. Ófeigsson, F. Sigmundsson, S. Hreinsdóttir, P. LaFemina and R. Bennett (2010). The 29 May 2008 earthquake doublet in SW Iceland, Geophys. J. Int., 181(2), 1128-1146, doi: 10.1111/j.1365-246X.2010.04565.x.

Decriem, J. and Th. Árnadóttir (2011). Transient crustal deformation in the South Iceland Seismic Zone observed by GPS and InSAR during 2000-2008, Tectonophysics, doi:10.1016/j.tecto.2011.09.028.

Einarsson, P., S. Björnsson, G. Foulger, R. Stefánsson, and Th. Skaftadóttir (1981). Seismicity pattern in the South Iceland seismic zone, in: Earthquake Prediction – An International Review (eds. D. Simpson and P. Richards). American Geophys. Union, Maurice Ewing Series 4, 141-151.

Einarsson, P., and J. Eiríksson (1982). Earthquake fractures in the districts Land and Rangárvellir in the South Iceland Seismic Zone. Jökull, 32, 113-120.

Einarsson, P (2008). Plate boundaries, rifts and transforms in Iceland. Jökull, 58, 35-58.

Feigl, K., J. Gasperi, F. Sigmundsson, and A. Rigo (2000). Crustal deformation near Hengill volcano, Iceland 1993-1998: Coupling between magmatic activity and faulting inferred from elastic modeling of satellite radar interferograms. J. Geophys. Res., 105, 25,65525,670.

Geirsson, H., T. Árnadóttir, C. Völksen, W. Jiang, E. Sturkell, T. Villemin, P. Einarsson, F. Sigmundsson, and R. Stefánsson (2006). Current plate movements across the Mid-Atlantic Ridge determined from 5 years of continuous GPS measurements in Iceland. J. Geophys. Res., 111, B09407, doi: 1029/2005JB003717.

Hackman, M. C., G. C. P. King, and R. Bilham (1990). Mechanics of the South Iceland Seismic Zone. J. Geophys. Res., 95, 17,339-17,351.

Hjaltadóttir, S. and K. S. Vogfjörð (2005). Subsurface fault mapping in Southwest Iceland by relative location of aftershocks of the June 2000 earthquakes. Icelandic Meteorological Office, Rit nr. 21.

Hjaltadóttir, S. (2010). Use of relatively located microearthquakes to map fault patterns and estimate the thickness of the brittle crust in Southwest Iceland, MSc. Thesis, University of Iceland, Reykjavík, October 2009, pp. 104. Also published as an Icelandic Meteorological Office Report, VÍ 2010-003.

Hreinsdóttir, S., T. Árnadóttir, J. Decrim, H. Geirsson, A. Tyggvasson, R.A. Bennett, P. LaFemina (2009). A complex earthquake sequence captured by the continuous GPS network in SW Iceland, GRL, VOL. 36, L12309, doi:10.1029/2009GL038391.

Jakobsdóttir, S. S., G. B. Guðmundsson, and R. Stefánsson (2002). Seismicity in Iceland 1991-2000 monitored by the SIL-system. Jökull 51, 87-94.

Jónsson, S., P. Segall, R. Pedersen, and G. Bjornsson (2003). Post-earthquake ground movements correlated to pore-pressure transients, Nature, 424, 179-183.

LaFemina, P. C., T. H. Dixon, R. Malservisi, T. Árnadóttir,E. Sturkell, F. Sigmundsson, and P. Einarsson (2005). Geodetic GPS measurements in south Iceland: Strain accumulation and partitioning in a propagating ridge system, J. Geophys. Res., 110, B11405, doi:10.1029/2005JB003675.

Linde, A.T., K. Agustsson, I.S. Sacks, R. Stefansson (1993). Mechanism of the 1991 eruption of Hekla from continuous borehole strain monitoring, Nature, 365, 737-740, 1993.

Pagli, C., R. Pedersen, F. Sigmundsson, and K. L. Feigl (2003). Triggered fault slip on June 17, 2000 on the Reykjanes Peninsula, SW-Iceland captured by radar interferometry, Geophys. Res. Lett., 30(6), 1273, doi:10.1029/2002GL015310, 2003.

Pedersen, R., K. L. Feigl, S. Jónsson, T. Árnadóttir, and F. Sigmundsson (2001), Coseismic inferferograms of two Ms6.6 earthquakes in the South Iceland seismic zone, June 2000, Geophys. Res. Lett., 28, 3341–3344.

Pedersen, R., F. Sigmundsson, K. L. Feigl, and T. Árnadóttir (2003), Fault slip distribution of two June 2000 Mw6.5 earthquakes in south Iceland estimated from joint inversion of InSAR and GPS measurements, Earth Planet. Sci. Lett., 213, 487–502.

Pétursson, G. G. and K. S. Vogfjörd (2009). Attenuation relations for near- and farfield peak ground motion (PGV, PGA) and new magnitude estimates for large earthquakes in SW-Iceland for large earthquakes in SW-Iceland. Icelandic Meteorological Office Report, VÍ 2009-012, pp. 43.

Roth, F. (2004). Stress Changes Modelled for the Sequence of Strong Earthquakes in the South Iceland Seismic Zone Since 1706. Pure & Applied Geophysics, 161, 1305-1327.

Rögnvaldsson, S. Th., and R. Slunga (1993). Routine fault plane solutions for local networks: A test with synthetic data. Bull. Seismol. Soc. Am., 83, 1232-1247.

Rögnvaldsson, S. Th., and R. Slunga (1994). Single and joint fault plane solutions for miqroearthquakes in South Iceland. Tectonophysics, 237, 73-80.
Sella, G. F., T. H. Dixon, and A. Mao (2002). REVEL: A model for recent plate velocities from space geodesy, J. Geophys. Res., 107(B4), 2081, doi:10.1029/2000JB000033.
Sigmundsson, F., P. Einarsson, S. Rögnvaldsson, G. R. Foulger, K. M. Hodgkinson, and G. Thorbergsson (1997). The 1994-1995 seismicity and deformation at the Hengill triple junction, Iceland: Triggering of earthquakes by minor magma injection in a zone of horizontal shear stress. J. Geophys. Res., 102, 15,151-15,161
Slunga, R., S. Th. Rögnvaldsson, and R. Bödvarsson (1995). Absolute and relative locations of similar events with application to microearthquakes in southern Iceland. Geophys. J. Int., 123, 409-419.
Stefánsson, R., and P. Halldórsson (1988. Strain release and strain build-up in the south Iceland seismic zone. Tectonophysics, 152, 267-276.
Stefánsson, R., R. Böðvarsson, R. Slunga, P. Einarsson, S. Jakobsdóttir, H. Bungum, S. Gregersen, J. Havskov, J. Hjelme, and H. Korhonen (1993). Earthquake prediction research in the South Iceland seismic zone and the SIL project, Bull. Seismol. Soc. Am., 83, 696716.
Vogfjörd, K. S., S. Hjaltadóttir and R. Slunga (2005a). Volcano-tectonic Interaction in the Hengill Region, Iceland during 1993-1998. Geophysical Research Abstracts, 7, 09947.
Vogfjörd, K. S., S. Hjaltadóttir and R. Slunga (2005b). The M~5 triggered events in the South Iceland Seismic Zone of June 17, 2000: Determination of fault plane, magnitude and mechanism. Geophysical Research Abstracts, 7, EGU-A-10274.
Vogfjord, K. S., S. Hjaltadottir, H. Geirsson and R. Slunga, 2009. Fault Interaction in the South Iceland Seismic Zone: The May 2008, M6.3 earthquake. Geophysical Research Abstracts, Vol. 11, EGU2009-11748-1.
Vogfjörd, K. S., E. Kjartansson, R. Slunga, P. Halldórsson, S. Hjaltadóttir, G. B. Gudmundsson, H. Sveinbjörnsson, S. Ármannsdóttir, B. Thorbjarnardóttir, S. S. Jakobsdóttir (2010). Development and Implementation of Seismic Early Warning Processes in South-West Iceland. an Icelandic Meteorological Office Report, VÍ 2010-012, pp. 83.

## 3.2 North Anatolian Fault Zone

Aktar, M., Özalaybey, S., Ergin, M., Karabulut, H., Bouin, M.-P., Tapırdamaz, C., Biçmen, F., Yörük, A., and Bouchon M. (2004), Fault zone heterogeneity and variations of seismicity parameters across 1999 Izmit-Düzce earthquake sequence, Tectonophysics, 391, 325–334, doi:10.1016/j.tecto.2004.07.020.
Armijo, R., Meyer, B., Navarro, S., King, G., and Barka, A. (2002), Asymmetric slip partitioning in the Sea of Marmara pull-apart: A clue to propagation processes of the North Anatolian Fault, Terra Nova, 14, 80– 86, doi:10.1046/j.1365 3121.2002.00397.x.
Barka, A., et al. (2002), The surface rupture and slip distribution of the 17 August 1999 Izmit earthquake (M 7.4), North Anatolian Fault, Bull. Seismol. Soc. Am., 92, 43– 60, doi:10.1785/0120000841
Bohnhoff, M., H. Grosser, and G. Dresen (2006), Strain partitioning and stress rotation at the North Anatolian fault zone from aftershock focal mechanisms of the 1999 I Izmit Mw = 7.4 earthquake, Geophys. J. Int., 166, 373–385, doi:10.1111/j.1365-246X.2006.03027.x.
Bouchon, M., Toksöz, M.N., Karabulut, H., Bouin, M.-P., Dietrich, M., Aktar, M., and Edie, M. (2002), Space and time evolution of rupture and faulting during the 1999 Izmit (Turkey) earthquake, Bull. Seismol. Soc. Am., 92, 256–266, doi:10.1785/0120000845.
Bulut, F., Bohnhoff, M., Ellsworth, W. L., Aktar, M., and Georg Dresen, Microseismicity at the North Anatolian Fault in the Sea of Marmara offshore Istanbul, NW Turkey, JOURNAL OF GEOPHYSICAL RESEARCH, VOL. 114, B09302, doi:10.1029/2008JB006244, 2009
Erdik, M., 2000, “Report on 1999 Kocaeli and Duzce (Turkey) Earthquakes”, http://www.koeri.boun.edu.tr/depremmuh/eqspecials/kocaeli/Kocaelireport.pdf

Hergert, T., and Heidbach, O., Slip-rate variability and distributed deformation in the Marmara Sea fault system, NATURE GEOSCIENCE, VOL 3, FEBRUARY 2010

Herring, T.A., King, R.W., McClusky, S.C., 2010. Introduction to GAMIT/GLOBK, Release 10.4, Massachusetts Institute of Technology, Cambridge.

Hubert-Ferrari, A., Barka, A., Jacques, E., Nalbant, S. S., B. Meyer, Armijo, R., Traponnier P., and King, G. C. P., (2000), Seismic hazard in the Marmara Sea following the 17 August 1999 Izmit earthquake, Nature, 404, 269– 273, doi:10.1038/35005054.

Kandilli Observatory and Earthquake Research Institute National Earthquake Monitoring Center, 2009 Annual Report, 2010.

Karabulut, H., Bouin, M.-P., Bouchon, M., Dietrich, M., Cornou, C., and Aktar, M., (2002), The seismicity in the eastern Marmara Sea after the 17 August 1999 Izmit earthquake, Bull. Seismol. Soc. Am., 92, 387–393, doi:10.1785/0120000820.

LePichon, X., Taymaz T., and Sengör, C., (1999), The Marmara fault and the future Istanbul earthquake, in ITU-IAHS International Conference on the Kocaeli Earthquake 17 August 1999, edited by M. Karaca and D. N. Ural, pp. 41– 54, Istanbul Tech. Univ., Istanbul.

Orgulu, G., and Aktar, M., (2001), Regional moment tensor inversion for strong aftershocks of the August 17, Izmit earthquake (Mw = 7.4), Geophys. Res. Lett., 28, 371– 374, doi:10.1029/2000GL011991.

Ozalaybey, S., Ergin, M., Aktar, M., Tapirdamaz, C., Bicman, F., and Yörük, A. (2002), The 1999 Izmit earthquake sequence in Turkey: Seismological and tectonic aspects, Bull. Seismol. Soc. Am., 92, 376 – 386, doi:10.1785/0120000838.

Ozener, H., 2000. "Monitoring Regional Horizontal Crustal Movements by Individual Microgeodetic Networks Established Along Plate Boundaries“, Ph.D. Thesis, Bogazici University KOERI Geodesy Department, Turkey.

Parsons, T., Toda, S., Stein, R.S., Barka, A., and Dieterich, J.H (2000), Heightened odds of large earthquakes near Istanbul: An interaction-based probability calculation, Science, 288, 661 – 664, doi:10.1126/science.288.5466.661.

Parsons, T. (2004), Recalculated probability of M _ 7 earthquakes beneath the Sea of Marmara, Turkey, J. Geophys. Res., 109, B05304, doi:10.1029/2003JB002667

Pinar, A., Honkura, Y., and Kuge, K. (2001), Seismic activity triggered by the 1999 Izmit earthquake and its implications for the assessment of future seismic risk, Geophys. J. Int., 146, F1–F7, doi:10.1046/j.0956-540x.2001.01476.x.

Reilinger, R., Toksoz, N., McClusky, S., and Barka A. (2000), 1999 Izmit,Turkey, earthquakes was no surprise, GSA Today, 10(1), 1 – 6.

Stein, R. S., Barka, A., and Dieterich, J.H. (1997), Progressive failure of the North Anatolian Fault since 1939 by earthquake stress triggering, Geophys. J. Int., 128, 594–604, doi:10.1111/j.1365-246X.1997.tb05321.x.

Tibi, R., Bock, G., Xia, Y., Baumbach, M., Grosser, H., Milkereit, C., Karakisa, S., Zunbul, S., Kind, R., and Zschau, J. (2001), Rupture processes of the 1999 August 17 Izmit and November 12 Düzce (Turkey) earthquakes, Geophys. J. Int., 144, F1–F7, doi:10.1046/j.1365-246x.2001.00360.x.

Toksoz, M. N., Shakal, A.F., and Michael, A.J. (1979), Space-time migration of earthquakes along the North Anatolian Fault and seismic gaps, Pure Appl. Geophys., 117, 1258–1270, doi:10.1007/BF00876218.

U.S. Geological Survey (2000), Implications for Earthquake Risk Reduction in the United States from the Kocaeli, Turkey Earthquake of August 17, 1999, U. S. Geol. Surv. Circ., 1193.

Wright, T., Fielding, E., and Parsons, B., (2001), Triggered slip: Observations of the 17 August 1999 Izmit (Turkey) earthquake using radar interferometry, Geophys. Res. Lett., 28, 1079–1082, doi:10.1029/2000GL011776.

URL1, http://www.koeri.boun.edu.tr/depremmuh/eski/EWRR/EWEngWeb/TurAnaSayfa_eng1.htm

URL 2, http://www.guralp.com/gsl-install-obs-network-under-the-sea-of-marmara/

URL 3, http://www.trimble.com/

URL 4, http://facility.unavco.org/software/teqc/teqc.html

## 3.3 Alto Tiberina Fault

Construction of the TABOO observatory was completed in the summer 2001, which means that the scientific production has just started.


Blewitt, G. (2008), Fixed point theorems of GPS carrier phase ambiguity resolution and their application to massive network processing: Ambizap, *J. Geophys. Res.*, 113, B12410, doi:10.1029/2008JB005736.

Byerlee, J.D., 1978. Friction of rocks. *Pure and Applied Geophysics* 116, 615–626.

Chiaraluce, L., Chiarabba, C., Collettini, C., Piccinini, D., Cocco, M., 2007. Architecture and mechanics of an active low-angle normal fault: Alto Tiberina Fault, northern Apennines, Italy. *Journal of Geophysical Research* 112, B10310. doi:10.1029/2007JB005015.

Collettini, C., Sibson, R.H., 2001. Normal faults normal friction? *Geology* 29, 927–930.

Jackson, J.A.,White,N.J., 1989.Normal faulting in the upper continental crust: observations from regions of active extension. *Journal of Structural Geology* 11, 15–36.

Nocquet, J. M., E. Calais, and B. Parsons (2005), Geodetic constraints on glacial isostatic adjustment in Europe, *Geophys. Res. Lett.,* 32, L06308, doi:10.1029/2004GL022174.

Sibson, R.H., 1985. A note on fault reactivation. Journal of Structural Geology 7, 751–754.

Wernicke, B., 1995. Low-angle normal faults and seismicity: a review. *Journal of Geophysical Research* 100, 20159–20174.

Williams, S. D. P. (2007), CATS: GPS coordinate time series analysis software, GPS Solutions, 12, 147-153, doi:10.1007/s10291-007-0086-4.

Zumberge, J. F., M. B. Heflin, D. C. Jefferson, M. M. Watkins, and F. H. Webb (1997), Precise point positioning for the efficient and robust analysis of GPS data from large networks*, J. Geophys. Res.*, 102, 5005-5018.


## 3.4 The Corinth Rift Laboratory


Armijo, R., B. Meyer, G. King, A. Rigo, D., Papastamatiou, Quaternary evolution of the Corinth rift and its implications for the Late Cenozoic evolution of the Aegean, *Geophys. J. Int.*, 126, 11-53, 1996

Avallone A., P. Briole, A.M. Agatza-Balodimou, H. Billiris, O. Charade, C. Mitsakaki, A. Nercessian, K. Papazissi, D. Paradissis, G, Veis, Analysis of eleven years of deformation measured by GPS in the Corinth Rift Laboratory area, *C.R. Geoscience*, 336, 301-312, 2004

Bernard, P., F. Boudin, S. Sacks, A. Linde, P.-A. Blum, C. Courteille, M.-F. Esnoult, H. Castarède, S. Felekis, and H. Billiris ; Continuous strain and tilt monitoring on the Trizonia island, Rift of Corinth, Greece, *C.R. Geoscience*, 336, 313-324, 2004

Bernard, P., P. Briole, B. Meyer, H. Lyon-Caen, et al., The Ms=6.2, June 15, 1995 Aigion earthquake (Greece): evidence for low angle normal faulting in the Corinth rift, *Journal of Seismology*,1, 131-150, 1997

Bernard, P., H. Lyon-Caen, P. Briole, A. Deschamps, F. Boudin, K. Makropoulos , P. Papadimitriou, F. Lemeille, G. Patau, H. Billiris, D. Paradissis, K. Papazissi, H. Castarède, O. Charade, A. Nercessian, A. Avallone, F. Pacchiani, J. Zahradnik, S. Sacks, and A. Linde, Seismicity, Deformation and seismic hazard in the western rift of Corinth : New insights from the Corinth Rift Laboratory (CRL) , *Tectonophysics*, 426,7–30, 2006

Bourouis S. and F.H. Cornet, Microseismic activity and fluid fault interactions: Some results from the Corinth Rift Laboratory (CRL), Greece, *Geophys. J. Int.*, 2009

Briole, P.; Rigo, A.; Lyon-Caen, H.; Ruegg, J.C.; Papazissi, K.; Mitsakaki, C.; Balodimou, A.; Veis, G.; Hatzfeld, D. and Deschamps, A.; Results from repeated Global Positioning System surveys between 1990 and 1995, *J. Geophys. Res.*,105, 25605—25625, 2001.

Cianetti S, Tinti E, Giunchi C, et al., Modelling deformation rates in the western Gulf of Corinth: rheological constraints, *Geophys. J. Int.*, 174, 749-757, 2008

Cociani, L., C.J. Bean, H. Lyon-Caen, F. Pacchiani, and A. Deschamps, Coseismic velocity variations caused by static stress changes associated with the 2001 Mw=4.3 Agios Ioanis earthquake in the Gulf of Corinth, Greece., *J. Geophys. Res.*, doi:10.1029/2009JB006859, 2010

Cornet, F.H., P. Bernard, and I. Moretti ; The Corinth Rift Laboratory, *C.R. Geoscience*, 336, 235-242, 2004

Cornet F.H., M.L. Doan, I. Moretti and G. Borm, Drilling through the active Aigion Fault : The AIG10 well observatory, *C.R. Geoscience*, 336, pp 395-406, 2004

De Martini P.M., D. Pantosti, N. Palyvos, F. Lemeille, L. McNeill and R. Collier ; Slip rates of the Aigion and Eliki faults from uplifted marine terraces, Corinth Gulf, Greece, *C. R. Geoscience*, 336, 325-334; 2004

Doan M. L. and F. H. Cornet : small pressure drop triggered near a fault by small teleseismic waves, *Earth Planet. Sci. Lett.*, 258, 2007, 207-218

Doan M.L. and F.H. Cornet, Thermal anomaly near the aigio fault, gulf of Corinth, Greece, maybe due to convection below the fault, *Geoph. Res. Lett*, 34, L06314, 2007

Gautier S., Latorre D., Virieux J., Deschamps A., Skarpelos C., Sotiriou A., Serpetsidaxi A. and Tselentis A., A new passive tomography of the Aigion area (Gulf of Corinth, Greece) from the 2002 dataset, *Pageoph*, 163, 431-453, doi : 10.1007/500024-005-0033-7, 2006

Gautier, S., J. Virieux and G. Nolet, Finite-frequency tomography in a crustal environment: application to the western part of the Gulf of Corinth, *Geophysical Prospecting*, 56, 493-526, 2008

Giurgea V., D. Rettenmaier, L. Pizzino, I. Unkel, H. Hötzl, A. Förster, F. Quatrocchi, Preliminary hydrogeological interpretation of the Aigion area from the AIG10 borehole data, *C.R. Geoscience*, 336, 467-476, 2004

Jansky J, Zahradnik J, Sokos E, et al., Relocation of the 2001 earthquake sequence in Aegion, Greece, *Studia Geophysica et Geodica*, 48, 331-344, 2004

Jansky, J., V. Plicka, H. LyonCaen, and O. Novotny, Estimation of velocity in the uppermost crust in a part of the western Gulf of Corinth, Greece, from the inversion of P and S arrival times using the neighbourhood algorithm, *J. Seismol.*, 11, 199- 204, 2007

Latorre D., J. Virieux, T. Monfret and H. Lyon-Caen, Converted seismic wave investigation in the gulf of Corinth from local earthquakes, *C. R. Geoscience*, 336, 259-267, 2004

Latorre D., J. Virieux, T. Monfret, V. Monteiller, T. Vanorio, J.L. Got and H. Lyon-Caen, A new seismic tomography of Aigion area (Gulf of Corinth-Greece) from the 1991 dataset, *Geophys. J. Int.*, 159, 1013-1031, 2004

Lemeille F., F. Chatoupis, M. Foumelis, D. Rettenmaier, I. Unkel, L. Micarelli, I. Moretti, C. Bourdillon, C. Guernet, C. Müller, 2004.Recent syn-rift deposits in the hanging wall of the Aigion Fault, *C. R. Geoscince*, 336, 281-290, 2004

Leonardi V. and P. Gavrilenko, Hydrologic measurements in wells in the Aigion area (Corinth Gulf, Greece): Preliminary results, *C.R. Geoscience*, 336, 385-394, 2004

Lyon-Caen, H., P. Papadimitriou, A. Deschamps, P. Bernard, K. Makropoulos, F. Pacchiani, G. Patau ; First results of CRLN seismic arraay in the western Corinth rift: evidence for old fault reactivation, *C.R. Geoscience*, 336, 343-352, 2004

Naville C., S. Serbutoviez, I. Moretti, J.M. Daniel, A. Throo, F. Girard, A. Sotiriou, A. Tselentis, C. Skarpzelos, C. Brunet and F. Cornet, Pre-drill surface seismic in the vicinity of the AIG-10 well and post-drill VSP, *C. R. Geoscience*, 336, 407-414, 2004

Pacchiani F. and H. Lyon-Caen, Spatio-temporal evolution of the 2001 Agios Ioanis seismic swarm (Corinth Rift, Greece) *Geophys. J. Int.*, 2009, doi: 10.1111/j.1365-246X.2009.04409.x

Palyvos N., D. Pantosti, P. M. De Martini, D. Sorel, K. Pavlopoulos, The Aigion-Neos Erineos normal fault system (Western Corinth Gulf Rift, Greece): Geomorphological signature, recent earthquake history and induced coastal changes during the Holocene, *J. Geophys. Res.*, 110, B09302, doi: 10.1029/2004JB003165, 2005

Palyvos, N., Mancini, M., Sorel, D., Lemeille, F., Pantosti, D., Julia, R., Triantaphyllou, M., De Martini, P.-M., Geomorphological, stratigraphic and geochronological evidence of fast

Pleistocene coastal uplift in the westernmost part of the Corinth Gulf Rift (Greece), *Geological Journal*, vol. 45 (1), 78-104. DOI: 10.1002/gj.1171, 2010

Pantosti D., P.M. De Martini, I. Koukouvelas, L. Stamatopoulos, N. Palyvos, S. Pucci, F. Lemeille, S. Pavlides, Paleosismological investigations of the Aigion fault (Gulf of Corinth, Greece), *C.R. Geoscience*, 336 425-434, 2004

Pham, V. N., P. Bernard, D. Boyer, P. Papadimitriou, G. Chouliaras, and A. Charrier ; Electrical conductivity and crustal structure beneath the Central Hellenides around the Gulf of Corinth (Greece) and their relationship with the seismotectonics, *Geophys. J. Int.* 142, 948-969, 2000

Pik R, Marty B, Helium isotopic signature of modern and fossil fluids associated with the Corinth rift fault zone (Greece): Implication for fault connectivity in the lower crust, *CHEMICAL GEOLOGY*, 266, 67-75, 2009

Pitilakis K., Makropoulos K., Bernard P., Lemeille F., Berge-Thierry C., Tika Th., Manakou M., Diagourtas D., Raptakis D., Kallioglou P., Makra K. Pitilakis D. Bonilla L.F. ; The Corinth Gulf Soft Soil Array (CORSSA) to study Site Effects, *C.R. Geosciences*, 336, 353-365, 2004

Pizzino L., Quattrocchi F., Cinti D., Galli G. ; Fluid Geochemistry along the Eliki and Aigion seismogenic segments (Gulf of Corinth, Greece), *C. R. Geoscience*, 336, 367-374, 2004

Rietbrock A., C. Tiberi, F. Sherbaum and H. Lyon-Caen, Seismic slip on a low angle normal fault in the Gulf of Corinth: evidence from high resolution cluster analysis of microearthquakes, *Geophys. Res. Lett.*, 23, 14, 1817-1820, 1996

Rigo A., H. Lyon-Caen, R. Armijo, A. Deschamps, D. Hatzfeld, K. Makropoulos, P. Papadimitriou, and I. Kassaras, 1996. A Microseismic Study in the Western Part of the Gulf of Corinth (Greece): Implications for Large-Scale Normal Faulting Mechanisms, Geophys. J. Int., 126, 663-688.

Sulem J., Stress orientation evaluated from strain localisation analysis in Aigion Fault, *Tectonophysics*, 442, 3-13, 2007

Wyss M., Pacchiani F., Deschamps A. and G. Patau, mean magnitude variations of earthquakes as a function of depth show different crustal stress distribution depending on tectonic setting, *Geophys. Res. Lett.*, 35, L01307, 2008

Zahradnik J., J. Jansky, E. Sokos, A. Serpetsidaki, H. Lyon-Caen P. Papadimitriou ; Modeling the M=4.7 mainshock of the February-July 2001 eathquake sequence in Aegion, Greece, J. of Seismology, 8, 247-257, 2004

Zahradnik J., J. Jansky, and V. Plicka, Detailed Waveform Inversion for Moment Tensors of M 4 Events: Examples from the Corinth Gulf, Greece *Bull. Seism. Soc. Am.*, 98, 2756 - 2771, 2008

## 3.5 Irpinia Fault System

Allen, R.V.(1978) Automatic Earthquake Recognition and Timing From Single Traces, Bull. Seism. Soc. Am., 68, 1521-1532.

Allen, R.V. (1982), Automatic Phase Pickers: Their Present Use and Future Prospects, Bull. Seism. Soc. Am. 72, S225-S242.

Bernard P. and Zollo A. (1989). The Irpinia (Italy) 1980 earthquake: detailed analysis of a complex normal faulting, J. Geophys. Res., B94, 1631-1647.

Bobbio A., Vassallo M. and Festa G.(2009). A Local Magnitude Scale for Southern Italy. Bull. Seism. Soc. Am., 99, 4, doi: 10.1785/0120080364

Colombelli S., Amoroso O., Zollo A. and Kanamori H. (2011). Test of a threshold-based Earthquake Early Warning method using Japanese data, Accepted by BSSA.

Emolo A., Iannaccone G., Zollo A. and Gorini A. (2004). Inferences on the source mechanisms of the 1930 Irpinia (Southern Italy) earthquake from simulations of the kinematic rupture process, Ann. Geophys., 47, 1743-1754.

Lancieri M., Zollo A. (2008). Bayesian approach to the real-time estimation of magnitude from the early P and S wave displacement peaks., J Geophys Res 2008; 113(B12), doi:10.1029/2007JB005386

Dietz, L. (2002). Notes on Configuring BINDER_EW: Earthworm's Phase Associator; 15

http://folkworm.ceri.memphis.edu/ew-doc/ovr/binder_setup.html.
Lomax A., Satriano S. and Vassallo M. (2011). Automatic picker developments and optimization: FilterPicker - a robust, broadband picker for real-time seismic monitoring and earthquake early-warning. Accepted by Seismological Research Letters.
Pantosti D. and Valensise G. (1990). Faulting mechanism and complexity of the 23 November 1980, Campania-Lucania earthquake, inferred from surface observations, J. Geophys. Res., 95, 15319-15341.
Pino A.N.,. Palombo N., Ventura G., Perniola B. and Ferrari G (2008). Waveform modeling of historical seismograms of the 1930 Irpinia earthquake provides insight on "blind" faulting in Southern Apennines (Italy), J. Geophys. Res., 113, B05303
Satriano C, Lomax A and Zollo A. (2008). Real-time evolutionary earthquake location for seismic early warning., Bull. Seism. Soc. Am.; 98(3):1482–94, doi:10.1785/ 0120060159.
Tertulliani A., Anzidei M., Maramai A., Murru M. and Riguzzi F. (1992). Macroseismic study of the Potenza (Southern Italy) earthquake of 5 May 1990, Nat. Hazards, 6, 25-38.
Westaway R. (1987). The Campania, Southern Italy, earthquakes of 1962 August 21, Geophys. J. R. Astr. Soc. 8, 1-24.
Westaway R. and Jackson J. (1987). The earthquake of 1980 November 23 in Campania-Basilicata (southern Italy), Geophys. J. R. Astr. Soc. 90, 375–443.
Zollo A., Amoroso O., Lancieri M., Wu YM. and Kanamori H. (2010). A threshold-based earthquake early warning using dense accelerometer networks. Geophys. J. Int., 183, 963–974 doi: 10.1111/j.1365-246X.2010.04765.x.

## 3.6 Valais Region

Burjanek J., Gassner-Stamm G. and Fäh D.; 2010: *Array-measurements in the area of Visp and St. Niklaus*. COGEAR, 3.1.2, Swiss Seismological Service SED. 77 p.
Burjanek J., Stamm G., Poggi V., Moore J.R. and Fäh D.; 2010: *Ambient vibration analysis of an unstable mountain slope*. *Geophysical* Journal International, 180(2), 820-828.
Fäh D., Giardini D., Bay F., Bernardi F., Braunmiller J., Deichmann N., Furrer M., Gantner L., Gisler M., Isenegger D., Jimenez M.-J., Kästli P., Koglin R., Masciadri V., Rutz M., Scheidegger C., Schibler R., Schorlemmer D., Schwarz-Zanetti G., Steimen S., Sellami S., Wiemer S. and Wössner J.; 2003: *Earthquake Catalogue Of Switzerland (ECOS) And The Related Macroseismic Database.* Eclogae geol. Helv., 96, pp. 219–236.
Fäh D., Giardini D., Kästli P., Deichmann N., Gisler M., Schwarz-Zanetti G., Alvarez-Rubio S., Sellami S., Edwards B., Allmann B., Bethmann F., Wössner J., Gassner-Stamm G., Fritsche S. and Eberhard D.; 2011: *ECOS-09 Earthquake Catalogue of Switzerland Release 2011*. Report and Database. Public catalogue, 17.4.2011. Swiss Seismological Service ETH Zürich, Report SED/RISK/R/001/20110417
Fäh, D., Moore, J., Burjanek, J., Iosifescu, I., Dalguer, L., Dupray, F., Michel, C., Woessner, J., Villiger, A., Laue, J., Marschall, I., Gischig, V., Loew, S., Marin, A., Gassner, G., Alvarez, S., Balderer, W., Kästli, P., Giardini, D., Iosifescu, C., Hurni, L., Lestuzzi, P., Karbassi, A., Baumann, C., Geiger, A., Ferrari, A., Laloui, L., Clinton, J., Deichmann, N., 2011b; *Coupled seismogenic geohazards in alpine regions*. Bolletino di Geofisica Teorica ed Applicata, in press.
Fréchet J., Thouvenot F., Frogneux M., Deichmann N. and Cara M.; 2011: *The Mw 4.5 Vallorcine (French Alps) earthquake of 8 September 2005 and its complex aftershock sequence.* Journal of Seismology, 15, 43-58, DOI:10.1007/s10950-010-9205-8.
Fritsche S. and Fäh D.; 2009: *The 1946 magnitude 6.1 earthquake in the Valais: site-effects as a contributor to the damage*. Swiss Journal of Geosciences, 102, 423-439.
Fritsche S., Fäh D., Gisler M. and Giardini D.; 2006: *Reconstructing the damage field of the 1855 earthquake in Switzerland: historical investigations on a well-documented event.* Geophysical Journal International, 166, 719-731.

Fritsche S., Fäh D., Gisler M., Schwarz-Zanetti G. and Giardini D.; 2010: *Historical Earthquakes in Valais: Primary and Secondary Effects*. Swiss J. Geosci., submitted.

Gisler, M., Fäh, D., Deichmann, N., 2004; *The Valais earthquake of December 9, 1755*. Eclogae Geol. Helv., 97, 411-422.

Kastrup U., Zoback M.-L., Deichmann N., Evans K., Giardini D. and Michael A.J.; 2004: *Stress field variations in the Swiss Alps and the northern Alpine foreland derived from inversion of fault plane solutions*. J. Geophys. Res.,109, B1, doi: 10.1029/2003JB002550B01402, 2004

Maurer H., Burkhard M., Deichmann N., Green A.G.; 1997: *Active Tectonism in the Western Swiss Alps.* Terra Nova, 9, 91-94.

Maurer H. and Deichmann N.; 1995: *Microearthquake cluster detection based on waveform similarities, with an application to the western Swiss Alps.* Geophys. J. Int., 123, 588-600.

Moore J.R., Gischig V., Burjanek J., Loew S. and Fäh D.; 2011: *Site effects in unstable rock slopes: dynamic behavior of the Randa instability (Switzerland)*. Bull. Seismol. Soc. Am., in press.

Roten D., Fäh D., Cornou C. and Giardini D.; 2006*: 2D resonances in Alpine valleys identified from ambient vibration wavefields*. Geophys. J. Int., 165, 889-905.

Roten D., Fäh D., Olsen K.B. and Giardini D.; 2008: *A comparison of observed and simulated site response in the Rhone valley*. Geophysical J. Int., 173, 3, 958-978.

Roten D., Fäh D., Bonilla F., Alvarez-Rubio S., Weber T. and Laue J.; 2009: *Estimation of nonlinear site response in a deep Alpine valley*. Geophys. J. Int., 178, 1597–1613.

Steimen S., D. Fäh, F. Kind, C. Schmid and D. Giardini, 2003. *Identifying 2-D Resonance in Microtremor Wave Fields*. Bull. Seism. Soc. Am., 93, 583 - 599.